

Contribution of Membrane Transporters to the Disposition of Organic Cations

Dissertation

Presented in Partial Fulfillment of the Requirements for the Degree Doctor of Philosophy
in the Graduate School of The Ohio State University

By

Muhammad Erfan Uddin, M.S.

Graduate Program in Pharmaceutical Sciences

The Ohio State University

2022

Dissertation Committee

Alex Sparreboom, PhD | Advisor

Shuiying Hu, PhD | Co-advisor

Cynthia A. Carnes, PharmD, PhD | Committee Member

Navjot Pabla, PhD | Committee Member

Copyrighted by
Muhammad Erfan Uddin
2022

Abstract

Membrane transporters play a pivotal role in maintaining cellular integrity via the removal of toxic metabolites or entry of essential nutrients. Despite regulating cellular influx and efflux, tissue-specific expression of transporters contributes to local drug accumulation and drug-drug interactions (DDIs), and functional alterations in these transporters can directly influence an individual's susceptibility to drug-induced toxicity. Here, we provide an overview of membrane transporters with a role in drug-induced toxicity and discuss novel strategies to improve therapeutic outcomes. We highlighted the contribution of membrane transporters in chemotherapy-induced various toxicities (Chapter 1). We then evaluated *in vitro* and *in vivo* functional regulation of organic cation transporter 1 (OCT1), a most abundant cationic transporter expressed in the liver, and identified an OCT1 specific biomarker isobutyryl L-carnitine (IBC) in plasma (Chapter 2). Next, we evaluated the interactions with FDA-approved tyrosine kinase inhibitors (TKIs) with MATE1 transporter, which is highly expressed in the apical membrane of renal tubular cells, and evaluated the effect of MATE1 inhibition on the safety or DDI liability of oxaliplatin-based chemotherapy (Chapter 3). Finally, we characterized the transport mechanism of dofetilide, a class III anti-arrhythmic drug. We investigated the *in vitro*, *ex vivo*, and *in vivo* DDI potential of dofetilide, and the influence of MATE1

transporter on dofetilide disposition. In addition, we developed a physiologically-based pharmacokinetic (PBPK) model to predict transporter-mediated DDIs (Chapter 4).

Dedication

Dedicated to Muhammad Kamal Uddin, a father who dreamed of this journey.

Acknowledgments

I would like to express my sincere gratitude and special thanks to my mentor, Dr. Alex Sparreboom, for his immense support, guidance, and providing extraordinary opportunities throughout my time in graduate school. I would like to acknowledge and thank Dr. Shuiying Hu for her critical insight and encouragement. Similarly, I would like to acknowledge Drs. Cynthia A. Carnes and Navjot Pabla for their guidance throughout my Ph.D. education which was critical to the completion of my research projects. I would like to thank Dr. Sharyn Baker for her continuous motivation and guidance on my projects. Special thanks to Alice. A. Gibson for her training and advice throughout my research. I would also like to thank the members, past and present, of the Experimental Cancer Pharmacology Laboratory for their support and guidance, including Dr. Daelynn Buelow, and each of the members of the PK team (Drs. Eric D. Eisenmann, Kevin M. Huang, Jason T. Anderson, Zahra Talebi, Dominique A. Garrison, Mingqing Chen, Yang Li, Yan Jin, Mahesh Nepal). I would also like to acknowledge Eli Lilly, and the American Heart Association (AHA) predoctoral fellowship for their financial support during my graduate studies.

Vita

- 2008 – 2012 Bachelor of Pharmacy (B.Pharm.)
Department of Pharmacy
International Islamic University Chittagong, Bangladesh
- 2014 – 2017 Master of Science in Biological Sciences (M.S.)
Department of Biological Sciences
Youngstown State University, Youngstown, OH
- 2017 –2022 Graduate Research Associate
Division of Pharmaceutics and Pharmacology
College of Pharmacy
The Ohio State University, Columbus, OH

Publications

Uddin ME, Talebi Z, Chen S, Jin Y, Gibson AA, Noonan AM, Cheng X, Hu S, Sparreboom A. In Vitro and In Vivo Inhibition of MATE1 by Tyrosine Kinase Inhibitors. *Pharmaceutics*. 2021; 13(12):2004.

Eisenmann ED, Fu Q, Muhowski EM, Jin Y, **Uddin ME**, Garrison DA, Weber RH, Woyach JA, Byrd JC, Sparreboom A, Baker SD. Intentional modulation of ibrutinib pharmacokinetics through CYP3A inhibition. *Cancer Research Communications*. 2021 Nov 9;1(2):79–89.

Uddin ME, Moseley A, Hu S, Sparreboom A. Contribution of Membrane Transporters to Chemotherapy-Induced Cardiotoxicity. *Basic & Clinical Pharmacology & Toxicology*. 2021 Jul 8.

Uddin ME, Garrison DA, Kim K, Jin Y, Eisenmann ED, Huang KM, Gibson AA, Hu Z, Sparreboom A, Hu S. Influence of YES1 Kinase and Tyrosine Phosphorylation on the Activity of OCT1. *Frontiers in Pharmacology*. 2021 Mar;12:291.

Hayden E, Chen M, Pasquariello KZ, Gibson AA, Petti JJ, Shen S, Qu J, Ong SS, Chen T, Jin Y, **Uddin ME**, Huang KM, Paz A, Sparreboom A, Hu S, Sprowl JA. Regulation of

OATP1B1 function by tyrosine kinase-mediated phosphorylation. *Clinical Cancer Research*. 2021 Mar 4;clincanres.0023.2021.

Huang KM, Zavorka Thomas M, Magdy T, Eisenmann ED, **Uddin ME**, DiGiacomo DF, Pan A, Keiser M, Otter M, Xia SH, Li Y, Jin Y, Fu Q, Gibson AA, Bonilla IM, Carnes CA, Corps KN, Coppola V, Smith SA, Addison D, Nies AT, Bundschuh R, Chen T, Lustberg MB, Wang J, Oswald S, Campbell MJ, Yan PS, Baker SD, Hu S, Burrige PW, Sparreboom A. Targeting OCT3 attenuates doxorubicin-induced cardiac injury. *Proceedings of the National Academy of Sciences*. 2021 Feb 2;118(5).

Huang KM, Leblanc, AF, **Uddin ME**, Chen M, Eisenmann ED, Gibson AA, Yang L, Hong KW, DiGiacomo D, Xia SH, Alberti P, Chiorazzi A, Housley SN, Cope T, Sprowl JA, Wang J, Loprinzi CL, Noonan A, Lustberg MB, Cavaletti G, Hu S, Sparreboom A. Neuronal uptake transporters contribute to oxaliplatin neurotoxicity in mice. *Journal of Clinical Investigation*. 2020 July; 27.

Huang KM, **Uddin ME**, DiGiacomo D, Lustberg MB, Hu S, Sparreboom A. Role of organic cation transporters in chemotherapy-induced toxicity. *Expert Opinion on Drug Metabolism and Toxicology*. 2020 Jun;16(6):493-506.

Uddin ME, Sun X, Huang KM, Hu S, Carnes CA, Sparreboom A, Fu Q. Development and validation of a UPLC-MS/MS analytical method for dofetilide in mouse plasma and

urine, and its application to pharmacokinetic study. Journal of Pharmaceutical and Biomedical Analysis. 2019 Aug;172:183-188.

Leblanc AF, Huang KM, **Uddin ME**, Anderson JT, Chen M, Hu S. Murine Pharmacokinetic Studies. Bio-Protocol. 2018 Oct; 8(20).

Fields of Study

Major Field: Pharmaceutical Sciences

Specialization: Pharmaceutics and Pharmacology

Table of Contents

Abstract.....	ii
Dedication.....	iv
Acknowledgments.....	v
Vita.....	vi
List of Tables	xiii
List of Figures.....	xiv
Chapter 1. Role of Membrane Transporters in Drug-induced Toxicities	1
1.1 Abstract	1
1.2 Introduction.....	2
1.3 Organic Cation Transporters.....	3
1.4 Dose-limiting toxicities associated with chemotherapeutic agents	6
1.4.1 Nephrotoxicity	6
1.4.2 Neurotoxicity	11
1.4.3 Ototoxicity	13
1.5 Role of transporters in drug-induced cardiotoxicity	15
1.5.1 Cardiac expression of xenobiotic transporters.....	16
1.5.2 Pharmacological role of xenobiotic transporters in cardiomyocytes.....	17
1.5.3 SLC-based intervention strategies to prevent cardiotoxicity	24
1.5.4 Future Perspective.....	28
Chapter 2. Influence of YES1 Kinase and Tyrosine Phosphorylation on the Activity of OCT1.....	32
2.1 Abstract.....	32
2.2 Introduction.....	33
2.3 Materials and Methods.....	34
2.4 Results.....	40
2.4.1 Conserved tyrosine phosphorylation of OCT1	40
2.4.2 TKI-based inhibition of OCT1 <i>in vitro</i>	42
2.4.3 TKI-mediated modulation of OCT1 <i>in vivo</i>	43
2.4.4 Kinase-mediated regulation of OCT1 function.....	44
2.5 Discussion.....	62

2.6 Acknowledgments.....	66
Chapter 3. <i>In Vitro</i> and <i>In Vivo</i> Inhibition of MATE1 by Tyrosine Kinase Inhibitors.....	67
3.1 Abstract.....	67
3.2 Introduction.....	68
3.3 Materials and Methods.....	69
3.4 Results and Discussion	77
3.4.1 TKI-mediated inhibition of MATE1 <i>in vitro</i>	77
3.4.2 Computational evaluation of MATE1-TKIs interaction.....	79
3.4.3 Influence of TKIs on MATE1 regulation <i>in vitro</i>	81
3.4.4 Effect of TKI treatment on MATE1 function <i>in vivo</i>	82
3.4.5 Modulation of oxaliplatin pharmacokinetics by TKI treatment	84
3.5 Conclusions.....	103
3.6 Acknowledgments.....	103
Chapter 4. Involvement of Membrane Transporters and Dofetilide-induced Proarrhythmia	104
4.1. Development and Validation of a UPLC-MS/MS Analytical Method for Dofetilide	104
4.1.1 Abstract	104
4.1.2 Introduction.....	105
4.1.3 Materials and Methods.....	106
4.1.4 Results.....	112
4.1.4.1 UPLC-MS/MS spectrometry and specificity	112
4.1.4.2 Linearity, accuracy, precision, and selectivity.....	112
4.1.4.3 Recovery, matrix effect, and stability	113
4.1.4.4 Pharmacokinetic studies.....	113
4.1.5 Discussion	124
4.1.6 Conclusion	126
4.1.7 Acknowledgments.....	126
4.2 Contribution of MATE1 to Dofetilide-induced Proarrhythmia	127
4.2.1 Abstract	127
4.2.2 Introduction.....	128
4.2.3 Materials and Methods.....	131
4.2.4 Results and Discussion	139

4.2.4.1 Identification of MATE1 as a high-affinity carrier of dofetilide	139
4.2.4.2 MATE1 deficiency exacerbates dofetilide-induced proarrhythmia.....	142
4.2.4.3 Inhibition of MATE1 attenuates renal elimination of dofetilide	143
4.2.4.4 Contraindicated drugs of dofetilide inhibit MATE1 function	146
4.2.4.5 Influence of CYP3A in the disposition of dofetilide	148
4.2.4.6 Dofetilide PBPK Model predicts transporter-mediated DDI.....	149
4.2.5 Acknowledgments.....	151
Chapter 5. Conclusion.....	181
Bibliography	184

List of Tables

Table 1: Features of TKIs used in the experiments	50
Table 2: Plasma pharmacokinetic parameters of cisplatin and oxaliplatin in mice and a human patient with cancer*	102
Table 3: Precursor molecular/product ion for quantification, confirmation, and detection parameters for each analyte	115
Table 4: Assay performance data for the quantitation of dofetilide in mouse plasma and urine	119
Table 5: Recovery and matrix effect of dofetilide and its metabolites in mouse plasma	120
Table 6: Short-term stability of dofetilide and its metabolites in mouse plasma and urine	121
Table 7: Pharmacokinetics parameters of dofetilide oral and IV administration in mice	123
Table 8. Influence of contraindicated drugs on the pharmacokinetic parameters of dofetilide in female mice	171
Table 9. Pharmacokinetic parameters of dofetilide after giving an intravenous dose (2.5 mg/kg) in mice	173
Table 10. Influence of contraindicated drugs on the pharmacokinetic parameters of dofetilide in male mice.....	174
Table 11. Observed and predicted pharmacokinetic parameters of dofetilide with the presence and absence of cimetidine and ketoconazole	175
Table 12. Input parameters of dofetilide in PBPK model.....	177

List of Figures

Figure 1: Proposed drug transport mechanisms in cardiomyocytes	31
Figure 2: Phosphotyrosine proteomics screen	46
Figure 3: Inhibition of organic cation transporters by TKIs.....	47
Figure 4: Inhibition of organic cation transporters 3 (OCT3) by TKIs	49
Figure 5: TKI-mediated OCT1 inhibition.....	51
Figure 6: TKI-mediated inhibition of OCT1 function	53
Figure 7: Targeted metabolomics and endogenous OCT1 biomarker identification.....	55
Figure 8: Genetic and pharmacological inhibition of YES1 kinase impairs OCT1 activity	57
Figure 9: Influence of YES1 inhibition on OCT1 and OCT2 function	59
Figure 10: Schematic diagram showing the role of YES1 kinase in regulating OCT1 function	61
Figure 11: Modulation of MATE1 function by TKIs in vitro	88
Figure 12: In silico analysis of mechanisms underlying MATE1 inhibition by TKIs.....	90
Figure 13: Influence of TKIs on MATE1 expression.....	92
Figure 14: Characteristics of MATE1 inhibition by TKIs.....	94
Figure 15: Renal transport of oxaliplatin in mice and humans.....	96
Figure 16: Influence of MATE1 deficiency on cisplatin disposition	97
Figure 17: Influence of MATE1 inhibition on oxaliplatin disposition	98
Figure 18: Influence of TKI pre-treatment on oxaliplatin and cisplatin disposition	100
Figure 19: MS/MS chromatograms and proposed fragmentation pathways of dofetilide	116
Figure 20: Representative chromatograms of dofetilide analytes.....	117
Figure 21: Concentration of dofetilide in plasma and urine	122
Figure 22: Inhibition of MATE1 enhances dofetilide accumulation in the heart	152
Figure 23: MATE1 deficiency exacerbates dofetilide-induced proarrhythmia	154
Figure 24: Inhibition of MATE1 attenuates renal elimination of dofetilide.....	156
Figure 25: Contraindicated drugs of dofetilide restrain MATE1 function	158
Figure 26: CYP3A does not influence in the disposition of dofetilide.....	160
Figure 27: Physiologically based pharmacokinetics (PBPK) model predicts transporter-mediated drug-drug interactions of dofetilide.....	162
Figure 28: Influence of MATE1 in the disposition of dofetilide	164
Figure 29: Drug-drug interactions increase dofetilide plasma exposure	166
Figure 30: Plasma exposure and renal elimination of dofetilide	167
Figure 31: Structure of the physiologically based pharmacokinetic (PBPK) model for dofetilide	169
Figure 32: Workflow of dofetilide physiologically based pharmacokinetic (PBPK) model	170

Chapter 1. Role of Membrane Transporters in Drug-induced Toxicities

****Disclaimer****

The following chapter contains excerpts from articles published and copyrighted by:

Expert Opinion on Drug Metabolism and Toxicology,¹ and *Basic and Clinical Pharmacology and Toxicology*.² Permissions obtained from Tylor & Francis, and John Wiley & Sons, Inc.

1.1 Abstract

Expression and localization of drug transporters contribute to a dynamic interplay between the maintenance of cellular integrity via the removal of toxic metabolites or entry of essential nutrients. Moreover, members of the ATP-binding cassette (ABC) and solute carrier (SLC) superfamilies are recognized as important determinants governing the therapeutic response of many drugs. Disruption of these sensitive transport systems through changes in gene expression, genetic variations or drug-drug interactions has the potential to contribute to chemoresistance, endogenous toxin-mediated diseases, diminished therapeutic efficacy, and increased sensitivity to drug-induced organ damage. The following review focuses on specific examples within the SLC subfamily of organic cation transporters (OCTs), and multidrug and toxin extrusion proteins (MATEs) as

critical determinants of the dose-limiting toxicity profiles associated with chemotherapeutic agents.

1.2 Introduction

ABC and *SLC* family members comprise of over 400 genes encoded in the human genom.^{3,4} While the function of these gene families is to regulate the entry of essential nutrients and the removal of endogenous toxins, the *SLC* family also contributes to the cellular and systemic distribution profile of many therapeutic drugs.⁵⁻⁷ Specifically, OCT1 [*SLC22A1*], OCT2 [*SLC22A2*], OCT3 [*SLC22A3*], OCTN1 [*SLC22A4*], and OCTN2 [*SLC22A5*] are the major organic cation-type transporters encoded by the *SLC22A* subfamily that facilitate drug accumulation. Due to their expression on the basolateral membranes of enterocytes, hepatocytes, proximal tubules and other endothelial peripheral tissues, OCTs play a critical role in the vectorial transport of organic cations.⁸⁻¹¹ Independent of Na⁺ and H⁺, OCTs translocate substrates across a biological membrane driven by membrane potential and the electrochemical gradient of the protonated molecule.⁸ Additionally, the subfamily of MATEs, including MATE1 [*SLC47A1*] and MATE2-K [*SLC47A2*], mediate the efflux of diverse substrates consisting primarily of organic cations, but also certain anions and zwitterions, from the liver and kidney.^{12,13} MATEs have emerged as clinically relevant efflux transporters that work in concert with OCTs to mediate apical efflux into the bile and urine. Unlike OCTs, the bi-directionality of MATE transport is dependent on the proton concentration gradient, and driven by exchange of protons in the bile or urine.¹⁴ It is important to note that other members within

this family, including OCTL2 [*SLC22A14*], OCT6 [*SLC22A16*], OCTN3 [*SLC22A21*], and UST6 [*SLC22A25*]^{15,16} as well as members of the *ABC* family such as MDR1 [*ABCB1*], MRP1 [*ABCC1*], MRP2 [*ABCC2*], MRP4 [*ABCC4*], and BCRP [*ABCG2*],^{17,18} are also capable of governing intracellular levels of organic cations. Since 40% of FDA-approved therapeutic drugs exist as organic cations under physiological conditions,¹⁹ OCTs and MATEs are recommended for evaluation during drug development by the Food and Drug Administration (FDA).²⁰

1.3 Organic Cation Transporters

Organic cation transporter 1 (OCT1). OCT1 is the most abundant cationic uptake transporter expressed in the liver in humans.¹¹ The localization of OCT1 is predominantly expressed on the sinusoidal membrane (blood facing) of hepatocytes, and it serves as the rate-determining step in the translocation of endogenous^{21,22} and xenobiotic cationic compounds from the systemic circulation into the liver,²³ and thus contributes as an initial step in hepatic metabolism and excretion. In addition to OCT1, efflux transporters of *ABC* superfamily of transporters such as MDR1,¹⁷ and MATE1¹⁴ work in a concerted manner to assist in the biliary excretion and detoxification of endogenous cationic toxins. OCT1 has been implicated in drug-drug interactions, and contributes to pharmacokinetic and pharmacodynamic variability of substrates in humans.^{24,25} OCT1 is also expressed on the bronchial epithelial cells,²⁶ endothelial cells of the heart, brain, and enterocytes.^{8,27} In contrast to the dominant OCT1 expression in human livers, rodents also express Oct1 on enterocytes²⁸ and epithelial cells found in the S1 and S2 segments of proximal tubular cells.

In the rodent kidney, Oct1 is redundant with Oct2, and these proteins jointly fulfill a function that is equivalent to that of OCT2 in humans. Targeted disruption of Oct1 in rodents reduced liver accumulation of prototypical transport substrates such as tetraethylammonium (TEA) and the neurotoxin 1-methyl-4-phenylpyridinium (MPP).^{29,30}

Organic cation transporter 2 (OCT2). Unlike OCT1, OCT2 presents a more restricted expression pattern. OCT2 is highest on the basolateral membrane (blood facing) along S2 and S3 segments of proximal tubular cells.^{10,29,30} OCT2 plays a key role in facilitating the translocation of cationic compounds from systemic circulation into renal proximal tubular cells and working in concert with efflux transporters (e.g., primarily MATE1 and MATE2-K) to mediate excretion of substrates into the urine. Although OCTs share many overlapping substrates, OCT2 also efficiently transports monoamine neurotransmitters, as evidenced by moderate expression across different types of neuronal cells.^{8,27} Due to its high expression in proximal tubular cells, OCT2 has been implicated in mediating drug-drug interactions and it is therefore recommended for evaluation during development by the FDA.²⁰

Organic cation transporter 3 (OCT3). In contrast to the wealth of knowledge accumulated in recent years on OCT1 and OCT2, relatively little is known about the third member of the *SLC22A* family, OCT3. OCT3 exhibits a promiscuous expression pattern in most major organs and peripheral tissues, with highest expression in the heart, placenta and skeletal muscles.^{10,31,32} Although OCT3 is generally not considered a significant

contributor to drug-drug interactions, recent studies have highlighted OCT3 as an important transporter in the heart and cardiovascular disease,³³ and carriers of polymorphic variants in OCT3 (rs2048327, rs1810126, rs1810126 and rs3088442) are at reduced risk of coronary artery disease development.³⁴⁻³⁶ While OCT3 is present in most tissues, the genetic deletion of Oct3 in mice does not affect viability and fertility, and does not lead to any overt and/or abnormal pathology.³⁷ Oct3 deficiency in mice is associated with diminished accumulation of prototypical substrates such as metformin and MPP in homogenized hearts.^{37,38}

Organic cation/carnitine transporter 1 and 2 (OCTN1 and OCTN2). In comparison with OCT1-3, OCTN1 and OCTN2 can transport substrates either dependently or independently of Na⁺. Driven by a proton gradient, OCTNs can recognize zwitterions as well as organic cations and even certain anions, and share a high degree of membrane topology.^{39,40} OCTN1 is the only known transporter of ergothioneine, whereas OCTN2 is believed to be an essential carnitine transporter. Both OCTN1 and OCTN2 are widely expressed in human tissues. Localization of OCTNs in proximal tubular cells is restricted to the apical membrane (urine side),^{8,10} where it may function in the reabsorption of essential cations from the urine. OCTNs are also expressed on the apical membrane of enterocytes, and OCTN2 is expressed in skeletal muscles, heart, lung and eye, where it may be involved in regulating L-carnitine uptake and tissue homeostasis.⁴¹⁻⁴³ Genetic deletion of Octn1 provides viable offspring,⁴⁴ whereas Octn2 deletion displays embryonic lethality without L-carnitine supplementation.⁴⁵ The clinical relevance of OCTN1- and

OCTN2-mediated drug-drug interactions remains largely unstudied but is likely limited due to the narrow substrate specificity of these transporters.

Multidrug and extrusion protein 1 and 2-K (MATE1 and MATE2-K). MATE1 and MATE2-K are poly-specific efflux transporters that translocate organic cations, and certain anions, in a Na⁺ independent and pH-dependent manner.^{7,8} MATE1 is apically expressed on the cannicular and brush-border membrane of hepatocytes as well as on proximal tubular cells, and mediates the efflux of organic cations into the bile and urine, respectively.⁴⁶ MATE2-K, a splice variant, is restricted to kidneys in humans and the redundant expression of this additional antiporter on the luminal membrane of proximal tubules in humans suggests that MATEs evolutionary adapted to mediate the clearance of endogenous toxins or xenobiotics.¹⁴ The tissue distribution of Mate1 in rodents is generally consistent with that observed for MATE1 in humans, with the exception of MATE2-K being absent in the kidney of mice and rats, while Mate1 is additionally absent in the liver of rats.^{13,47}

1.4 Dose-limiting toxicities associated with chemotherapeutic agents

1.4.1 Nephrotoxicity

Cisplatin is a standard of care drug for the treatment of various malignant solid tumors in both pediatric and adult populations.⁴⁸⁻⁵¹ The clinical utility of cisplatin is limited by the onset of debilitating toxicities, including nephrotoxicity,⁵²⁻⁵⁴ which can cause severe renal impairment. Approximately one-third of patients receiving cisplatin develop acute

kidney injury (AKI) during the course of treatment, and in severe cases, patients display a permanent incomplete recovery of renal function despite discontinuation of treatment. More than 50 percent of the drug is excreted into the urine within the first 24 hours,^{55,56} and renal cortical concentrations of platinum are orders of magnitude greater than that observed in the systemic circulation and compared to other organs,⁵⁷ suggesting a key renal-mediated mechanism of accumulation. The pathophysiology of cisplatin-induced nephrotoxicity involves renal tubular apoptosis and necrosis, particularly in the S3 segment of proximal tubular cells and of the distal nephron, manifesting clinically as imbalances in salt and essential nutrients, tubular acidosis and a reduced glomerular filtration rate (GFR).⁵⁸⁻⁶⁰ Although proper hydration of patients and prophylactic treatment with diuretics can manage the symptoms of nephrotoxicity, the prevalence of this side effect remains high and greatly diminishes quality of life.^{59,61}

Renal concentrations of platinum are highest in the S2 and S3 segment of proximal tubular cells,^{52,62} highlighting a key cell-specific and transporter-mediated process. In rodents, the deficiency of both Oct1 and Oct2 conferred protection against cisplatin-induced nephrotoxicity⁶³ while the OCT2 808G>T (rs316019) genetic variant in humans was associated with reduced changes in serum creatinine, a hallmark of acute kidney injury, after one cycle of cisplatin treatment as compared to baseline and to patients lacking this variant.⁶⁴⁻⁶⁶ Furthermore, sexually dimorphic expression of Oct2 in proximal tubular cells of male rodents correlated with a greater propensity and susceptibility to cisplatin-mediated tubular injury compared to female rodents.^{10,67} Cisplatin is also a transported substrate of MATE1, and rodent deficiency for Mate1 was associated with diminished urinary

excretion of total platinum, potentiating nephrotoxicity.⁶⁸ The pharmacologic targeting of these transport mechanisms using OCT2 and MATE1 inhibitors protected or exacerbated nephrotoxicity, respectively.^{69–71} The translational significance of OCT2-dependent intervention strategies, in which cisplatin is administered after an OCT2 inhibitor to restrict access of the chemotherapy into tubular cells, remains somewhat disappointing. This may be explained by the partial reduction in biomarkers of cisplatin-induced nephrotoxicity (e.g., serum creatinine and blood urea nitrogen), the use of non-specific OCT2 inhibitors lacking potency at clinically-achievable concentrations, the incomplete recovery of pathological damage in the kidneys that occurs despite the OCT2 inhibition,⁶³ and/or the failure of the intervention strategy to modulate uptake mechanisms that mediate cisplatin-induced AKI in an OCT2-independent manner. Regarding the latter, it should be pointed out that several reports have suggested the existence of a negatively charged N-acetylcysteine S-conjugate (NAC-1) derived from cisplatin that can act as an intermediate, highly reactive nephrotoxic thiol. NAC-1 is generated by cisplatin conjugation with glutathione and cysteine before accumulation in proximal tubular cells.⁷² NAC-1 was recently found to be a transported substrate of the organic anion transporters OAT1 [*SLC22A6*] and OAT3 [*SLC22A8*], which are also expressed on the basolateral membrane of proximal tubules, and can contribute to cisplatin nephrotoxicity independently of Oct2 in a signaling pathway that is upstream of p53.⁷³ However, similar to Oct2-deficient rodents, genetic deficiency of Oat1 and Oat3 or pharmacological inhibition with probenecid only offers partial reduction in serum markers and pathological damage.⁷⁴ This study further demonstrated that concomitant administration of the Bcr-Abl tyrosine kinase

inhibitor nilotinib, which can simultaneously inhibit both Oct2-mediated uptake of cisplatin⁷⁵ and Oat1/Oat3-mediated uptake of NAC-1 through non-competitive mechanisms, afforded complete protection against cisplatin-induced proximal tubular injury *in vivo*.⁷⁴

Compared to cisplatin, the related drug oxaliplatin lacks significant nephrotoxic activity, despite being a transported substrate of the rodent Oct2 and Mate1, and human OCT2, MATE1 and MATE2-K.⁷⁶ While Oct2 transports both platinum agents with similar kinetics, the extent of total platinum accumulation in the kidney was far greater in cisplatin-treated animals compared to oxaliplatin.⁷⁷ The differences observed in the accumulation and elimination of these platinum agents is potentially related to differences in transport kinetics for Mate1 in mice, and MATE1 and MATE2-K in humans,⁷⁷ suggesting higher luminal efflux of oxaliplatin into the urine compared to cisplatin. However, this explanation of differential tubular secretion rates for cisplatin and oxaliplatin as a driving discriminatory mechanism for their different nephrotoxic properties is not completely satisfactory, and is inconsistent with comparative *in vivo* studies in mice indicating that the renal excretion of both agents is strongly dependent on Mate1. It also largely ignores intrinsic differences in renal metabolic activation pathways that results in the formation of potent nephrotoxins in the case of cisplatin but not oxaliplatin, and fails to recognize the differing contribution of other potentially critical renal *ABC* efflux transporters in the process, such as MRP2 and MRP4.

Similar to oxaliplatin, the novel platinum derivative, phenanthriplatin, is a high affinity substrate for both OCT2 and MATE1/2-K, and it has been argued that these are

kinetically favorable attributes that would be efficacious in the treatment of OCT-expressing tumors, while efficient MATE-mediated efflux may decrease the renal tubular residence time and thereby prevent the debilitating toxicity profiles observed in the kidneys following cisplatin treatment.⁷⁸ Similar observations have been documented with the alkylating agent, ifosfamide, which is associated uniquely with nephrotoxic activity and the development of renal Fanconi syndrome.⁷⁹ Bioactivation of ifosfamide mediated by OCT2 transport into proximal tubular cells has been proposed as a differentiating mechanism between ifosfamide on the one hand and cyclophosphamide's lack of nephrotoxic activity on the other.⁸⁰ Although the nephrotoxic properties of these chemotherapeutic agents is predominantly attributed to originate with basolateral OCT2-mediated uptake and subsequent apical MATE1- and MATE2-K-mediated efflux, it should be pointed out that significant differences in transport kinetics and transporter-mediated interactions involving MATEs could potentially contribute to lower or higher incidences of nephrotoxicity in patients, depending on relative interindividual differences in functional expression of these proteins. While interindividual differences in expression may predict susceptibility to drug-induced organ damage in tissues with a clear functional role of uptake transporters, it is important to note that these expression differences also contribute as mechanisms of chemoresistance in tumor cells. Consistent with this notion, several studies have demonstrated that the down-regulation of OCT6 in lung and colon cancer tissues is associated with cellular resistance to cisplatin and oxaliplatin.^{81,82} Thus, intervention strategies aimed at targeting uptake transporters to ameliorate drug-induced

toxicity must be evaluated for antagonized therapeutic efficacy due to unintended inhibition of transport mechanisms regulating entry into tumor cells.

1.4.2 Neurotoxicity

In addition to their varying degrees to which cisplatin and oxaliplatin induce AKI, platinum agents can also cause severe and debilitating, dose-limiting peripheral neurotoxicity, and this has resulted in extensive preventative efforts as evidenced by the increasing emergence of large numbers of neuroprotective clinical trials.⁸³ Clinical manifestation of neurotoxicity occurs immediately after infusion and is characterized by paresthesia, ataxia, and dysesthesia in the extremities of the body.^{84,85} Within the nervous system, platinum agents are unable to penetrate the blood-brain barrier, but rather preferentially accumulate in peripheral sensory neurons present along dorsal root ganglia (DRG) of the spinal cord.⁸⁶ In peripheral sensory neurons, induction of nuclear and mitochondrial DNA damage, disruption of ion channels while glial activation of astrocytes and microglial cells are mechanisms of pharmacological interest in preventing mechanical and thermal neuropathic pain.⁸⁷ At higher cumulative doses, incomplete recovery and permanent dysfunction of sensory neurons represents a major clinical problem.⁸⁶

Somewhat unexpectedly, several studies have demonstrated that OCT2 transcripts are detectable in rodent and human DRG samples, suggesting a carrier-mediated mechanism of accumulation into these structures.⁸⁸ Consistently, the genetic deletion of Oct2 in mice prevented the onset of acute oxaliplatin-induced thermal and mechanical allodynia, while this phenotypic preservation occurred in the absence of detectable changes

across structurally similar and putative *SLC* or *ABC* transporters of relevance to oxaliplatin.⁸⁸ This protection can also be recapitulated in wild-type animals using pretreatment with dasatinib, a pharmacological SRC-family kinase inhibitor, which inhibits both mouse and human OCT2 through a noncompetitive mechanism that regulates the post-translational modification of OCT2 through tyrosine phosphorylation by the kinase YES1.⁸⁹ Interestingly, other reports have suggested oxaliplatin is also a transported substrate of rat Octn1 and the use of genetic targeting constructs or pharmacologic inhibition with ergothioneine, an Octn1-specific substrate, protected rats from chronic forms of oxaliplatin neurotoxicity.^{90–92} However, due to the reported expression of Octn1 on the mitochondrial membrane and intrinsic antioxidant activity of ergothioneine, the observed neuroprotection may be independent of a direct contribution to the transmembrane transport of oxaliplatin into target cells. This hypothesis would be consistent with data suggesting that ergothioneine can reduce cellular concentrations of oxaliplatin in Octn1-deficient DRG neurons of mice.⁴⁴ Furthermore, it is unknown whether ergothioneine competes or exhibit inhibitory activity against putative transporters of relevance to oxaliplatin in neurons. The discrepant findings reported for the involvement of transporters involved in oxaliplatin-induced peripheral neurotoxicity in rodents may also be attributed to differences in transport kinetics or expression between the two species, and further studies are required to delineate the translational contribution of human OCT2, OCTN1, and other *SLC* family members to this side effect.

1.4.3 Ototoxicity

Cisplatin is unique among platinum chemotherapeutics in its ability to frequently induce severe hearing-loss (ototoxicity), where the incidence ranges from 20 to 80% in pediatric patients, and this side effect may permanently affect early speech and ultimately hamper social development.^{93,94} Excessive generation of reactive oxygen species (ROS) increases in cochlear inflammatory responses and induction of apoptosis mediated by platinum-DNA adduct formation have been proposed as mechanisms of cisplatin ototoxicity.^{95,96} However, antioxidant or anti-inflammatory drugs used prophylactically do not prevent permanent damage, and only offer moderate protection in the management of cisplatin-induced cochlear injury.^{94,95} It is possible that the initial accumulation of cisplatin into the cochlea cells represents a key trigger for the following pathophysiological changes in cisplatin-induced hearing loss. Indeed, both mouse Oct2 and human OCT2 are expressed in the organ of corti and stria vascularis of the cochlea, and genetic deficiency or pharmacological targeting of Oct2 with cimetidine protected rodents against toxicity.⁷¹ A retrospective and exploratory analysis of 11 SNPs in the human *SLC22A2* gene identified a genetic variant, c.808G>T; Ser270Ala (rs316019), that conferred significant protection against cisplatin-induced ototoxicity in a pediatric cohort.⁹⁷ *In vitro* insertion of the 808G>T allele into OCT2, located within the transmembrane domain,⁹⁸ reduced transport kinetics (e.g., V_m and K_m) of OCT2 substrates (e.g., MPP and dopamine)⁹⁸⁻¹⁰⁰ and a moderate increase in serum creatinine,¹⁰¹ supporting the notion that the observed human variant functionally reduces transport affinity of cisplatin and cellular injury. Of note, pantoprazole, an inhibitor of OCT2,¹⁰² did not ameliorate ototoxicity or nephrotoxicity in a pediatric cohort of osteosarcoma patients treated with cisplatin.¹⁰³ While prediction of

the applied dosing schedules for pantoprazole-mediated OCT2 inhibition was performed using pharmacokinetic modeling and simulations, these strategies were not adequately validated and ultimately lack rationally designed preclinical and clinical studies to document the local (cochlea or kidney) and systemic (blood) changes in endogenous substrates of OCT2 as a pharmacodynamic biomarker of OCT2 function. While the reported intervention study with pantoprazole was negative, caution is warranted against the conclusion that the proposed OCT2 inhibition concept is intrinsically flawed, and different results could have been obtained with a more potent inhibitor given at a dose and schedule known to affect cochlear biomarkers of OCT2 function.

In connection with MATE1 function, it is worth pointing out that, in an adult cohort of patients with head and neck squamous cell carcinoma (HNSCC) receiving cisplatin-containing therapy, the presence of one or two copies of the *SLC47A1* variant (rs2289669) significantly predisposed patients to cisplatin-induced ototoxicity.¹⁰⁴ However, it is uncertain whether this variant produces a gain or loss of function phenotype. Pharmacogenomic analysis of this same variant in patients with type 2 diabetes receiving metformin indicated a reduced function phenotype, as demonstrated by an increase in glucose lowering, a marker of pharmacodynamic response to metformin.¹⁰⁵ On the other hand, the protective effects observed among HNSCC patients suggested a gain of function since MATE1-mediated cisplatin efflux and treatment response was unaffected in the HNSCC cohort.¹⁰⁴ The unique bi-directional antiporter characteristics of MATE1, compared to other *SLCs*, suggest that the function of this variant may be dependent on tissue localization and cellular polarity of MATE1-expressing cells.

1.5 Role of transporters in drug-induced cardiotoxicity

In the pre-cloning era, it was widely believed that the predominant mechanism of accumulation of small-molecule xenobiotics is by the direct movement of unionized drug through the phospholipid bilayer (“passive diffusion”).^{106,107} However, the saturable cellular uptake of many anticancer drugs in cell-based models and the cationic properties of many cardiotoxic anticancer drugs, including anthracyclines and TKIs, at physiological pH support instead the existence of a solute carrier (SLC)-mediated mechanism.¹⁰⁸ Transport proteins in this SLC class are vital to the growth and health of all living organisms and evolved to ensure the regulated delivery of many substrates, both endogenous and natural products. Indeed, many SLCs are now known to provide essential roles involved in various physiological processes that depend on the uptake of amino acids, neurotransmitters, organic cations and anions, and vitamins. SLCs can also mediate the uptake of certain xenobiotics that structurally resemble essential nutrients by hitchhiking on the same transporters,¹⁰⁹ thereby playing an unintended role in response to such therapeutics. The localization of SLCs varies depending on their specific subfamilies, thus resulting in functional differences in transport properties.¹⁶ The SLC superfamily includes over 400 genes in the human genome, and is currently organized into 57 families that are highly diverse in structure, function, and localization.¹¹⁰ SLCs regulate the movement of substrates across the membrane by the use of predominantly facilitative transport or secondary active transport. Because of this, SLC transporters depend on an electrochemical gradient to expedite the drive of substrate compounds

through cell membranes or ion gradients created by ATP-pumps in order to facilitate molecules against the concentration gradient.¹¹⁰

While the SLC superfamily is composed of transporters that are mainly involved in the influx of molecules into a cell, transporters of the ATP-binding cassette (ABC) superfamily consist primarily of transporters that are involved in the efflux molecules out of a cell. The human genome contains 49 ABC genes that are divided into seven subfamilies based on the amino acid sequences, and the gene products are widely expressed in multiple organs of relevance to the absorption and disposition of drugs, including the liver, kidney, intestine, blood-brain barrier, blood-testis barrier, and placenta.¹¹⁰ Examples of ABC transporters that are expressed at high levels in cardiomyocytes and cardiac capillary endothelial cells of the mammalian heart include ABCB1 (P-glycoprotein; P-gp) and ABCG2 (BCRP), which also contribute to the resistance of cancer cells to many chemotherapeutic drugs.¹¹¹

1.5.1 Cardiac expression of xenobiotic transporters

Several studies have confirmed the expression of certain SLCs in cardiomyocytes that are known to transport a broad range of clinically-relevant xenobiotics.^{111,112}

Although still largely unexplored, one strategy that could potentially offer cardioprotection is to intentionally inhibit this transport process with pharmaceuticals in order to restrict access of cardiotoxic drugs to the site of injury, and thereby prevent or diminish downstream pathways that result in clinical manifestations of cardiotoxicity (**Figure 1**). Among the class of SLCs, the importance of organic cation transporters

(OCTs) as mediators of cardiomyocyte uptake transporters has been reasonably well established, and this collective work has demonstrated particularly high cardiac expression of the carnitine transporter OCTN2,¹¹³ as well as (in decreasing order) the related transporters OCT3, OCTN1, OCT1, and MATE1.¹¹⁴ It is worth pointing out that MATE1 acts as an efflux transporter in cardiomyocytes.¹¹⁵ The role of organic anion transporting polypeptides (OATPs) in drug transport has historically focused mainly on the liver as a key organ of elimination that expresses high levels of OATP1B1 and OATP1B3, although recent studies have indicated that some of the related, but more broadly expressed transporters in this class, such as OATP2B1, OATP3A1, and OATP4A1, are also detectable in the mammalian heart. In contrast to SLCs, ABC transporters use energy from ATP hydrolysis and several members of this family are expressed in the heart.

1.5.2 Pharmacological role of xenobiotic transporters in cardiomyocytes

In the late 1990s, the molecular entities responsible for the uptake transport of cationic xenobiotics were identified as the polyspecific transporters OCT1, OCT2, and OCT3. These transporters have a relatively broad substrate profile that is at least partially overlapping, but their tissue expression profile is diverse such that OCT1 is primarily expressed in the liver and OCT2 in the kidney, while OCT3 is generally regarded as a less important contributor to the disposition of xenobiotic substrates. Due to the dominance of OCT1 and OCT2 in organs of elimination, OCT3 has traditionally received relatively scant attention. More recently, however, reduced oral bioavailability and

attenuated pharmacological response to certain substrate drugs such as metformin have been detected in OCT3-deficient mice, suggesting that OCT3 may significantly contribute to the distribution of certain substrate drugs to OCT3-expressing tissues.¹¹⁶ Indeed, studies involving OCT3-deficient mice have highlighted that OCT3 is an important transporter in the heart,¹¹⁶ where it regulates the cardiac uptake of xenobiotic substrates, including tetraethylammonium, dehydrocorydaline, and metformin^{114,116,117}. Using the same mouse model, it was recently reported that the ability of doxorubicin to accumulate in the heart is dependent on Oct3 and that pharmacological inhibition of OCT3 by concomitant administration of nilotinib, a Bcr-Abl tyrosine kinase inhibitor, prevented doxorubicin-induced cardiac injury without affecting its antitumor efficacy.¹¹⁸ Gene expression analyses have revealed the absence of OCT3 alterations at the transcript level in cardiac samples obtained from both patients and mice treated with doxorubicin. This suggests that doxorubicin-induced cardiac injury in cancer patients may be a direct consequence of inherent expression differences in OCT3 at baseline and provides justification for genotyping of OCT3 status in order to predict a patient's susceptibility to cardiac injury. Such strategy is supported by the recent demonstration that certain polymorphic variants in the OCT3 gene (*SLC22A3*) contribute to the incidence and severity of coronary artery disease,¹¹⁹ and that these variants are associated with reduced transport function.¹²⁰ In this context, it is worth noting that OCT3 functions as an efficient transporter of several other cardiotoxic anticancer drugs, including cisplatin, oxaliplatin, melphalan, and vincristine, and that known OCT2 substrates, such as erlotinib, ibrutinib, ifosfamide, mitoxantrone, and vandetanib¹²¹ are possibly also

transported by OCT3, given the overlapping substrate specificity of these two transporters. These prior observations provide support for the possibility that the cardiotoxic potential of some or all of these agents is similarly dependent on OCT3, and this warrants further investigation.

Although the cardiac effects of HMG-CoA inhibitors (statins) remain subject to controversial discussion, the mechanism of their uptake into the human heart has been investigated in recent years, and this work may shed light on transport mechanisms of certain cardiotoxic anticancer drugs. These studies have demonstrated that OATP2B1 is a high-affinity uptake transporter for some, but not all, statins that is expressed in the vascular endothelium of the human heart,¹²² suggesting an involvement in the cardiac uptake of substrate drugs. Although the interaction of OATP2B1 with anticancer drugs has not been extensively explored, some transported substrates have been identified, including erlotinib,¹²³ and this knowledge provides a potentially fruitful avenue for future investigation. Since OATP2B1 has only a single mouse ortholog with high sequence homology and a similar tissue expression profile compared with the human transporter,¹²⁴ the use of recently developed single-gene knockout models can provide particularly useful and translationally-relevant information regarding the biological role of this transporter in the heart in response to a challenge with anticancer drugs.¹²⁵

In contrast to OATP2B1, the contribution of the liver-specific transporters OATP1B1 and OATP1B3 to the hepatic transport and elimination of anticancer drugs has been extensively evaluated, both *in vitro* and *in vivo*. This work has revealed that hepatic OATP transporters can affect the pharmacokinetic properties of a remarkably broad range

of substrates that include charged organic anions (e.g., methotrexate), charged organic cations (e.g., imatinib), polar zwitterions (e.g., fexofenadine), and uncharged hydrophobic agents (e.g., taxanes). Although OATP1B1 and OATP1B3 are not expressed in the heart, it has been argued that deficiency of these transporters in the liver results in impaired elimination, and that this process may result in an altered distribution to tissues such as the heart. Evaluating this hypothesis for doxorubicin, investigators observed that the absence of OATP1B-type transporters in mice resulted in modestly reduced heart-to-plasma concentration ratios but without markedly altered doxorubicin levels in the heart.¹²⁶ Although these findings suggest at best a minor role of hepatic OATPs proteins in the cardiac disposition of doxorubicin, this conclusion should not be extrapolated to other substrates that are potentially more susceptible to modulation of this elimination pathway.

As outlined previously, ABC transporters such as ABCB1 (P-gp), ABCC1 (MRP1), and ABCG2 (BCRP) generally act to extrude drugs or toxic xenobiotic compounds from cells or tissues, and several of these, in particular ABCB1, have been specifically studied in relation to cardiotoxicity.^{127,128} This is expected since a majority of cardiotoxic anticancer drugs are sensitive to transport by ABCB1, including cytotoxic chemotherapeutics such as the anthracyclines doxorubicin and idarubicin as well as TKIs such as imatinib, and this mechanism contributes potentially to both resistance of cancer cells and protection of healthy cells. Preclinical studies have demonstrated that the retention of both doxorubicin and its main metabolite doxorubicinol in the hearts of ABCB1^{-/-} mice is substantially prolonged although plasma levels were increased by only

1.2-fold compared with wild-type mice.¹²⁹ While these data suggest that pharmacological inhibition of endogenous ABCB1 enhances the risk of doxorubicin-induced cardiotoxicity (**Figure 1C**), a hypothesis that has been verified in multiple animal models,^{130,131} clinical evidence of this thesis remains controversial.¹³² It is also worth pointing out that many cancer drugs are very efficiently transported by ABCB1, yet still cause cardiotoxicity to varying degrees in patients, and this observation seems inconsistent with ABCB1 exerting a critical protective function in the heart against insults with cardiotoxic therapeutics. Loss of ABCC1 (MRP1) function has been found to have detrimental effects on cardiac function after doxorubicin treatment. One study showed that *Abcc1*^{-/-} mice receiving chronic doxorubicin treatment demonstrated significantly more severe left ventricle dysfunction as well as decreases in left ventricular fractional shortening (LVFS) and left ventricular ejection fraction (LVEF) as compared with wild-type mice.¹³³ Furthermore, a number of genetic polymorphisms in the ABCC1 gene (e.g., rs3743527 and rs246221) is associated with the development of anthracycline-induced cardiotoxicity.¹³⁴ However, subsequent studies have demonstrated that increased sensitivity of *Abcc1*-deficient mice to doxorubicin-induced cardiotoxicity is unrelated to altered anthracycline transport but possibly linked with a role of ABCC1 in regulating extracellular redox states.¹³⁵ In this scenario, loss of ABCC1-mediated efflux diminishes the ability to scavenge ROS in the extracellular environment and facilitates in causing anthracycline-induced cardiotoxicity (**Figure 1C**).

In addition to SLCs and ABC transporters directly contributing to treatment-related cardiotoxicity via direct transport of anticancer drugs, effects of these drugs

themselves on the function of transporters playing a role in the regulation of cardiac muscle cell homeostasis by supplying nutrients and how such process could result in impaired cardiac function remain largely unexplored. Such drug-transporter interactions would be particularly relevant for transporters with a role in myocardial contractility, glucose transport, amino acid transport, vitamin transport, and regulation of the human ether-a-go-go (hERG) channel.¹³⁶ Glucose transport in the heart is regulated by the transporters GLUT1 (SLC2A1) and GLUT4 (SLC2A4), where GLUT1 facilitates the basal cardiac glucose uptake and GLUT4 mediates contraction-mediated movement of glucose into peripheral organs, including the heart.¹³⁷ The connection of these glucose transporters is derived from the notion that treatment with many anticancer drugs, including dasatinib, imatinib, sorafenib, and sunitinib, is associated with significant declines in blood glucose levels,¹³⁸ and that the hypoglycemic effect of these drugs, as well as ibrutinib,¹³⁹ has been confirmed in many subsequent studies. Recent studies have verified that the mechanistic basis of this clinical observation is consistent with the interaction of these TKIs with amino acid residues at the glucose binding site of GLUT1 to inhibit glucose uptake,¹⁴⁰ and that these effects are either reversible (e.g., gefitinib, imatinib, and pazopanib) or even irreversible, (e.g., nilotinib). The ability of TKIs to alter glycemia and cause cardiotoxic events may be of particular importance in the diabetic heart. Recent studies in this area have suggested that the cardiotoxic TKI crizotinib reduced blood glucose in diabetic rats independently of insulin and glucagon by a mechanism that involved changes in regulators of cardiac metabolism, including

GLUT4.¹⁴¹ Further study is warranted to definitively establish the contribution of GLUT1/GLUT4-mediated mechanisms to the cardiotoxicity induced by these TKIs.

The hERG potassium channel conducts the movement of I_{Kr} , which is essential for the repolarization of cardiac action potentials. A slight blockage of the hERG channel could generate a beneficial class III arrhythmia effect while a decrease in hERG currents as a result of genetic or adverse drug effects may lead to lengthening the QT interval or increase risk of life-threatening arrhythmias.¹⁴² While most new investigational agents undergo extensive cardiac safety studies in advance of clinical trials, including the ability to modulate potassium channels, it should be pointed out that the extent of hERG block induced by drugs is highly sensitive to cardiac expression of uptake and efflux transporters that jointly regulate drug levels in the heart *in vivo*. While this seems intuitively obvious, this issue is rarely considered in experimental model systems used to verify the cardiac safety of xenobiotics. Specific examples of this concept include the demonstration that overexpression of OCTN1 in human cardiomyocytes intensifies hERG block induced by the OCTN1 substrate quinidine, while overexpression of the efflux transporter ABCB1 attenuates KCNA5 channel block by erythromycin (an ABCB1 substrate).¹⁴³ These studies provide further support for the idea that modifying cardiac drug concentrations, for example through unintended concurrent treatment with inhibitors of critical influx and efflux transporters could modulate the effects of blocking ion channels in patients, and potentially cause serious arrhythmias such as *Torsade de pointes*.¹⁴⁴

1.5.3 SLC-based intervention strategies to prevent cardiotoxicity

The demonstration that certain SLCs play a pivotal role in a clinically relevant, potentially life-threatening cardiotoxicity, by directly regulating accumulation and retention of anticancer drugs, warrants the further exploratory use of specific transport inhibitors in treatment regimens in patients with cancer. Specifically, it can be envisaged that translational interventions targeting known uptake transport mechanisms could be strategically exploited as a preventative strategy and may offer benefits over alternative, previously proposed approaches that target one of many pleiotropic signaling pathways that may also influence apoptotic pathways in tumor cells. The success of such a strategy depends at least in part on optimizing local exposure to cardiomyocytes by applying the right dose and schedule of SLC inhibitors. Likewise, utilization of potent transporter inhibitor might have some off-target effect in terms of reducing drug absorption, distribution or elimination. Thus, the use of transporter inhibitor should only be considered when drug clearance (via organs such as liver and kidney) and antitumor efficacy of chemotherapeutic agents are not compromised. Such agents would ideally have high potency, high specificity, low drug–drug interaction potential, and favorable pharmaceutical properties. The incentive for such an approach is underscored by the notion that a leading cause of drug attrition during pharmaceutical development is cardiotoxicity and that proper exploration of this SLC inhibitor concept can ultimately result in many preventable patient deaths. In addition to pharmacological inhibition of transporter, administration of siRNA therapeutics to downregulate tissue-specific influx transporters that are known to contribute cardiac injury might be taken into consideration

as a future treatment strategy in order to minimize chemotherapy-induced cardiotoxicity. An alternative approach could be the induction of efflux transporter such as ABCB1 by downregulating heat-shock factor 1 (HSF-1) in advance of cardiotoxic chemotherapy to increase cardiac ABCB1 activity and ameliorate doxorubicin-induced cardiotoxicity. For example, it has been demonstrated that ablation of HSF-1 in mice increases the expression of ABCB1 in the heart, which significantly reduced doxorubicin-induced heart failure and diminished left ventricular dysfunction.¹⁴⁵ In addition, a recent study has demonstrated that genetic manipulation can cause a directional change of ABCB1 from an efflux into influx transporter, dependent on multiple mutations in a pair of transmembrane helices.¹⁴⁶ The implications of this finding for therapy-related cardiotoxicity are presently unclear.

One particularly useful model to identify and validate cardioprotective strategies is through the use of human-induced pluripotent stem cell-derived cardiomyocytes (hiPSC-CMs),¹⁴⁷ which retain SLC and ABC expression signatures that resemble those observed in human heart specimens. This model also allows hiPSC-CMs to be generated from patients with inherited heart disease to predict the effectiveness of selected interventions in patients of diverse genetic backgrounds. Models based on hiPSC-CMs are also amenable to genetic manipulation and high throughput screening (HTS) to allow rapid identification of novel transporter modulators and select hit leads for further evaluation.¹⁴⁸ Alternatively, *ex vivo* evaluation of rodent cardiomyocytes directly obtained from animals of a desired genetic constitution (e.g., deletion of a specific SLC with or without transgenic expression of human transporters) has proven useful in

demonstrating transporter-dependence of particular drug phenotypes in advance of *in vivo* testing.¹⁴⁹ These procedures allow adverse effects of drugs on the heart to be detected by measuring drug uptake, mechanical performance, energetics, mitochondrial function, glucose uptake, and/or cell viability, depending on the specific drug or drug combinations being tested.¹⁵⁰ In advance of clinical testing, selection of a proper, predictive nonclinical *in vivo* model and an optimal technique for imaging-based cardiac assessment is required to arrive at a strategy that could be clinically beneficial. In this context, cardiac magnetic resonance imaging (cMRI) techniques are particularly useful in measuring and analyzing drug-induced cardiotoxicity as they capture early myocardial changes, worsening cardiac function, left ventricular (LV) volume, and LVEF. Besides cMRI, positron emission tomography (PET) is often applied and still considered as the gold standard to measure myocardial metabolism and inflammation due to its high spatial and temporal resolution. PET imaging provides changes in myocardial glucose metabolism that can be detected early during the treatment of cancer chemotherapeutics.¹⁵¹ Moreover, PET tracers are beneficial in determining the earliest modifications within the myocardium because it provides information on alterations in mitochondrial membranes and subsequent production of ROS.¹⁵² Hence, PET imaging is advantageous to predict the incidence of cardiotoxicity and optimize dose regimens accordingly. In terms of elucidating the underlying mechanisms of drugs that have the propensity to trigger cardiovascular toxicity or arrhythmogenicity, PET scanning could be an ideal approach in order to evaluate the distribution of radiolabeled cardiotoxic agents in several tissues.^{153,154} In contrast, more conventional approaches such as echocardiograms provide an inferior

spatial resolution that decreases accuracy, and these cannot be used to detect subclinical myocardial damage or small changes in LVEF.¹⁵⁵

In addition to imaging-based strategies, serum biomarkers have been developed to specifically assess the prognosis of cardiac injury as well as transporter-mediated drug-drug interactions. For example, cardiac troponins, such as troponin I (TnI) and troponin T (TnT), and brain-type natriuretic peptide (BNP) and its N-terminal fragment (NT-proBNP) are present in the cardiomyocytes and released into the bloodstream in the event of any disruption in sarcolemma or stress in the myocardial wall.¹⁵⁶ Recently developed analytical technology allows detection of such biomarkers at low levels to detect ventricular dysfunction.^{157,158} It should be noted that the degree of cardioprotection offered by genetic-deficiency in an animal model usually cannot be phenocopied by pharmacological inhibitors when given at empirical or typical therapeutic doses and schedules, even when such inhibitors can completely inhibit transport function in *in vitro* models. This suggests that optimization strategies are required to refine the regimen of potentially useful inhibitors in order to ensure optimal transport modulation at the site of injury. One approach that warrants further exploration focuses on the development and validation of endogenous and exogenous cardiac biomarkers that are specific to a particular transporter. Such a strategy can ultimately be employed to guide the identification of optimal doses and schedules of transport inhibitors that can be used in conjunction with cardiotoxic drugs in order to refine preventative treatments. Liposomal formulation could also be considered as an alternative strategy to minimize drug-induced cardiotoxicity, and such formulations commonly result in substantial alterations in

pharmacokinetic profiles. For example, liposomal formulations of anthracyclines result in high concentrations in the systemic circulation and extended half-life, while minimizing free anthracycline release into the blood. This larger size formulation also reduces the infiltration of anthracyclines into normal vasculature of the heart and simultaneously facilitates access into the more porous tumor endothelium.¹⁵⁹

1.5.4 Future Perspective

Drug-induced cardiotoxicity remains a significant clinical concern with many chemotherapeutic agents,¹⁶⁰ including approved drugs and investigational agents. Recent advances in understanding the role of SLCs and ABC transporters have shed light on new approaches to the development of cardioprotective strategies against both acute and chronic forms of toxicity. Current evidence suggests that transporters can potentially contribute in distinct ways to chemotherapy-induced cardiotoxicity – (a) when the drug is itself a transported substrate of a cardiac uptake transporter, (b) when the drug inhibits the transport of essential nutrients or vitamins in the heart, and (c) when drug-transporter interactions take place at a site of drug elimination that impacts exposure to the heart.

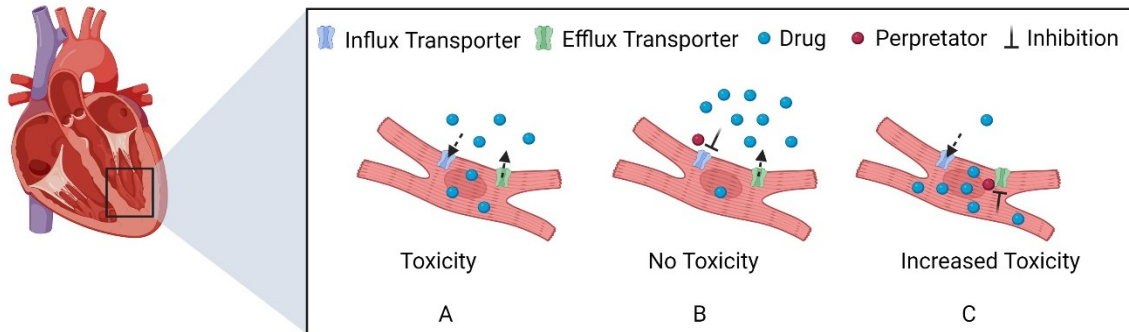
Substantial progress has been made in recent years toward an understanding of the functional significance of cardiac SLC and ABC transporter proteins, although various aspects in this area require more work before it becomes more useful clinically as a prospective tool for the development of drug-specific intervention strategies. For example, although cardiac expression profiles of a select set of SLC and ABC transporters have been documented,^{110,111} only few studies have provided compelling

direct evidence of a causal connection of drug-induced cardiotoxicity and a specific transporter. Indeed, the mechanism(s) by which most anticancer drugs accumulate into cardiomyocytes, which is often required as an initiating event in the development of cardiac injury, remains essentially unknown and unstudied. This is an unsustainable situation in need of an appropriate and cost-effective solution, especially in light of the recognition that membrane transporters in cardiomyocytes are predicted to contribute to drug-specific adverse cardiac events.¹⁶¹ The availability of hiPSC-CMs used in combination with transportome-wide gene knockout strategies enables new designs for preliminary, exploratory genetic studies using matched samples from healthy volunteers or patients with a predefined genotype of the desired signature. The implementation of such proof-of-principle approaches will unequivocally establish drug-transporter associations -or the lack thereof- in a statistically sound and unbiased fashion, and the information could also be obtained faster and provide opportunities to rapidly transition to functional *in vivo* validation studies. This type of research necessitates an interdisciplinary-team approach that includes expertise in experimental therapeutics and cancer pharmacology, transcriptomics, metabolomics, genome-based drug screens, pluripotent stem-cell-based cardiovascular disease modeling, predictive model organisms, and state-of-the-art cardiac imaging.

It is expected that, within the next decade, the importance of SLC and ABC transporters in the etiology of cardiac injury observed with classical anticancer drugs will be defined; however, this field of research is equally important for small-molecule targeted drugs and may be of importance for the rational development of new agents

designed to avoid cardiac complications observed with former generations of drugs. Similar to the discoveries of functional transporters that facilitate the cardiac uptake of anticancer drugs, it is expected that successful identification and development of predictive biomarkers in the near future will have a profound impact on attempts to further optimize cancer chemotherapeutic treatment. Such biomarker strategies will allow optimization of rationally-designed combinatorial treatments, and open new avenues to enhance the therapeutic window of chemotherapy-based regimens in a routine clinical setting. This in turn would have a significant impact on the morbidity and mortality associated with the usage of drugs in the treatment of diverse malignant diseases.

Figure 1: Proposed drug transport mechanisms in cardiomyocytes



Proposed drug transport mechanisms in cardiomyocytes. (A) Normal drug transport in cardiomyocytes by influx and efflux transporters. **(B)** No toxicity of therapeutic agents due to genetic (polymorphism) or pharmacologic (perpetrator) inhibition of influx transporters. **(C)** Drug-induced toxicity due to inhibition of efflux transporters leading to accumulating drugs in the cardiomyocytes.

Chapter 2. Influence of YES1 Kinase and Tyrosine Phosphorylation on the Activity of OCT1

****Disclaimer****

The following chapter contains excerpts from an article published and copyrighted by *Frontiers in Pharmacology*.¹⁶² Permission obtained from Frontiers.

2.1 Abstract

Organic cation transporter 1 (OCT1) is a transporter that regulates the hepatic uptake and subsequent elimination of diverse cationic compounds. Although OCT1 has been involved in drug-drug interactions and causes pharmacokinetic variability of many prescription drugs, details of the molecular mechanisms that regulate the activity of OCT1 remain incompletely understood. Based on an unbiased phospho-proteomics screen, we identified OCT1 as a tyrosine-phosphorylated transporter, and functional validation studies using genetic and pharmacological approaches revealed that OCT1 is highly sensitive to small molecules that target the protein kinase YES1, such as dasatinib. In addition, we found that dasatinib can inhibit hepatic OCT1 function in mice as evidenced from its ability to modulate levels of isobutyryl L-carnitine, a hepatic OCT1 biomarker identified from a targeted metabolomics analysis. These findings provide novel insight into the post-translational regulation of OCT1 and suggest that caution is

warranted with polypharmacy regimes involving the combined use of OCT1 substrates and kinase inhibitors that target YES1.

2.2 Introduction

In the last two decades, considerable advances have been made towards understanding the pharmacological role of cationic transporters belonging to the SLC22A subfamily. The advent of heterologous overexpression systems and genetically-engineered murine models has substantiated that the members of this subfamily facilitate the cellular uptake of a large number of structurally diverse endogenous metabolites and an increasingly large number of cationic xenobiotics. Organic cation transporter 1 (OCT1, *SLC22A1*) is the most abundant cationic transporter expressed on the sinusoidal membrane of hepatocytes,²¹ and is a rate-limiting step in the sodium-independent uptake and elimination of many xenobiotic substrates.^{5,25,163}

The *in vivo* contribution of OCT1 to the hepatic elimination of xenobiotics was first conclusively demonstrated for the prototypical organic cation, tetraethylammonium (TEA), in mice harboring a genetic deletion of OCT1.^{164,165} Many subsequent studies have focused on the biguanide analog metformin, a first-line medication for the treatment of type 2 diabetes. These studies have led to the recognition that the glucose-lowering effects of metformin are partially dependent on OCT1,^{166,167} and that OCT1 deficiency is associated with diminished metformin uptake in hepatocytes.^{25,168} More recently, OCT1 has also been identified as a critical determinant of the therapeutic efficacy of fenoterol,¹⁶⁹ morphine,¹⁷⁰ sumatriptan,¹⁷¹ thiamine,¹⁷² tramadol,¹⁷³ and tropisetron.¹⁷⁴

Due to its predominant role in determining the efficacy of many clinically-important drugs, multiple regulatory aspects of OCT1 have been widely studied. For example, polymorphic variants in OCT1¹⁷⁵ have been linked to the pharmacokinetics and glycemic response in diabetic patients receiving metformin,¹⁷⁶ and epigenetic mechanisms have been identified that can functionally modulate OCT1 and can profoundly affect therapeutic outcomes of substrate drugs.¹⁷⁷ Although post-translational modification via phosphorylation has been reported to influence the function of transporters,^{178,179} surprisingly, this has not been extensively studied as a regulatory mechanism of OCT1. We previously reported that the related transporter OCT2 (*SLC22A2*) is sensitive to inhibition by several FDA-approved tyrosine kinase inhibitors (TKIs) through a mechanism that involves YES1-mediated tyrosine phosphorylation.¹⁸⁰ Since OCT1 and OCT2 share structural features, a high degree of sequence homology, and have overlapping substrate recognition sites and conserved tyrosine motifs,^{11,181} we hypothesized that the activity of OCT1 is also dependent on kinase-mediated tyrosine phosphorylation. In the current study, we tested this hypothesis by employing phosphoproteomics screens, genetic strategies, pharmacological approaches, and metabolomics analyses in heterologous models overexpressing mouse or human OCT1, as well as OCT1-deficient mice.

2.3 Materials and Methods

Cell culture and reagents. Human embryonic kidney (HEK293) cells were obtained from the American Type Culture Collection (ATCC, Manassas, VA). HEK293

cells stably transfected with mouse OCT1 (mOCT1) or human OCT1 (hOCT1) were cultured in Dulbecco's Modified Eagle Media (DMEM) media supplemented with 10% fetal bovine serum (FBS) and grown at 37°C in a humidified incubator containing 5% CO₂. Radiolabeled [¹⁴C] TEA and [¹⁴C] metformin were obtained from American Radiochemicals (St. Louis, MO). Cellular uptake assays were performed 48 hours following transient transfection by Lipofectamine 3000 Transfection Reagent (Thermo Fisher Scientific, Waltham, MA). ON-TARGETplus Human YES1 siRNA was obtained from Dharmacon (Lafayette, CO). RNA extraction kits were obtained from Omega Bio-tek (Norcross, GA). Reference standards of decynium22, a positive control inhibitor, as well as the TKIs bosutinib, dasatinib, gilteritinib, ibrutinib, lapatinib, sunitinib, vandetanib, and CH6953755 were obtained from MedChemExpress (Monmouth Junction, NJ).

Cellular accumulation studies. Uptake assays were performed with radiolabeled TEA (2 μM) or metformin (5 μM) as described previously^{182,183} in the presence or absence of TKIs. The results were normalized to uptake values in cells stably transfected with an empty vector treated with vehicle alone. Prior to cellular accumulation experiments, cells were grown to 90% confluence on poly-lysine coated multi-well plates. For uptake studies, cells were rinsed with warm PBS and incubated in the presence of a vehicle or inhibitor, prepared in serum and phenol red-free DMEM media for 15 min. Subsequently, media was removed followed by the addition of radiolabeled TEA and metformin along with inhibitor, and cellular uptake was measured after a 15-min co-incubation period. Total radioactivity originating from TEA and metformin was

determined using liquid scintillation counting after lysing the cells with 1 N NaOH, a neutralizing step with 2 N HCl. A Pierce protein assay (Thermo Fisher Scientific, Columbus, OH) was used to normalize radioactivity readings to account for variation in cell number between samples.

Site-directed mutagenesis. The YES1 plasmid with pCMV6-Entry (C-terminal FLAG-tagged) backbone was obtained from Origene (Rockville, MD). Mutants in OCT1 and YES1 were generated using QuikChange XL Site-Directed Mutagenesis Kit (Agilent Technologies, Santa Clara, CA). Mutagenesis primers were designed using QuikChange Primer Design software and generated according to the manufacturer's instructions. Successful mutagenesis was confirmed by Sanger sequencing and constructs used for transient transfection experiments.

siRNA-mediated knockdown. HEK293 cells overexpressing hOCT1 were plated at a density of 1.25×10^5 per well in a 12-wells plate and incubated overnight at 37°C with 5% CO₂. The next day, cells were transfected with 50 nM siRNA targeting YES1, positive control siRNA, and negative control siRNA (Dharmacon, Lafayette, CO) according to manufacturer protocols. After 48 hours of exposure to siRNA, OCT1 function was evaluated with TEA or metformin as described above.

RT-qPCR. Total RNA was extracted from cells treated with siRNA by E.Z.N.A. Total RNA Kit I (Omega Bio-tek), and reverse transcribed to cDNA by qScript XLT cDNA SuperMix (QuantaBio, Beverly, MA). Primer sequences included YES1 (Hs00736972_m1) and human GAPDH (Hs02758991_g1), and quantitative RT-PCR was performed using TaqMan™ Fast Advanced Master Mix (Thermo Fisher Scientific,

Waltham, MA). The Ct values of the YES1 gene were subtracted from the mean of GAPDH (Δ Ct). All samples were analyzed in triplicate, and the mean value of Δ Ct was calculated.

Protein analysis. Cell treated with non-targeting siRNA and YES1 siRNA were lysed using sonication. Pierce Bicinchoninic Acid (BCA) Protein Assay Kit (Thermo Fisher Scientific, Waltham, MA) was used to determine protein concentrations. Next, an equal amount of protein was separated on a Bis-Tris 4-12% SDS-polyacrylamide gel with MOPS buffer according to the instructions from manufacturer (Life Technologies, Grand Island, NY) and transferred to PVDF membranes. Western blot analysis was performed using antibodies against YES1 (Product # 3201S), vinculin (Product # 13901S), and HRP-conjugated secondary anti-rabbit (Product # 7074) obtained from Cell Signaling Technology (Danvers, MA). Proteins were visualized by chemiluminescence using the SignalFire ECL Reagent (Cell Signaling Technology, Danvers, MA) or SuperSignal West Femto Maximum Sensitivity Substrate (Invitrogen, Carlsbad, CA) using film.

Proteomics and metabolomics studies. In order to evaluate the tyrosine-phosphorylation landscape of ADME proteins in FVB mice, the genetic background strain used in our transporter-deficient *in vivo* models, tissue samples were subjected to a PhosphoScan analysis (Cell Signaling, Danvers, MA). This analysis provides purification and characterization of tyrosine phosphorylation sites in cellular proteins when paired with liquid chromatography tandem mass-spectrometry (LC-MS/MS) technology. The assay comprises enhanced phospho-tyrosine-containing peptides using P-Tyr-100, a mouse anti-phospho-tyrosine antibody paired with protein G agarose beads. Following

protease-mediated digestion, immune-affinity purification of peptides, and MS analysis on phospho-peptides, spectra were assessed using Sequest 3G and the Sorcerer 2 platform (Sage-N Research, Milpitas, CA).

For metabolomics studies, plasma and tissue samples were collected from wild-type mice and OCT1/OCT2 (OCT1/2)-deficient mice (Taconic, Petersburg, NY). Tissue samples were washed with ice-cold 0.9% saline, and snap-frozen using liquid nitrogen. Further preparation of plasma and tissue samples for metabolomics analysis was done using LC-MS/MS, as previously described.¹⁸⁴

Animal experiments. For all *in vivo* studies, plasma and tissue samples were collected from both males and females wild-type mice, OCT1/2-deficient mice, and mice additionally deficient for MATE1 (OCT1/2/MATE1), following an established protocol.¹⁸⁵ Mice were maintained under pathogen-free conditions at the Ohio State University Laboratory Animal Resources, and all *in vivo* experiments were approved by University Animal Care and Use Committee (protocol number: 2015A00000101-R1). Mice were accommodated in a temperature-, and light-controlled environment with access to water and food. OCT1/2/MATE1-deficient mice was obtained by crossing male OCT1/2-knockout mice with female MATE1-knockout mice to generate heterozygous breeders. The MATE1-deficient mice used to generate this model were kindly provided by Dr. Yan Shu (University of Maryland, Baltimore, MD), and backcrossed onto an FVB background. Next, heterozygous males and females were used to obtain OCT1/2/MATE1-knockout mice. Genetic deletion of OCT1/2 and MATE1 was confirmed by performing RT-PCR analysis.

Dasatinib was dissolved in 80 mM citric acid (pH 3.1) and administered via oral gavage at a dose of 15 mg/kg. For studies involving TEA, dasatinib was given orally 30 min before the intravenous administration of [¹⁴C] TEA (0.2 mg/kg) via the caudal vein. Concentrations of total TEA-derived radioactivity in plasma and homogenized liver samples were measured by liquid scintillation counting.

Quantification of isobutyryl L-carnitine (IBC). A Vanquish UHPLC paired with a Quantiva triple quadrupole mass spectrometer (Thermo Fisher Scientific) was used to perform LC-MS/MS analysis of IBC and the internal standard, isobutyryl L-carnitine-d₃ (Cayman Chemical, Ann Arbor, MI). Chromatographic separation of analytes was achieved on an Accucore aQ column (150 mm × 2.1 mm, dp = 2.6 μm) with a C18 AQUASIL guard cartridge (2.1 mm × 10 mm, dp = 3 μm). The temperature of the column and autosampler was retained at 40°C and 4°C, respectively. The mobile phase contains solvent A (0.1% formic acid in water) and solvent B (0.1% formic acid in acetonitrile-methanol, 50:50 v:v). The gradient elution was 5.0 min at a flow rate of 0.4 mL/min, and conditions were as follows: 0-0.5 min, 0% B; 0.5-2.3 min, 30% B; 2.3-3.8 min, 30% to 95% B; 3.8-4.2 min, 95% B; 4.2-5.0 min, 0% B. The extracted samples (5 μL) were injected for analysis, and following parameters were established for the mass spectrometer: 40 Arb, 12 Arb, 3.3 Arb, 350°C, and 375°C for sheath gas, aux gas, sweep gas, ion transfer tube, and vaporizer temperature, respectively. The ion source was managed by heated ESI in positive ion mode with ion spray voltage at 3500 V. Argon was used as a collision gas at a pressure of 1.5 mTorr. Precursor molecular ions and product ions were recorded for confirmation and detection of IBC (232.144 > 85.083)

and the internal standard (236.056 > 85.056). Assay validation studies demonstrated that the within-day precision and between-day precision ranged from 0-6.16%, and the accuracy ranged from 92.8-105%. The lower limit of quantification for IBC was 0.1 ng/mL.

Statistical analysis. All data are presented as mean \pm SEM, either as the experimental readings or after normalization to baseline values, and then expressed as a percentage. All experiments were conducted in triplicate unless specified, and were performed on at least two independent occasions. Comparisons between two groups were analyzed by unpaired two-sided Student's t-test with Welch's correction while one-way ANOVA with Dunnett's post-hoc test was performed for comparing more than 2 groups. Statistical analyses were conducted using GraphPad Prism version 8.1.2 (GraphPad Software, San Diego, CA), and $P < 0.05$ was considered as the cutoff for statistical significance.

2.4 Results

2.4.1 Conserved tyrosine phosphorylation of OCT1

In order to initially demonstrate that OCT1 is tyrosine phosphorylated, in a manner similar to that reported previously for OCT2,¹⁸⁰ an unbiased MS-based proteomics analysis was performed to identify all tyrosine-phosphorylated proteins, membrane-localized or intracellular, from murine tissues (**Figure 2A**). A total of 802 redundant phosphorylated peptide assignments to 438 non-redundant phosphorylated peptides for the phospho-tyrosine motif antibody were identified, applying a 5% false-

positive rate to filter the results. The hits included multiple transporters (**Figure 2B**), including OCT1, but also several ion channels and enzymes (**Figure 2C**). These preliminary findings thus verified our hypothesis, suggest that tyrosine-phosphorylation may be a much more widespread regulatory mechanism of ADME proteins than held previously, and that these proteins are potentially sensitive to off-targeted de-regulation by clinically-used TKIs.

We previously reported that several TKIs can modulate OCT2 function through inhibition of the protein kinase YES1, and that tyrosine-to-phenylalanine (Y-F) OCT2 mutants at three sites (241, 362, and 377) considerably diminished OCT2 function without affecting OCT2 expression in plasma membrane.¹⁸⁰ In addition, OCT2 has a proline-rich (PXXPR) sequence, which is known to attach the Src Homology 3 (SH3) domain present in YES1 kinase, and mutations in this proline-rich SH3 binding domain decreased OCT2 function and tyrosine-phosphorylation. Interestingly, all these OCT2 domains, including the functionally most relevant 362 residue, are uniquely conserved in phylogenetically-linked transporters, such as OCT1, and across model organisms (**Figure 3A-B**). In addition, a naturally-occurring single nucleotide variant in the OCT1 gene, causing a P283L change, is known to reduce OCT1 function and alter metformin transport in humans,¹⁸⁶ and this site is located in the proline-rich SH3 binding sequence of OCT1.

To investigate directly if the regulation of OCT2 by phosphorylation is conserved in OCT1, we performed functional assays after mutagenesis of relevant sites, and found that OCT1 mutants lacking the putative phosphorylation sites in OCT1 at residues 240,

361, and 376, corresponding to the 241, 362, and 377 sites in OCT2, had significantly reduced transport function (**Figure 3C**). Moreover, we found that distinct OCT2-inhibiting TKIs, including bosutinib, dasatinib, gilteritinib, ibrutinib, sunitinib, and vandetanib, but not the negative-control TKI lapatinib, also inhibit OCT1 function (**Figure 3D**). These results support the possible existence of a common inhibitory mechanism by which TKIs can modulate the function of OCT1 and OCT2, a conclusion that is consistent with the notion that the OCT1- and OCT2-inhibitory properties of the studied TKIs are strongly correlated. Interestingly, compared to OCT1 and OCT2, a highly distinct TKI-mediated inhibitory profile was observed for the related transporter OCT3 (**Figure 4**), with some TKIs (e.g., dasatinib, sunitinib) potently inhibiting all three transporters and some (e.g., bosutinib, gilteritinib, ibrutinib) having no influence on OCT3 function.

2.4.2 TKI-based inhibition of OCT1 *in vitro*

Dose-response experiments with select TKIs (**Table 1**) indicated that dasatinib, gilteritinib, ibrutinib, and vandetanib potently inhibited OCT1 function in a species-independent manner (**Figure 5**), and regardless of the test substrate at concentrations that are clinically achievable at the recommended daily doses. Among the tested TKIs, dasatinib was found to be the most potent inhibitor against both mOCT1 (IC_{50} , 1.09 μ M) and hOCT1 (IC_{50} , 0.56 μ M) (**Figure 6A**), and was selected for further mechanistic studies. In line with previous observations for OCT2-inhibitory TKIs,^{89,187} inhibition of mOCT1 and hOCT1 by TKIs was independent of the substrate concentration, and a

Dixon plot of the reciprocal velocity against the TKI concentration to derive inhibition constants indicated that the mechanism of inhibition is non-competitive (**Figure 6B-C**). This conclusion is consistent with our previous observation that TKs such as dasatinib are not themselves transported substrate of OCT1.¹⁸⁸

2.4.3 TKI-mediated modulation of OCT1 *in vivo*

The notion that the OCT1-inhibitory properties of dasatinib are species-independent is consistent with and recapitulates several prior observations,^{25,180,189,190} and suggests that mice can serve as a suitably predictive model for humans. To directly assess the influence of dasatinib on the function of OCT1 *in vivo*, the pharmacokinetic profile of TEA was examined in wild-type mice and OCT1/2-deficient mice receiving a single oral dose of dasatinib, given 30 min before the administration of TEA. We found that the hepatic uptake of TEA, as determined from the liver-to-plasma concentration ratio, was dramatically reduced in the OCT1/2-deficient mice, and that the genotype could be phenocopied by a single dose of dasatinib (**Figure 6D**). Similar observations were made in the murine kidney (**Figure 6E**), an organ that expresses both OCT1 and OCT2.¹⁹¹

In order to provide further evidence that the ability of dasatinib to modulate TEA disposition is causally related to modulation of hepatic OCT1, we next performed an LC-MS/MS-based targeted metabolomics study in samples from wild-type mice and OCT1/2-deficient mice that was designed to identify a liver-specific endogenous biomarker of OCT1. This study revealed that among 121 metabolites examined, the hepatic concentration of several compounds, including isobutyryl-l-carnitine (IBC), was

substantially elevated in OCT1/2-deficient mice compared to wild-type mice (**Figure 7A**), in both male and female animals. We also observed that reduced hepatic levels of IBC in wild-type mice were accompanied by significantly elevated levels in plasma (**Figure 7B**), that IBC levels in the kidney were negligible (**Figure 7B**) regardless of mouse genotype, and that additional deficiency of MATE1 (**Figure 7C**), which forms a functional unit with OCT1 in the liver and with OCT2 in the kidney, did not influence the results. These findings suggest that IBC, a natural 4-carbon acylcarnitine involved in fatty acid oxidation and organic acid metabolism, serves as a *bona fide* biomarker for hepatic OCT1 function, a conclusion that is in line with a recent clinical report¹⁹². We next evaluated the impact of dasatinib on concentrations of IBC and found that administration of the TKI resulted in a transient, statistically significant increase in the plasma levels of IBC in wild-type mice, but not in OCT1/2-deficient mice or OCT1/2/MATE1-deficient mice (**Figure 7D**). Taken together, these data indicate that dasatinib, given at a dose that affects the liver uptake of TEA, causes significant inhibition of hepatic OCT1 function.

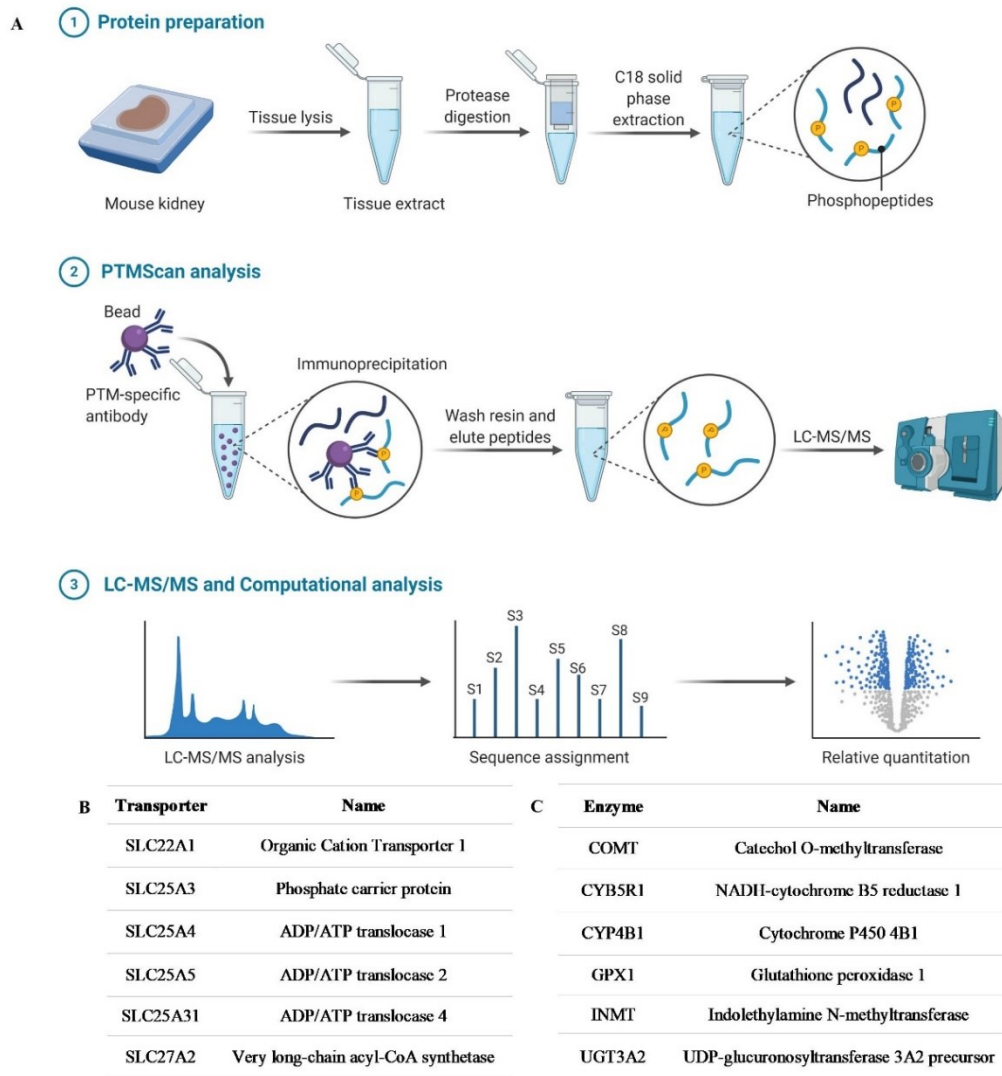
2.4.4 Kinase-mediated regulation of OCT1 function

The existence of tyrosine motifs that are conserved between OCT1 and OCT2, and the similarity in sensitivity to inhibition by TKIs between these two transporters raises the possibility that the tyrosine phosphorylation and activity of OCT1 are regulated by YES1, as described for OCT2.⁸⁹ In support of this hypothesis, we found that pre-treatment of OCT1-expressing cells with the selective YES1 inhibitor, CH6953755,

causes substantial inhibition of hOCT1-mediated transport of TEA (IC_{50} , 2.76 μ M) and metformin (IC_{50} , 2.31 μ M) (**Figure 8A, 9A-B**). This degree of inhibition by CH6953755 was also observed in models overexpressing mOCT1 (**Figure 9C**) or hOCT2 (**Figure 9D**). The connection of TKI-mediated OCT1 inhibition with the function of YES1 was further substantiated by the observed relationship between potency of target engagement by the studied TKIs, as determined by the affinity constant (K_d),^{193,194} and their ability to modulate OCT1-mediated transport (**Figure 9E**).

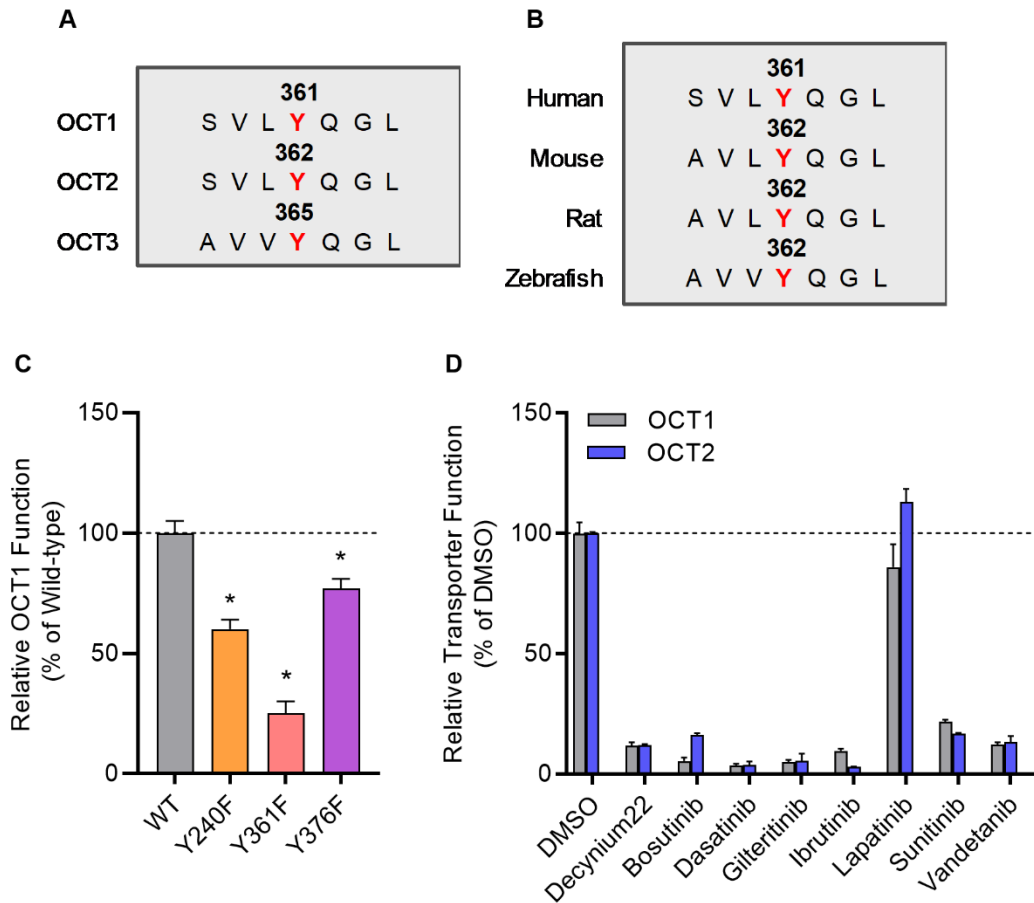
To demonstrate causality of this relationship, we found that even partial downregulation of YES1 expression by siRNA in HEK293 cells (**Figure 8B**) was already associated with a statistically significant loss of OCT1 transport function (**Figure 8C**). To unambiguously identify YES1 as the TKI-sensitive protein kinase that phosphorylates OCT1, we next carried out a screen utilizing a chemical genetics approach in which HEK293 cells expressing hOCT1 are transfected with either the wild-type or TKI-resistant (T348I gatekeeper) mutant of YES1,^{195,196} followed by dasatinib treatment and OCT1 uptake assays (**Figure 10**). These studies revealed that the TKI-resistant YES1 mutant was able to rescue OCT1 inhibition by dasatinib, whereas cells carrying the YES1 wild-type construct retained sensitivity to dasatinib-mediated OCT1 inhibition (**Figure 8D**).

Figure 2: Phosphotyrosine proteomics screen



Phosphotyrosine proteomics screen. (A) Schematic diagram depicting the PhosphoScan analysis from wild-type mouse kidney samples. Identified SLC transporters **(B)** and enzymes **(C)** that are tyrosine-phosphorylated from the phosphotyrosine proteomics screen.

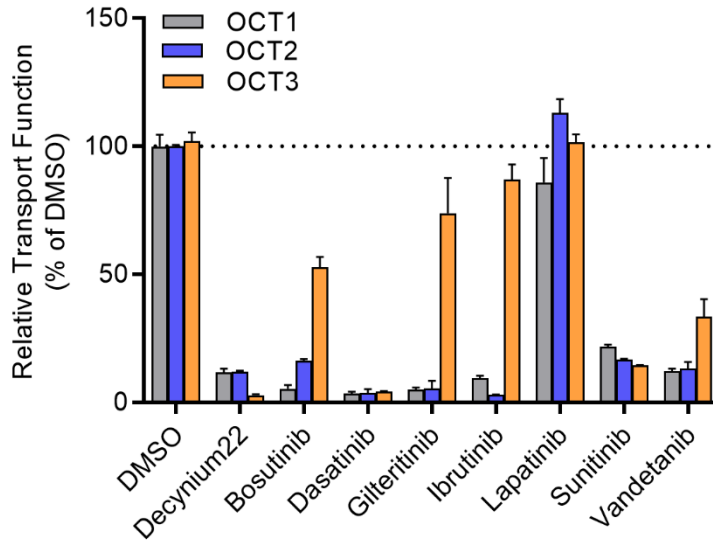
Figure 3: Inhibition of organic cation transporters by TKIs



Inhibition of organic cation transporters by TKIs. (A) The protein sequence of hOCT1, hOCT2, and hOCT3 was aligned by a multiple sequence alignment program (MAFFT). (B) OCT1 protein sequence from indicated organisms was aligned by a multiple sequence alignment program (MAFFT). (C) HEK293 cells were transiently transfected with wild-type (WT), Y240F, Y361F, and Y376F mutant plasmids, uptake assays were performed using [14C] TEA (2 μ M) for 15 min. Cellular accumulation of [14C] TEA was determined by liquid scintillation counter, and the graph represents

relative uptake values compared to wild-type after normalization of protein levels. **(D)** Relative transporter function in HEK293 cells stably transfected with hOCT1 was evaluated by a substrate drug TEA in the presence of FDA-approved TKIs (10 μ M) previously found to inhibit OCT2. Lapatinib was included as a negative-control TKI, and decynium22 as a non-TKI positive control inhibitor. The graph represents relative transport activity of indicated substrate drug compared to DMSO. *P < 0.05 vs. wild-type control. All values represent mean \pm SEM.

Figure 4: Inhibition of organic cation transporters 3 (OCT3) by TKIs



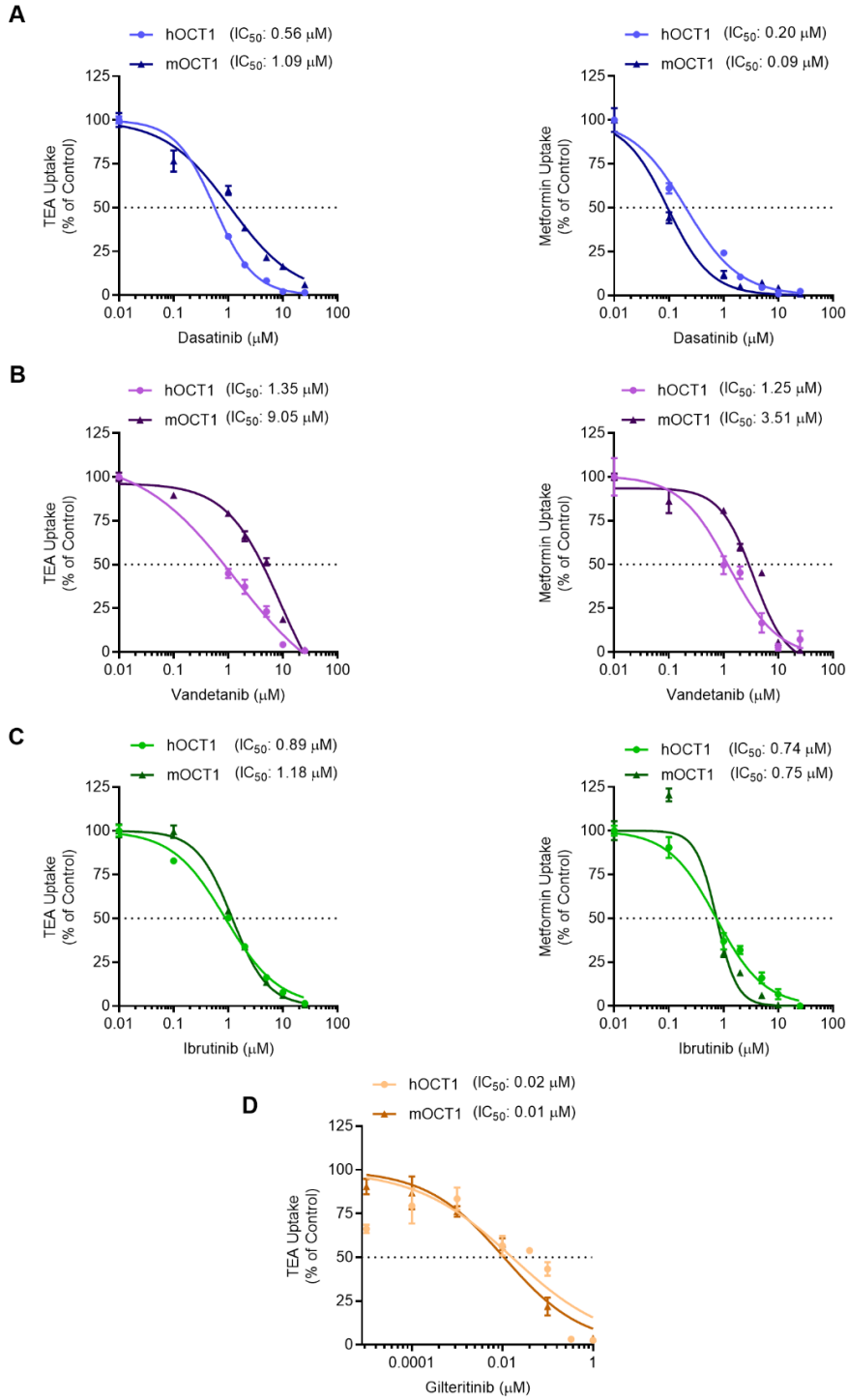
Inhibition of organic cation transporters 3 (OCT3) by TKIs. Relative transporter function was evaluated in HEK293 cells stably transfected with hOCT1, hOCT2, or hOCT3 using [¹⁴C] TEA (2 μM) in the presence or absence of various FDA -approved TKIs (10 μM) for 15 min. All values represent mean ± SEM.

Table 1: Features of TKIs used in the experiments

TKI	Indication(s)	Primary Target(s)	YES1 K_d (nM)	OCT1 IC₅₀ (μM)	OCT1 Inhibition	OCT2 Inhibition
Dasatinib	CML, GIST	BCR/ABL, SRC	0.3	0.56 - 1.09	Yes	Yes
Gilteritinib	AML	FLT3, AXL	445	0.02 - 0.01	Yes	Yes
Ibrutinib	CLL, MCL	BTK	27	0.89 - 1.18	Yes	Yes
Lapatinib	Breast cancer	HER2, EGFR	>10,000	-	No	No
Vandetanib	Thyroid cancer	EGFR, VEGFR	120	1.35 - 9.05	Yes	Yes

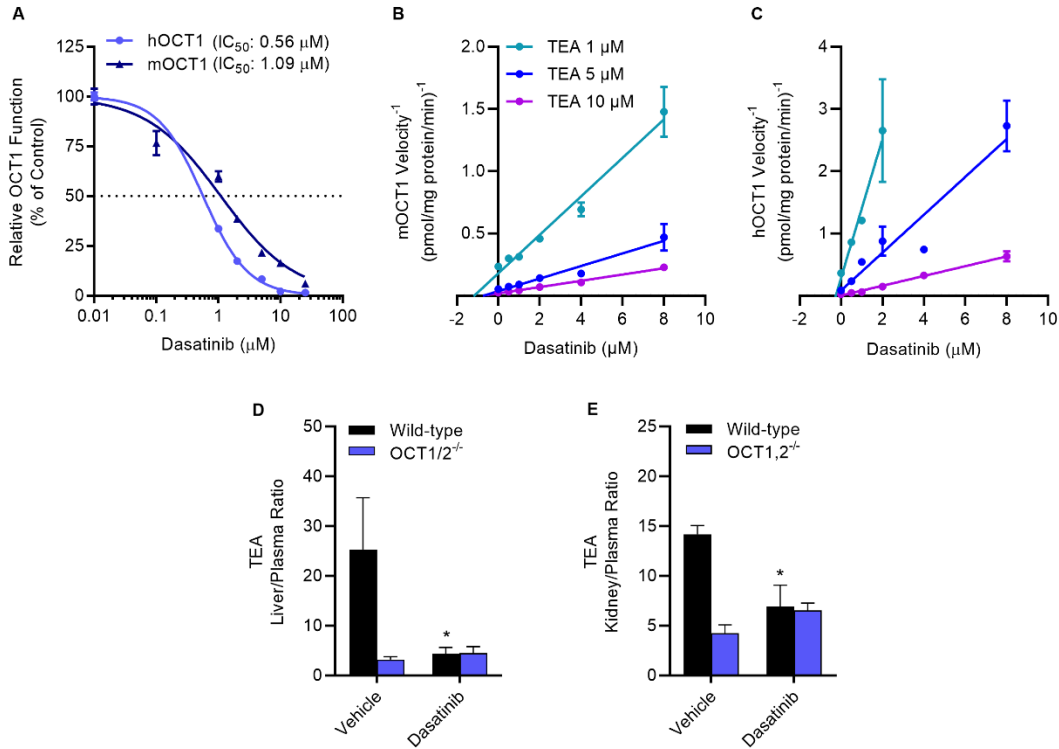
Abbreviations: CLL, chronic lymphocytic leukemia; CML, chronic myeloid leukemia; GIST, gastrointestinal stromal tumor; MCL, mantle cell lymphoma; AML, acute myeloid leukemia.

Figure 5: TKI-mediated OCT1 inhibition



TKI-mediated OCT1 inhibition. Uptake of [¹⁴C] TEA (2 μM) and [¹⁴C] metformin (5 μM) was measured in HEK293 cells overexpressing hOCT1 or mOCT1 after pre-incubation with dasatinib (**A**), vandetanib (**B**), ibrutinib (**C**), or gilteritinib [TEA uptake] (**D**) at various concentrations for 15 min, followed by the co-incubation of TEA and metformin for 15 min. All values represent mean ± SEM, and are expressed as a percentage over vector control.

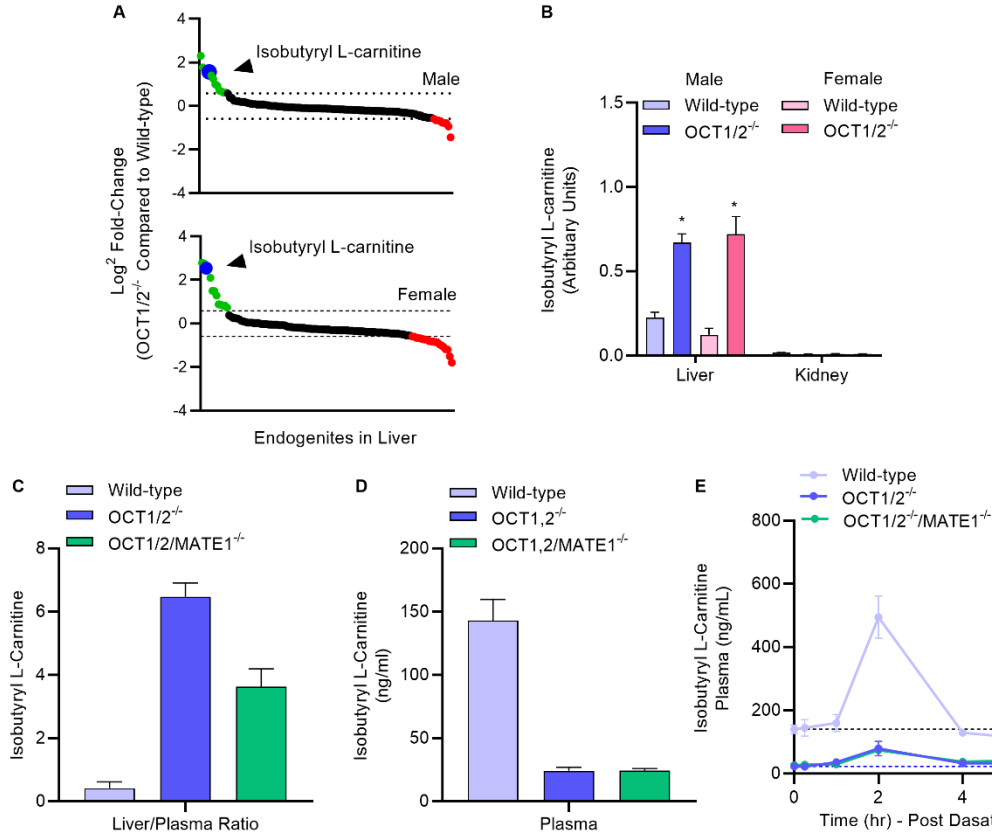
Figure 6: TKI-mediated inhibition of OCT1 function



TKI-mediated inhibition of OCT1 function. (A) Uptake of [^{14}C] TEA ($2 \mu\text{M}$) was measured in HEK293 cells overexpressing hOCT1 and mOCT1 after pre-incubation with dasatinib at various concentrations (0.1 – $25 \mu\text{M}$) for 15 min, followed by the co-incubation with TEA for 15 min. Data represent the mean \pm SEM and are expressed as a percentage over control. (B, C) Dixon plot showing varying concentrations of [^{14}C] TEA (1 , 5 , and $10 \mu\text{M}$) uptake assay in the presence of dasatinib (0.1 – $8 \mu\text{M}$) in HEK293 cells overexpressing hOCT1 and mOCT1, data expressed as $1/\text{velocity}$. In a Dixon plot, the point of intersection of the lines represent the negative inhibition constant ($-\text{K}_i$); this analysis revealed dasatinib-mediated inhibition constants of $0.18 \mu\text{M}$ for hOCT1 and

0.87 μM for mOCT1 (n = 3 per group). **(D, E)** Wild-type and OCT1/2-deficient male mice (n = 5) were treated with either vehicle or dasatinib (15 mg/kg) 30 min before an intravenous administration of [^{14}C] TEA (0.2 mg/kg). Liver **(D)** and kidney **(E)** samples were collected at 5 min after TEA treatment, and graphed as tissue-to-plasma ratios. *P < 0.05 vs. vehicle control. All values represent mean \pm SEM.

Figure 7: Targeted metabolomics and endogenous OCT1 biomarker identification

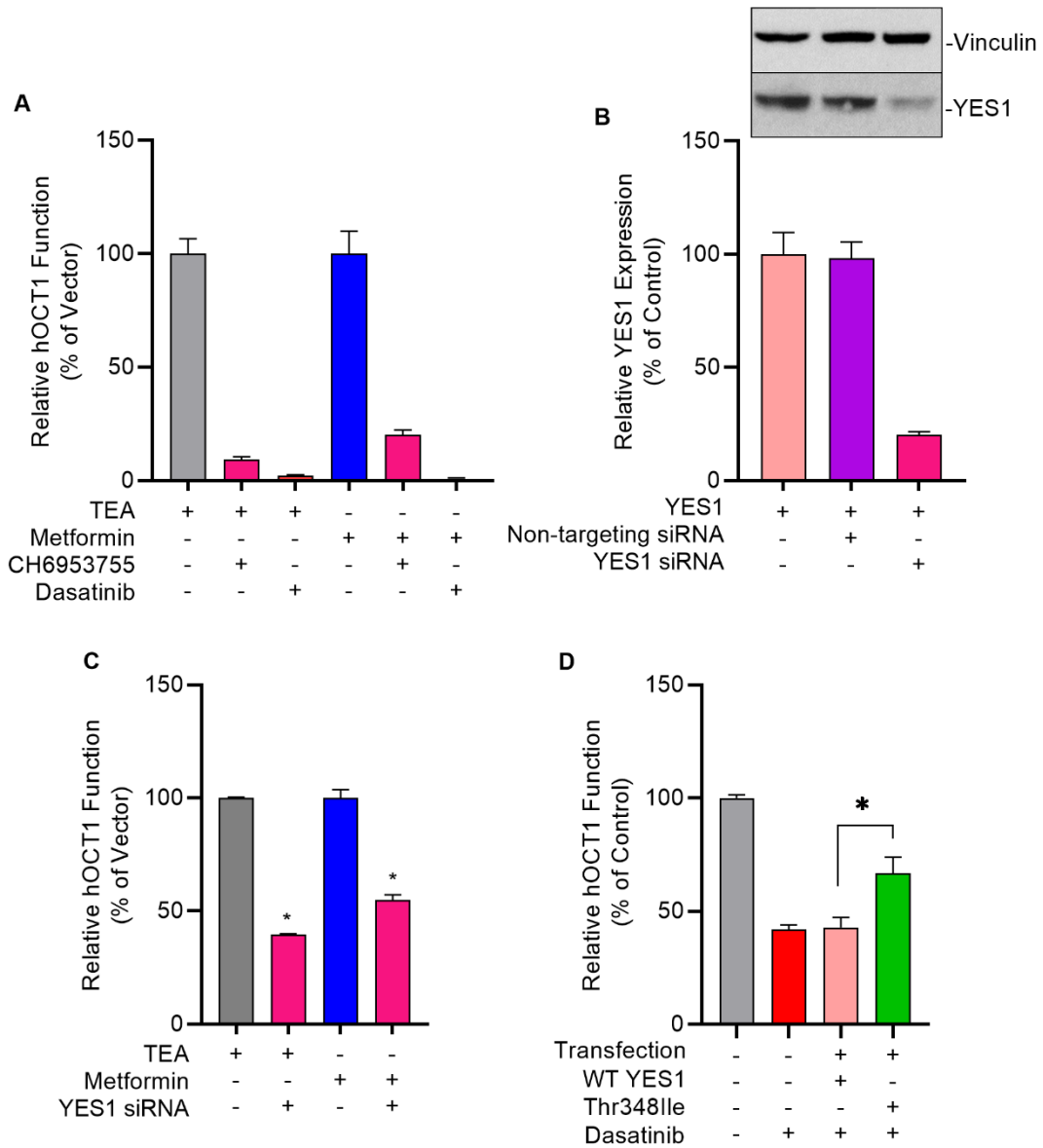


Targeted metabolomics and endogenous OCT1 biomarker identification.

(A) Differentially quantitated endogenous metabolites (“endogenites”) in the liver of male and female wild-type mice and OCT1/2-deficient mice. Endogenites highlighted in green and red were significantly increased and decreased, respectively in livers of OCT1/2-deficient mice. The blue symbol represents isobutyryl L-carnitine (IBC). (B) Liver and kidney concentrations of IBC in wild-type and OCT1/2-deficient mice (n = 5). (C, D) Liver-to-plasma ratio and plasma level of IBC at baseline in wild-

type mice, OCT1/2-deficient mice, and OCT1/2/MATE1-deficient mice (n = 5). **(E)** Plasma concentration-time profile of IBC in wild-type mice, OCT1/2-deficient mice, and OCT1/2/MATE1-deficient mice (n = 5) after a single oral dose of dasatinib (15 mg/kg). *P < 0.05 vs. wild-type. All values represent mean ± SEM.

Figure 8: Genetic and pharmacological inhibition of YES1 kinase impairs OCT1 activity



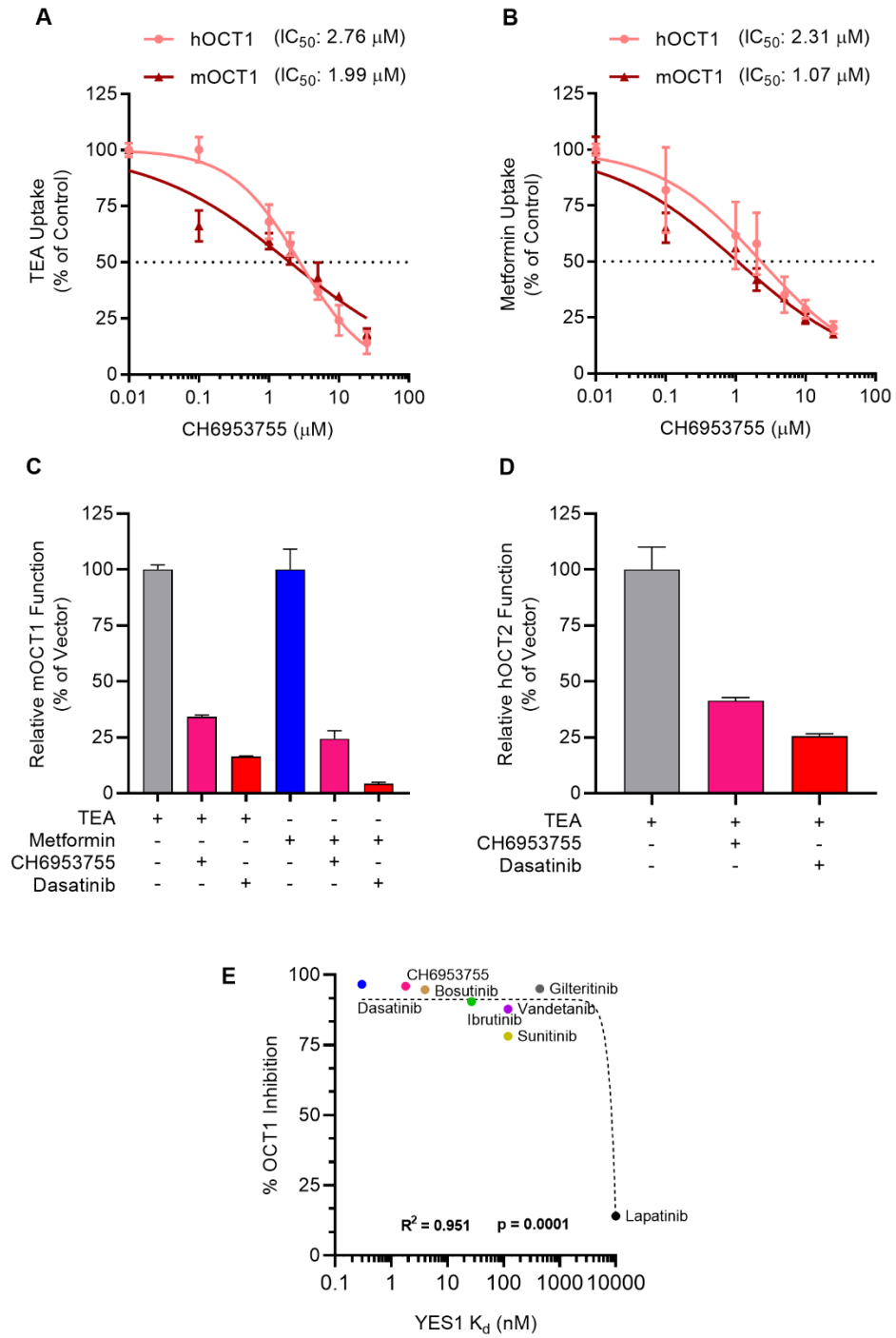
Genetic and pharmacological inhibition of YES1 kinase impairs OCT1 activity.

(A) HEK293 cells stably transfected with vector control (VC) and hOCT1 were pre-incubated with CH6953755 or dasatinib (10 μ M) for 15 min followed by the co-

incubation with [¹⁴C] TEA (2 μM) or [¹⁴C] metformin (5 μM). Data represents relative uptake values compared to VC control after normalization of protein levels.

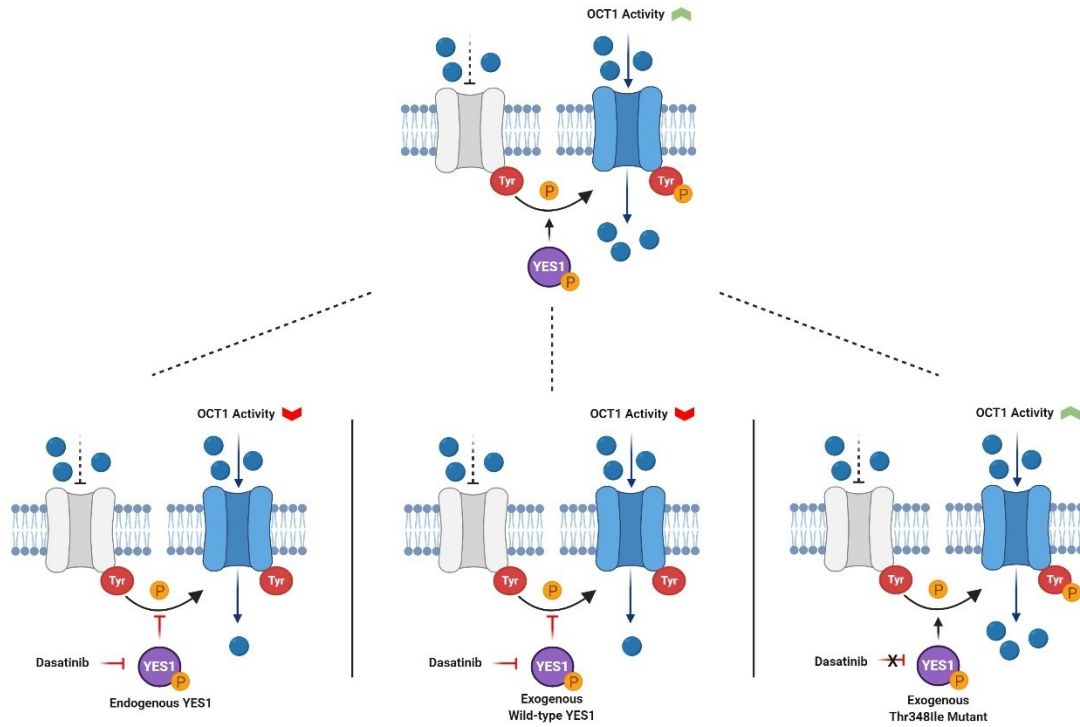
(B) Expression of YES1 protein (top) and gene (bottom) in hOCT1-expressing HEK293 cells 48 h after transfection with non-targeting siRNA or YES1 siRNA. **(C)** Influence of YES1 silencing by siRNA on hOCT1 function was measured in HEK293 cells using uptake assays with [¹⁴C] TEA or [¹⁴C] metformin. **(D)** Influence of YES1 mutants on dasatinib-mediated inhibition of hOCT1 function in HEK293 cells following transient transfection of constructs carrying either wild-type YES1 or the YES1 Thr348Ile gatekeeper mutant. After 48 h, cells were pre-treated with dasatinib (1 μM) for 15 min, followed by uptake assay using [¹⁴C] TEA. *P < 0.05 vs. control. All values represent mean ± SEM.

Figure 9: Influence of YES1 inhibition on OCT1 and OCT2 function



Influence of YES1 inhibition on OCT1 and OCT2 function. Dose-dependent inhibition of TEA (**A**) and metformin (**B**) transport in HEK293 cells overexpressing hOCT1 or mOCT1 after pre-incubation with CH6953755, a selective YES1 inhibitor, at various concentrations for 15 min followed by the co-incubation with [¹⁴C] TEA or [¹⁴C] metformin for 15 min. HEK293 cells stably transfected with vector control (VC), mOCT1 (**C**), or hOCT2 (**D**) were pre-incubated with CH6953755 or dasatinib (10 μM) for 15 min followed by the co-incubation with [¹⁴C] TEA (2 μM) or [¹⁴C] metformin (5 μM) for 15 min. The bars represent relative uptake values after normalization of protein levels as compared to vector control. (**E**) Correlation between YES1 kinase affinity constant (K_d) and percentage of OCT1 inhibition by various TKIs along with CH6953755, a selective YES1 inhibitor. All values represent mean ± SEM.

Figure 10: Schematic diagram showing the role of YES1 kinase in regulating OCT1 function



Schematic diagram showing the role of YES1 kinase in regulating OCT1 function.

Influence of exogenous YES1 targeting constructs carrying the reference sequence or a TKI-resistant mutant on OCT1 activity.

2.5 Discussion

In the present study, we identified OCT1 as a tyrosine-phosphorylated transporter from a phospho-proteomics screen, and demonstrated through functional validation studies using genetic and pharmacological approaches that OCT1 is highly sensitive to small molecules in the class of TKIs that target the protein kinase YES1, such as dasatinib. In addition, we found that dasatinib can inhibit hepatic OCT1 function in mice as evidenced from its ability to modulate levels of the prototypical substrates TEA and metformin as well as the OCT1 endogenous biomarker, isobutyryl L-carnitine. These findings provide novel insight into the posttranslational regulation of OCT1 and suggest that caution is warranted with polypharmacy regimes involving the use of OCT1 substrates in combination with TKIs that target YES1.^{187,197,198} This is particularly relevant in view of the fact that more than one-third of approved prescription drugs are positively charged at neutral pH, and that the membrane transport of many of these agents relies on facilitated carriers such as OCT1.

Previous studies have indicated that OCT1 expression is regulated at different levels, including transcriptionally, by intracellular trafficking, and through alteration of functional properties. Among these mechanisms, transcriptional regulation by hepatic nuclear factors (HNF1 and HNF4 α) has been well documented. This work has suggested that HNF1 ties to an evolutionary conserved region within intron 1,¹⁹⁹ whereas HNF4 α is involved in bile acid-dependent regulation of OCT1 in the liver via activation by the bile acid-inducible transcriptional repressor.²⁰⁰ In addition, OCT1 expression can be

regulated by hepatic growth factor,²⁰¹ and activity of the OCT1 promoter is affected by methylation.^{25,177,186}

In contrast to this knowledge on transcriptional mechanisms, details of short-term posttranslational regulation of OCT1 activity have remained incompletely understood. It was previously reported that substrate transport of OCT1 is reduced by activation of protein kinase A and by inhibition of calmodulin, CaM-dependent kinase II, or p56lck tyrosine kinase.²⁰² Our current findings add to this prior knowledge and demonstrate that many ADME proteins, including multi-specific drug-transporters such as OCT1, are directly regulated through tyrosine-phosphorylation by a mechanism that involves the kinase YES1 in a manner that is analogous to that previously reported for OCT2.¹⁸⁰ Our study also indicates that disruption of this phosphorylation process by YES1 by several clinically-used TKIs can result in dramatically impaired OCT1 function. Furthermore, our study suggests that phospho-proteomic analysis should be considered during the drug development process to predict potential drug-drug interactions and to avoid unwanted consequences when potent inhibitors of YES1 kinase are administered together with agents that undergo OCT1-dependent hepatic transport.^{171,203}

During the course of our investigation, we identified several FDA-approved TKIs as previously unrecognized, potent inhibitors of OCT1, including dasatinib, ibrutinib, sunitinib, and vandetanib. In addition, we confirmed the OCT1-inhibitory potential of several other TKIs, such as bosutinib and gilteritinib, which are listed as OCT1 inhibitors in their prescribing information. It should be pointed out that the mechanism by which these agents impede OCT1 transport function is not distinctly illustrated in the

prescribing information of most TKIs (e.g., reversible *vs.* irreversible; non-competitive *vs.* competitive). The presence or absence of either pre- and co-incubation of TKIs with probe substrates could influence on the inhibitory potential toward transporters, and lead to false-negative results. For example, addition of dasatinib in pre-incubation conditions potently inhibits OCT2 function in experimental studies,¹⁸⁰ whereas co-incubation designs, based on an *a priori* presumed competitive mechanism of inhibition, dasatinib was identified as only a weak inhibitor of OCT2 that is unlikely to have *in vivo* relevance.¹⁸⁷ Because of the discrepancies in published reports and prescribing information, we have previously argued that a reliable and reproducible approach needs to be implemented to explicitly determine TKI-transporter interactions with a statistically meaningful and unbiased manner is essential in order to evade contradictory results, and should ultimately be applied for the design of subsequent *in vivo* validation studies.¹⁶³ In addition, variations among different laboratory settings, including selection of the test substrate(s),²⁰⁴ demand that choosing appropriate model substrates should become an essential component in conducting *in vitro* cationic-type transport assays to generate useful and translationally-relevant predictions.

The lack of regulatory guidelines on the experimental design and clarification of *in vitro* studies to determine an inhibitory potential of drugs with transporters has likely influenced on many of the reported inconsistencies. Since TKI agents are most frequently prescribed as a chronic treatment (e.g., once or twice daily) along with numerous other medications, it is anticipated that researchers will be vigilant regarding the potential transporter-mediated drug-drug interactions of TKIs as a perpetrators in order to achieve

new mechanistic insights and to enhance the safety of currently used polypharmacy regimens. One approach explored in our current study to demonstrate direct *in vivo* modulation of hepatic OCT1 function following the administration of dasatinib is through the identification of novel biomarkers that could ultimately be utilized to guide the selection of optimal doses and schedules of potential perpetrators to be used in conjunction with OCT1 substrates. This was accomplished by probing for novel endogenous metabolites of OCT1 that reflect hepatic transport function and that can be detected in the circulation, by conducting targeted MS-based metabolomic analyses. This analysis was performed using plasma and liver specimens from wild-type mice and OCT1/2-deficient mice, and ultimately resulted in the identification of various structurally named molecules of possible significance, including isobutyryl-l-carnitine (IBC). Interestingly, while we were completing the current study, Luo et al reported that IBC is also a potentially useful endogenous biomarker to predict OCT1-mediated drug-drug interactions in humans.¹⁹² These collective findings are largely congruent with prior studies by Kim et al on the transport of carnitines in liver-specific OCT1-knockout mice.²⁰⁵ This work suggests that levels of certain short-chain acylcarnitines are increased in livers of OCT1-deficient mice but unchanged in plasma, and also that OCT1 serves to efflux carnitines out of cultured hepatocytes but not to take them up. This is consistent with the prior observation that acylcarnitines are not taken up by cells engineered to overexpress OCT1.²⁰⁶ In our metabolomics data, we did not observe apparent changes in the levels of IBC in the kidney, where OCT2 is most highly expressed, and we found that additional deficiency of MATE1 had no influence on the results. Although the baseline

differences of IBC in plasma between wild-type mice and the various OCT1-deficient strains suggests that levels are predominantly influenced by OCT1-mediated hepatic efflux, we found that dasatinib administration to wild-type mice was actually associated with an increase in the levels of IBC in plasma. Although this observation seems counterintuitive, it should be noted that OCT1 can serve as a bi-directional hepatic transporter to either mediate the electrogenic cellular influx or alternatively to mediate efflux of organic cations under *trans-zero* conditions, depending on the substrate concentration gradient. Regardless of the mechanistic basis, the recorded discrepancy with the recently published human study¹⁹² suggests that further investigation into the use of IBC as an OCT1 biomarker in the context of transport inhibitors is warranted.

In conclusion, we identified a novel regulatory mechanism for OCT1 function that involves tyrosine phosphorylation by the kinase YES1, and that is highly sensitive to inhibition by multiple TKIs, including dasatinib. OCT1 is highly expressed in hepatocytes and plays a crucial role in the elimination and pharmacological activity of many prescription drugs, and this makes OCT1 uniquely vulnerable to phosphorylation-mediated interactions with TKIs.

2.6 Acknowledgments

We would like to acknowledge the Genomics Shared Resource (GSR) at the Ohio State University for assistance with sequencing efforts.

Chapter 3. *In Vitro* and *In Vivo* Inhibition of MATE1 by Tyrosine Kinase Inhibitors

****Disclaimer****

The following chapter contains excerpts from an article published and copyrighted by

Pharmaceutics.²⁰⁷ Permission obtained from MDPI.

3.1 Abstract

The membrane transport of many cationic prescription drugs depends on facilitated transport by organic cation transporters of which several members, including OCT2 (*SLC22A2*), are sensitive to inhibition by select tyrosine kinase inhibitors (TKIs). We hypothesized that TKIs may differentially interact with the renal transporter MATE1 (*SLC47A1*) and influence the elimination and toxicity of the MATE1 substrate oxaliplatin. Interactions with FDA-approved TKIs were evaluated in transfected HEK293 cells, and *in vivo* pharmacokinetic studies were performed in wild-type, MATE1-deficient, and OCT2/MATE1-deficient mice. Of 57 TKIs evaluated, 37 potently inhibited MATE1 function by >80% through a non-competitive, reversible, substrate-independent mechanism. The urinary excretion of oxaliplatin was reduced by about 2-fold in mice with a deficiency of MATE1 or both OCT2 and MATE1 ($P < 0.05$), without impacting markers of acute renal injury. In addition, genetic or pharmacological inhibition of MATE1 did not significantly alter plasma levels of oxaliplatin, suggesting that MATE1 inhibitors are unlikely to influence the safety or drug-drug interaction liability of oxaliplatin-based chemotherapy.

3.2 Introduction

Membrane-transporters are key regulators of selective cellular permeability,²⁰⁸ and mediate the passage of many endogenous metabolites such as amino acids and nucleosides as well as small-molecule xenobiotics across the plasma membrane.²⁰⁹ Therefore, they are key determinants in normal physiology and pathophysiology, as well as therapeutic response to drugs. At the cellular level, transporter-mediated uptake or efflux can lead to emergence of drug sensitive or resistant phenotypes in target cells,²¹⁰ and as such affect therapeutic efficacy. On the other hand, transporter-mediated uptake in non-target tissues can result in drug-related toxicities,²¹¹ and several of the transporters involved in this processes have emerged as critical determinants of drug absorption, disposition, therapeutic efficacy, adverse drug reactions, and drug-drug interactions.

About 40% of approved prescription drugs are positively charged at neutral pH (“organic cations”), and the membrane transport of such agents is dependent on facilitated uptake carriers. The organic cation transporters OCT2 (*SLC22A2*) and MATE1 (*SLC47A1*) have particular relevance in this connection, since they are highly expressed at the basolateral and luminal membranes of renal tubular cells, respectively, and these proteins are considered major transporters in the secretion of organic cations from the circulation into the kidney and then from the kidney into the tubular lumen. The tissue distributions of OCT2 and MATE1 in mice are generally consistent with that in humans, with the exception of MATE2-K being absent in the kidney of mice.¹⁴ Human and mouse MATE1 exhibit mutual sequence identity (78%) with similar characteristics.⁸ Substrates for MATE1 are typical organic cations, e.g., tetraethylammonium (TEA), 1-methyl-4-

phenylpyridinium (MPP), metformin, cimetidine, procainamide, and oxaliplatin, which are also found to be transported by mouse MATE1.⁷⁰ Defects in OCT2 or MATE1 function resulting from reduced-function alleles in the *SLC22A2* and *SLC47A1* genes can lead to impaired drug elimination and cause increases in circulating concentrations of xenobiotic substrates.²¹² These prior genetic studies suggest that unintentional alteration of organic cation transporter function, for example by the use of drugs with OCT2- and/or MATE1-inhibitory properties, can potentially lead to deleterious phenotypic changes in patients.²¹³

Previous studies have identified a number of widely used anticancer drugs in the class of tyrosine kinase inhibitors (TKIs) as particularly potent inhibitors of OCT2⁸⁹ as well as the phylogenetically-linked transporters OCT1²¹⁴ and OCT3.²¹⁵ However, a systematic approach to evaluate the ability of TKIs to interact with MATE1 and subsequently affect endogenous homeostasis and xenobiotic handling of substrate drugs such as oxaliplatin is still lacking. In the current study, we characterized the interaction of FDA-approved TKIs with MATE1 *in vitro* in cells, *in silico* by molecular docking simulations, and *in vivo* in genetically-engineered mouse models and a patient with cancer.

3.3 Materials and Methods

Cellular models and cell culture conditions. Parental HEK293 cells were obtained from American Type Culture Collection (ATCC; Manassas, VA). Cells were cultured in DMEM supplemented with 10% FBS and grown in a humidified incubator

containing 5% CO₂ at 37 °C. Lipofectamine 2000 or LTX (Life Technologies, Rockville, MD) was used for transient transfections. TKIs were obtained from Sigma-Aldrich (St. Louis, MO) or Selleckchem (Houston, TX). Radiolabeled compounds were obtained from American Radiolabeled Chemicals (St. Louis, MO) or Moravek (Brea, CA). Oxaliplatin was obtained from Tocris (Minneapolis, MN), and cisplatin from Sigma-Aldrich (St. Louis, MO).

Uptake assays. Uptake experiments in cells overexpressing mouse (m) and human (h) OCT2 or MATE1 were performed with radiolabeled tetraethylammonium (TEA) as the model substrate, using standard methods^{216,217} in the presence or absence of TKIs. The cell culture and uptake conditions for cells expressing mMATE1 or hMATE1 were described previously.²¹⁵ Since several xenobiotics can inhibit OCT2- and/or MATE1-mediated transport of certain substrates, drugs with higher affinities than TEA,²¹³ the ability of select TKIs to inhibit the uptake of metformin and oxaliplatin was also evaluated. To ensure that inhibition via high-affinity binding sites can be detected,²¹³ substrate concentrations were selected that are ≥ 100 -fold below the K_m values for OCT2 and MATE1. Considerations of inhibitor concentration selection in the *in vitro* studies were based on prior criteria²¹³ in order to exceed the anticipated unbound plasma concentrations of investigated TKIs and demonstrate inhibitory potential. Since the inhibitory potential of various xenobiotics against OCT2 and MATE1 is dependent on preincubation with perpetrator drugs,^{89,218,219} a 15-min preincubation period with the TKIs was employed unless stated otherwise. All results were normalized to uptake values in cells transfected with an empty vector or DMSO-treated groups.

In the uptake experiments, cells were seeded in 12- or 24-well plates (6-well plates for oxaliplatin) in phenol red-free DMEM containing 10% FBS, and were incubated at 37°C for 24 h. After removal of the culture medium and rinsing with PBS, cells were preincubated with either DMSO or inhibitors followed by addition of substrate and uptake measurement after 10-15 min for TEA (2 μ M) or metformin (5 μ M) and 60 min for oxaliplatin (50-75 μ M). MATE1-overexpressed cells were pre-incubated with transport media containing 30 mM ammonium chloride for 20 min at 37 °C following previously published protocol (pH 7.4 for hMATE1²²⁰⁻²²² and pH 8.4 for mMATE1^{12,223}) to ensure interactions can be evaluated between outward-facing MATE1 and substrate uptake before adding inhibitors. Then, preincubation media was removed and cells were incubated with transport media (NH₄Cl free) containing radiolabeled compounds. The composition of transport buffer was as follows: 145 mM NaCl, 3 mM KCl, 1 mM CaCl₂, 0.5 mM MgCl₂, 5 mM D-Glucose, and 5 mM HEPES. Although the physiological function of MATE1 is to support luminal efflux, previous studies have shown that kinetic parameters of MATE1-mediated transport are not significantly different between the outward (uptake) and inward (efflux) orientations.²²⁴ The uptake of TEA and metformin was measured by liquid scintillation counting, as described previously.²²⁵ For uptake studies involving platinum drugs, cells were collected with TrypLE, and the pellets were lysed overnight in 0.2% nitric acid. After sonication, total platinum levels were determined by flameless atomic absorption spectrometry.²²⁵

Gene expression analysis. RNA was extracted using the Qiagen kit from treated cells in 12-well plates or kidney tissues obtained from untreated or treated mice. Taqman

primers Hs00217320_m1 and Mm00840361_m1 were obtained from Thermo Fisher Scientific (Waltham, MA) and used for the hMATE1 and mMATE1 genes. The primers Hs02786624_g1 and Mm99999915_g1 were used as the house-keeping control genes for hGAPDH and mGAPDH, respectively.

Computational modeling. Ligand-based pharmacophore modelling and molecular docking were performed with Schrodinger Suite 2018.^{226,227} TKIs were classified as active and inactive based on their cellular uptake activities, where TKI-mediated inhibition of MATE1 function was considered ‘active’ if transport function was reduced to $\leq 10\%$ of baseline values, and ‘inactive’ was defined as inhibition resulting in residual cellular uptake values of $> 50\%$ of baseline values. A total 43 TKIs was used in pharmacophore construction. Common chemical features were extracted through the alignment of all active TKIs to capture the essential interactions between the ligands and a potential protein target. Molecular docking predicts the preferred binding conformation and orientation of a ligand within a protein target and the binding poses are evaluated based on an energy function also known as scoring function. Machine learning-based QSAR (ML-QSAR) models were constructed as binary classification with support vector machine (SVM) and artificial neural network (ANN).^{228,229} A group of 58 tested compounds was randomly divided into a training and a testing dataset in an 8:2 ratio. All TKIs were converted to Morgan circular fingerprints. For the ANN-based QSAR models, 20 runs were taken, and the ANN was trained with 150 epochs in each run. Linear discriminative analysis (LDA) and t-distributed stochastic neighbor embedding (t-SNE) were performed to explore the chemical space spanned by these TKIs. In the LDA

analysis, we randomly selected 100 known allosteric modulators or competitive inhibitors, and then converted their SMILES representations to Morgan Circular fingerprint using RDKit. The 2D chemical structures of the tested TKIs were also converted to Morgan Circular fingerprint. The molecular fingerprints and labels of all compounds were fitted with the LDA model using *sklearn*, and results were plotted as probability density distributions. In the t-SNE analysis, principal component analysis (PCA) was performed for the first 20 dimensions of the molecular fingerprints for all compounds using *sklearn*. The PCA results were then fed into t-SNE model using *sklearn*, and the result was visualized with a scatter plot. The source codes for ML-QSAR, similarity comparison, LDA and t-SNE are available at <https://github.com/sijiechenchenchen>.

Murine pharmacokinetic studies. For pharmacokinetic studies, plasma and tissue samples were collected from male wild-type mice (8-12 weeks old), and age-matched MATE1-deficient [MATE1(-/-)] mice, and mice additionally deficient for OCT1 and OCT2 [OCT1/2/MATE1(-/-)], following an established protocol.²³⁰ All animals were backcrossed on an FVB strain, were given a standard diet and water *ad libitum*, and housed and handled in accordance with the University Laboratory Animal Resources (ULAR) Animal Care and Use Committee at The Ohio State University (2015A00000101-R1). The expected gene deletions in OCT1/2/MATE1(-/-) mice were verified by PCR,²¹⁴ and these animals were observed to be viable and fertile without detectable serum biochemical abnormalities. Oxaliplatin was administered to mice as a single i.p. dose (10 mg/kg), with oxaliplatin dissolved in sterile PBS containing 5%

glucose. Dasatinib (15 mg/kg) was formulated in 80 mM citric acid (pH 3.1) and given orally 30 min prior to the administration of oxaliplatin. Concentrations of total platinum in plasma and tissues were measured by flameless atomic absorption spectrometry, as previously reported,^{217,231} by interpolation of unknown readings on linear calibration curves prepared in drug-free nitric acid (0.2%) using linear-least squares regression analysis.

In order to examine the influence of transporter deficiency on the elimination of total platinum after oxaliplatin administration, male wild-type, MATE1(-/-), and OCT1/2/MATE1(-/-) mice were kept individually in Nalgene metabolic cages for a period of 3 days prior to oxaliplatin administration (10 mg/kg, i.p.). Animals had free access to a standard diet and water, and were housed in a temperature- and light-controlled environment. Changes in the animals' appearance (e.g., kyphosis and altered grooming), behavior (e.g., altered nesting), and/or activity (e.g., altered exploring) were monitored throughout the experiments. The bodyweight of each individual mouse was recorded before and during the experiment. Urine samples were collected in sterile 1.5 ml Eppendorf tubes at 8, 24, 48, and 72 h post-administration of oxaliplatin. Drug levels in urine were analyzed by a validated method based on flameless atomic absorption spectrometry,²¹⁷ and urinary excretion of oxaliplatin was expressed as a percentage of the total administered dose.

Immunoblotting assays. Kidneys were isolated from mice, then minced and incubated in 500 μ l of RIPA buffer (Cell Signaling Technology) containing 1% SDS and protease and phosphatase inhibitors. After sonication, the lysate was incubated for 10 min

on ice, and then centrifuged at $15,000 \times g$ for 15 min. The supernatant was re-centrifuged and used for determination of total protein content by a BCA assay kit. For the immunoblotting, the membrane was blocked with 5% skim milk in 0.05% PBS-tween, and then incubated overnight with a primary antibody (NGAL # 0351) obtained from Santa Cruz Biotechnology (Dallas, TX), and with an HRP-conjugated secondary anti-rabbit antibody (7074) obtained from Cell Signaling Technology (Danvers, MA).

Human pharmacokinetic studies. The study subject was a patient with metastatic colorectal cancer receiving a once daily oral dose of dasatinib (100 mg) before initiation of mFOLFOX6-based therapy, which included oxaliplatin (85 mg/m^2), leucovorin (400 mg/m^2), and 5-fluorouracil (400 mg/m^2 by i.v. bolus and 2400 mg/m^2 by infusion over 46 hours). Dasatinib was administered in combination with standard doses of oxaliplatin given every 14 days, 24 h before and 30 min before each oxaliplatin infusion. In order to assess the degree of MATE1 inhibition by dasatinib, analyses of N-methylnicotinamide (see below) were performed in plasma samples collected at serial time points (up to 24 h after the end of infusion). Plasma samples were also subjected to dasatinib analysis by liquid chromatography with tandem mass spectrometric detection (LC-MS/MS)²³² and analyzed for total platinum levels by flameless atomic absorption spectrometry.²³³ The study protocol NCT04164069 was approved by the review board at the Ohio State University (Columbus, OH), and the patient provided informed consent prior to enrollment.

Quantification of N-methylnicotinamide. Levels of N-methylnicotinamide (NMN; purity >98%, Sigma Aldrich, St. Louis, MO) were determined using LC-MS/MS

using a Vanquish UHPLC coupled with a Quantiva triple quadrupole mass spectrometer (Thermo Fisher Scientific). An Accucore aQ C18 column (150 × 2.1 mm, dp = 2.6 μm) with a C18 AQUASIL guard cartridge (2.1 mm × 10 mm, dp = 3 μm) were employed for separation of the analytes of interest. The column and autosampler were maintained at temperatures of 40 °C and 4 °C, respectively. The mobile phase was composed of solvent A (0.1% formic acid in distilled water) and solvent B (0.1% formic acid in acetonitrile: methanol, 50:50, vol/vol), and a gradient elution was used for 5.0 min at a flow rate of 0.4 mL/min. The gradient conditions were as follows: 0-0.5 min, 0% B; 0.5-1.5 min, 0% to 20% B; 1.5-2.3 min, 20% B; 2.3-3.8 min, 20-95% B; 3.8-4.2 min, 95% B; 4.2-5.0 min, 0% B. Aliquots of 5 μL of the extracted samples were injected. The following parameters were set for the mass spectrometer: sheath gas, 40 Arb; aux gas, 12 Arb; sweep gas, 3.3 Arb; ion transfer tube temperature, 350 °C, and vaporizer temperature, 375 °C. The ion source was operated using heated ESI with the ion spray voltage set at 3500 V in positive ion mode. The collision gas argon was used at a pressure of 1.5 mTorr. An optimized selective reaction monitoring (SRM) mode was applied for the quantitation with the following parameters: m/z 137.062>94.012, collision energy at 20.05 V for N-methylnicotinamide and m/z 140.050>97.082, collision energy at 21.68 V for the internal standard, 3-carbamoyl-1-methyl-d3-pyridinium chloride (purity: >98%, Toronto Research Chemicals, North York, ON, Canada). A protein-precipitation method was used to extract N-methylnicotinamide from plasma samples. In brief, prior to analysis, frozen samples were thawed at room temperature, plasma aliquots of 10 μL were transferred to a 0.5-mL Eppendorf tube followed by the addition of 20 μL of an internal standard working

solution (100 ng/mL) and 70 μ L of methanol. The samples were vortex-mixed and centrifuged at 13,000 rpm for 9.5 min at 4 °C. Next, 60- μ L aliquots of the organic layer were transferred into WebSeal 96-well plates covered with a Webseal mat (Thermo Fisher Scientific,), and a 5- μ L volume of each was injected into the LC-MS/MS system. The lower limit of quantitation for N-methylnicotinamide was determined to be 1 ng/mL, and linear calibration curves ranged from 1 to 1000 ng/ml. The within-run and between-run precisions were within 5.27%, while the accuracy ranged from 93.5 to 104%.

Statistical Analyses. All data are presented as mean \pm standard error of the mean (SEM), and experimental results from uptake studies were normalized to total protein content and baseline values, and expressed as a percentage. All experiments were performed using multiple replicates and were performed independently on at least two independent occasions. An unpaired two-sided Student's t-test with Welch's correction was used for comparisons between two groups (control/baseline vs. treatment/genotype), and a one-way ANOVA with Dunnett's post-hoc test was used for comparing more than 2 groups. $P < 0.05$ was used as the statistical cut-off across all analyses.

3.4 Results and Discussion

3.4.1 TKI-mediated inhibition of MATE1 *in vitro*

In our previously reported screens of inhibitors against the organic cation transporters OCT1, OCT2, and OCT3, several TKIs were identified as agents with potent transporter-modulatory properties.^{89,214,215} Due to their unique inhibitory activity against these transporters, we performed a screen of FDA-approved TKIs and sought to

determine whether these agents are also modifiers of transport function in cells overexpressing the related transporter, MATE1. In order to determine the extent of interactions between TKIs and MATE1, the uptake of the prototypical substrate TEA was evaluated in cells overexpressing hMATE1 in the presence or absence of a pre-incubation with each individual TKI. The known MATE1 inhibitor cimetidine was used as a positive control inhibitor. This screen revealed that all 57 TKIs, except for alectinib, inhibited MATE1 function by at least 25% with an inhibitor to substrate concentration ratio of 5:1, and more than half of the TKIs inhibited by more than 80% (**Figure 11A**).

Subsequent investigation with various anti-leukemic TKIs, including dasatinib, ibrutinib, imatinib, nilotinib, and/or ponatinib, indicated that the TKI-MATE1 interaction is dependent on the pre-incubation time (**Figure 11B**), and is only partially reversible such that MATE1 function is not fully restored even after an 8-h washout period (**Figure 11C**). This suggests that even short-term exposure to TKIs followed by their removal can result in sustained inhibition of MATE1 for prolonged time periods. Since certain inhibitors of organic cation transporters function in a substrate-dependent manner,²³⁴ we verified that TKIs retained MATE1-inhibitory potential when using metformin as an alternative, secondary substrate (**Figure 11D**). Furthermore, a Dixon plot of the reciprocal velocity against the TKI concentration to derive inhibition constants (K_i) indicated that the mechanism of inhibition is non-competitive (**Figure 11E**). conclusion is consistent with a previous observation that certain anti-leukemic TKIs, including nilotinib (K_i , 1.54 μM), can exert selectively potent inhibitory effects against MATE1 at clinically-relevant concentrations.²¹⁸

3.4.2 Computational evaluation of MATE1-TKIs interaction

To gain insight into the mechanistic basis of the finding that an unexpectedly large number of TKIs have potent MATE1-inhibitory properties, two ligand-based models were constructed, including pharmacophore models and ML-QSAR models (**Figure 12A**). The two ML-QSAR models using artificial neural network (ANN) and support vector machine (SVM) yielded q^2 values of 0.83 and 0.75 in the test dataset, respectively (**Figure 12B**). The good accuracy of the ML-QSAR models indicates that the inhibitory activities of TKIs are correlated with their chemical structural features, which in turn suggests a common inhibitory mechanism. To probe the mechanisms by which these TKIs interact with human MATE1, we generated a pharmacophore model with the maximum hypothesis match of the 24 ‘active’ TKIs that reduced the function of MATE1 by >90%. The low accuracy of the model ($q^2=0.51$) indicates, however, that these TKIs do not share a common pharmacophore and, hence, are unlikely bind to the same well-defined pocket (site) on MATE1. The main reason for the poor performance of this pharmacophore model is related to the diverse structures of the active TKIs, as indicated by the low Tanimoto similarity scores (**Figure 12C**), where most TKIs show less than 0.3 similarity across the three comparisons.

The notion that TKIs are non-competitive inhibitors of MATE1 suggests that the TKIs do not occupy the orthosteric binding site for substrates. To investigate if the active TKIs act as allosteric modulators of MATE1, we compared their chemical characteristics with those of existing allosteric drugs. We randomly selected 100 compounds belonging

to allosteric modulators or competitive inhibitors, and conducted linear discriminant analysis (LDA) to classify these compounds (**Figure 12D**).²³⁵ Our results show that LDA can distinctly separate the allosteric modulators from the competitive inhibitors, and our tested active TKIs populate the purple distribution region representing allosteric modulators. In addition, we employed t-distributed Stochastic Neighbor Embedding (t-SNE) to visualize if the TKIs, allosteric modulators, and approved drugs reside in the same chemical space (**Figure 12E**). Both LDA and t-SNE show that the active TKIs and allosteric drugs are clustered together, indicating that the active TKIs resemble allosteric modulators in terms of their physicochemical properties.

To further probe if and how these TKIs interact with MATE1, we computationally docked them to an atomic structural model of MATE1 predicted by AlphaFold2 (access code AF-Q96FL8-F1).²³⁶ The docking result does not show a consensus binding site/pose for these TKIs, consistent with the above pharmacophore model. Additionally, the docking scores show no significant difference among the active, neutral and inactive TKIs. The best binding poses of the active, inactive, and neutral TKIs show that their binding space overlaps, all occupying a large vacant volume between the C- and N-lobes of MATE1 (**Figure 12F**). Overall, these calculations suggest that the mechanism by which TKIs inhibit MATE1 is unlikely associated with binding to a common and well-defined binding pocket on the MATE1 protein.

3.4.3 Influence of TKIs on MATE1 regulation *in vitro*

Next, we evaluated the influence of MATE1-inhibitory TKIs on post-translational and transcriptional regulatory pathways as potential explanations for the observed inhibitory profiles. We previously reported that the transporter OCT2 is sensitive to inhibition by several FDA-approved TKIs through a mechanism that involves YES1-mediated tyrosine phosphorylation²¹⁴ Since OCT2 shares various structural features and has overlapping substrate specificity compared with MATE1,²³⁷ we hypothesized that the activity of MATE1 might also be dependent on kinase-mediated tyrosine phosphorylation. However, a recent unbiased MS-based phospho-proteomics screen did not identify MATE1 as a tyrosine-phosphorylated protein.⁸⁹ The absence of a common inhibitory mechanism by which TKIs can modulate the function of OCT2 and MATE1 is also consistent with the notion that the inhibitory properties of a subset of TKIs against these 2 transporters are not correlated (**Figure 13A**). Indeed, compared to OCT2, a highly distinct TKI-mediated inhibitory profile was observed for MATE1, with some TKIs (e.g., bosutinib, sunitinib) potently inhibiting both transporters and some (e.g., regorafenib, sorafenib) having no influence on OCT2 function. These findings are consistent with the observation that silencing of YES1 by siRNA in HEK293 cells influenced the function of OCT2 but not MATE1 (**Figure 13B**), and with the notion that MATE1 lacks the proline-rich (PXXPR) sequence present in OCT2 that binds the Src Homology 3 domain present in YES1⁸⁹ (**Figure 13C**).

An alternative route by which TKIs affect MATE1 function is through effects on transcription factors that result in gene expression changes. Previous studies have

suggested a possible role for PPAR α ,^{238,239} and basal transcription of the MATE1 gene is regulated by FXR²⁴⁰ and by binding of Sp1 close to the transcription start site,²⁴¹ by binding of AP-1/AP2-rep to the promoter region,²⁴² and by Nkx-2.5, SREBF1, and USF-1²⁴³. Of these transcription factors, Sp1 is of particular interest because exposure to nilotinib and dasatinib is known to influence Sp1 expression and binding to its target genes as well as influence kinases that phosphorylate Sp1 via mechanisms unrelated to their primary targets.²⁴⁴ To gain preliminary insights, we performed a transcriptomic analysis by RT-PCR of MATE1-overexpressing cells exposed to TKIs *in vitro* and found that dasatinib and nilotinib (in increasing order) downregulated the expression of MATE1 (**Figure 13D**). Although further investigation is required to the TKI-, dose-, and time-dependence as well as the mechanistic basis of these findings, they are consistent with the possibility that TKIs inhibits MATE1 through a transcriptional regulation mechanism.

3.4.4 Effect of TKI treatment on MATE1 function *in vivo*

In advance of evaluating the influence of TKIs on MATE1 function in mice, the comparative concentration associated with 50% inhibition of transport (IC₅₀) for human and mouse MATE1 was determined for several TKIs, including ibrutinib, imatinib, and nilotinib. These studies indicated that mouse MATE1 was more resistant to TKI-mediated inhibition than the human transporter; for example, the IC₅₀ for nilotinib against human MATE1 was >100 times lower than that against mouse MATE1 (0.38 vs 45.4 μ M, respectively) (**Figure 14A**). It is noteworthy that the same pattern of inhibition was observed for the known, non-TKI inhibitor of MATE1, cimetidine (IC₅₀, >50 μ M). The

finding that the MATE1-inhibitory property of certain xenobiotics is species-dependent is not unprecedented,²⁴⁵ and has been specifically reported previously for imatinib-mediated inhibition of dopamine transport (IC_{50} for human MATE1, 1.1 μ M; IC_{50} for mouse MATE1, 101 μ M).²⁴⁵ This suggests that phenotypic changes observed in mice could potentially under-predict observations made in humans.

To directly assess the influence of dasatinib on the function of MATE1 *in vivo*, levels of the endogenous dual OCT2/MATE1 substrate 1-N-methyl-nicotinamide (NMN) were measured as a potentially TKI-sensitive biomarker at baseline in mice that were either wild-type or deficient in MATE1,²⁴⁶ OCT1 and OCT2 (OCT1/2), which together are the functional equivalent of human OCT2,²⁴⁷ or both MATE1 and OCT1/2.²⁴⁸ We found that deficiency of either MATE1 or OCT1/2 was accompanied by significantly elevated levels of NMN in plasma (**Figure 14B**), and that simultaneous deficiency of MATE1 and OCT1/2, which form a functional unit with MATE1 in the kidney to regulate the tubular secretion of organic cations, resulted in further elevation of baseline levels. These findings suggest that NMN, a natural metabolite of niacin (or nicotinamide), serves as a *bona fide* biomarker for directional renal organic cation transport, a conclusion that is in line with a recent clinical report.²⁴⁹

We next evaluated the impact of dasatinib on concentrations of NMN in mice and found that oral administration of the TKI at a dose of 10 mg/kg resulted in a transient, statistically significant increase in the plasma levels of NMN in wild-type mice to a degree that resembles those observed in MATE1-deficient mice at baseline (**Figure 14B**). Similar observations were made in a patient with colorectal cancer who received a single

oral 100-mg dose of dasatinib (**Figure 14C**). The average circulating concentrations of dasatinib in this patient were consistent with previously reported findings in humans receiving dasatinib-based treatment,²⁵⁰ were similar to those observed in our preclinical studies in mice (**Figure 14D**), and suggest that these levels are in the range required for potent and sustained inhibition of MATE1 as predicted from *in vitro* model systems. The plausibility of dasatinib-mediated *in vivo* inhibition of MATE1 is further underscored by the notion that TKIs tend to accumulate in cells (administration of imatinib 25 μ M resulted in 4.2 mM intracellular concentrations in K562 cells)²⁵¹ and dasatinib is known to extensively accumulate in the mammalian kidney, the proposed site of interaction, with reported kidney-to-blood concentration ratios of >10 .²⁵² In view of the structural dissimilarity between TKIs, extending conclusions derived from studies with dasatinib to other TKIs is not necessarily appropriate, and suggests that further investigations are required to evaluate whether the mechanism of MATE1 inhibition is dependent on the TKI involved. In addition, while TKIs such as dasatinib potently inhibit MATE1 function *in vitro*, suggesting that concurrent treatment with such TKIs warrants caution, these interactions are not necessarily associated with a deleterious effect on renal function.

3.4.5 Modulation of oxaliplatin pharmacokinetics by TKI treatment

To further evaluate the influence of TKIs on the function of MATE1 *in vivo*, the plasma pharmacokinetic profile and urinary excretion of the anticancer drug oxaliplatin were examined in mice. Oxaliplatin is a small-molecule platinum coordination complex

used for the treatment of several gastrointestinal cancers that is cleared from plasma predominantly by renal elimination, with urinary excretion accounting for >50% of the dose and fecal excretion for about 2% of the dose.²⁵³ Previous reports demonstrated that oxaliplatin is a transported substrate of mouse, rat, and human OCT2^{9,217} as well as MATE1,^{248,254} and these transporters collectively provide a mechanistic account of the renal tubular secretion of oxaliplatin in rodents and humans (**Figure 15A**). Preliminary *in vitro* studies provided confirmation of the notion that oxaliplatin is a transported substrate of mouse and human OCT2 and mouse and human MATE1, where overexpression of the murine (**Figure 15B**) and human (**Figure 15C**) transporters was associated with 15-fold and 3-fold increases in uptake, respectively, compared with cells transfected with an empty vector control. Importantly, cells pre-treated with dasatinib showed a dramatically impaired ability to transport oxaliplatin.

In advance of the pharmacokinetic studies with oxaliplatin, we verified the utility of the MATE1-deficient mouse model by demonstrating its increased sensitivity to nephrotoxicity associated with the related agent cisplatin that results from an increase in residence time and extent of accumulation in proximal tubular cells associated with impaired MATE1 function. Indeed, we found that the administration of cisplatin to MATE1-deficient mice was associated with increases in several commonly used biomarkers of drug-induced acute kidney injury, including blood urea nitrogen (BUN) and neutrophil gelatinase-associated lipocalin (NGAL) compared with the values observed in wild-type mice (**Figure 16**). These findings are consistent with prior observations in similar genetically-engineered mouse models^{255–257} or studies involving

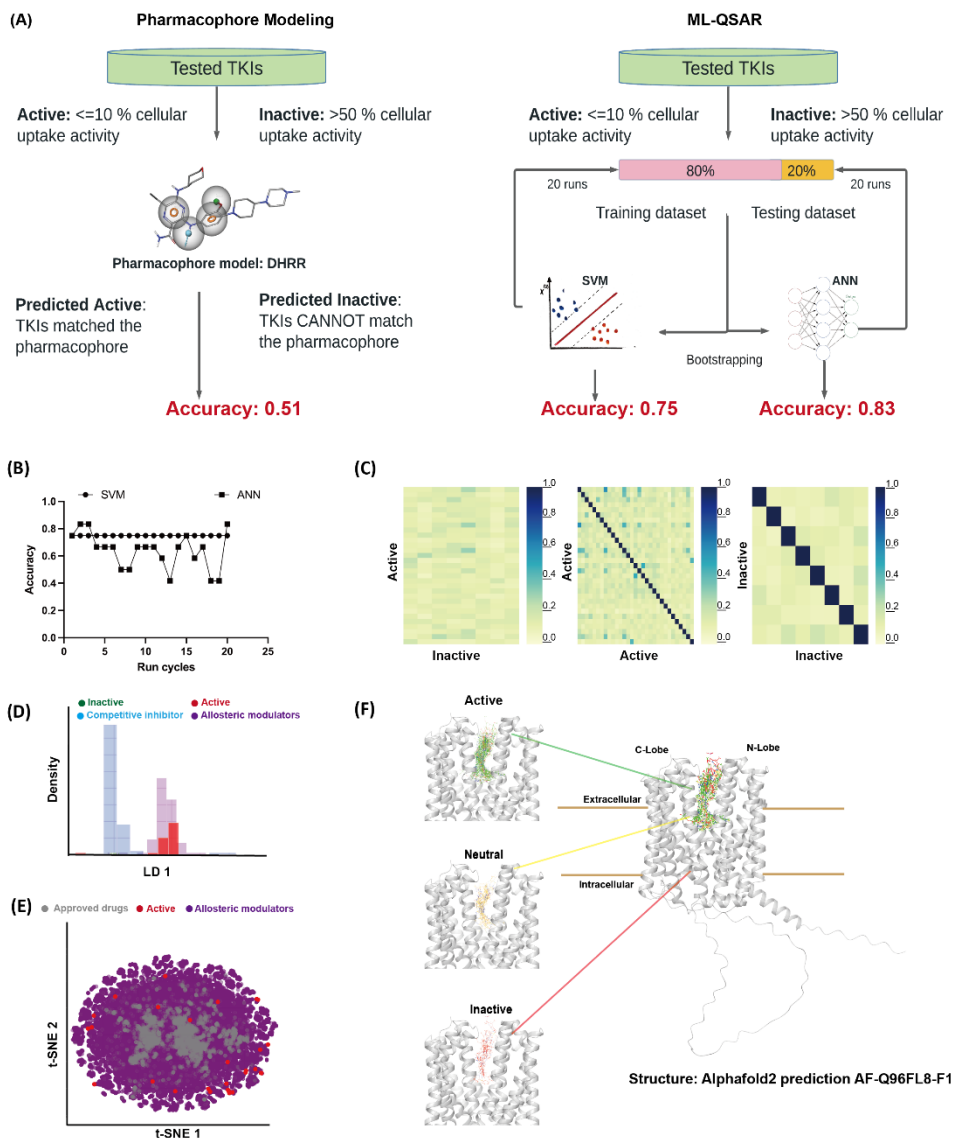
the administration of cisplatin together with inhibitors of MATE1,^{258,259} and are in line with observations made in patients receiving treatment with cisplatin who carry impaired function variants in *SLC47A1*, the gene that encodes MATE1.^{260–262}

The notion that oxaliplatin lacks nephrotoxic properties similar to those observed with cisplatin has been ascribed to comparative differences in transport kinetics for MATE1 in both mice and humans, and with a corresponding increase in luminal efflux into the urine.²³⁴ This, in turn, provides a plausible explanation for the differential extent of total drug accumulation in the kidney, which is much less for oxaliplatin than for cisplatin.^{235,263} Based on this prior knowledge, it has been speculated that genetic or pharmacological inhibition of MATE1 might also be associated with an oxaliplatin-mediated potentiation of nephrotoxicity.²⁶⁴ In contrast, we found that while the urinary excretion of oxaliplatin was substantially decreased by MATE1-deficiency over a 3-day collection period (**Figure 17A**), this was not accompanied by detectable changes in treatment-related weight loss (**Figure 17B**), a general marker of toxicity, or by specific markers of nephrotoxicity (**Figure 17C-D**). Similar observations were made in animals that were additionally deficient in OCT1 and OCT2 (**Figure 17A-D**). The translational significance of these findings was confirmed by the demonstration that the pretreatment of mice with dasatinib had no influence on markers of oxaliplatin-induced nephrotoxicity (**Figure 18A-B**). Interestingly, the plasma pharmacokinetic profile of oxaliplatin was unchanged by pretreatment with a single dose of dasatinib in wild-type mice (**Figure 17E**), and in the patient with colorectal cancer (**Figure 17F; Table 2**). This observation was made regardless of MATE1 or OCT1/2 genotype (**Figure 18C**), and the lack of a

detectable plasma pharmacokinetic interaction was also noted for cisplatin when given in combination with nilotinib (**Figure 18D; Table 2**). The paradoxical notion that urinary excretion of oxaliplatin can be impaired as a result of dysfunctional transport by MATE1 without concurrent changes in the apparent systemic clearance is possibly related to shunting of elimination. A related phenomenon has been documented previously for several other drugs where altered liver uptake or biliary secretion due to a genetic defect is associated with increases in the extent of urinary excretion.^{265,266} Although additional investigation will be required to assess the precise mechanistic basis and the pharmacodynamic implications of this phenomenon, the observations made in mice and humans provide evidence that MATE1 inhibitors are unlikely to influence the safety or drug-drug interaction liability of oxaliplatin-based chemotherapy.

removal of ibrutinib and [¹⁴C] TEA uptake assay was carried out at time 0, 1, 2, 4, and 8 h. Baseline MATE1 function was determined in untreated cells. **(D)** Influence of TKIs (pre + co-incubation) on comparative MATE1-dependent transport of [¹⁴C] TEA (2 μM) and metformin (5 μM). The graph represents relative uptake as compared to individual vector group after normalization of protein levels. Individual t-tests showed no significant difference between the two substrates. **(E)** Dixon plot of nilotinib-dependent MATE1 inhibition of varying concentrations of [¹⁴C] TEA. The velocity (v) was calculated based on the difference in uptake between cells with and without MATE1 overexpression. Data are shown as mean ± SEM.

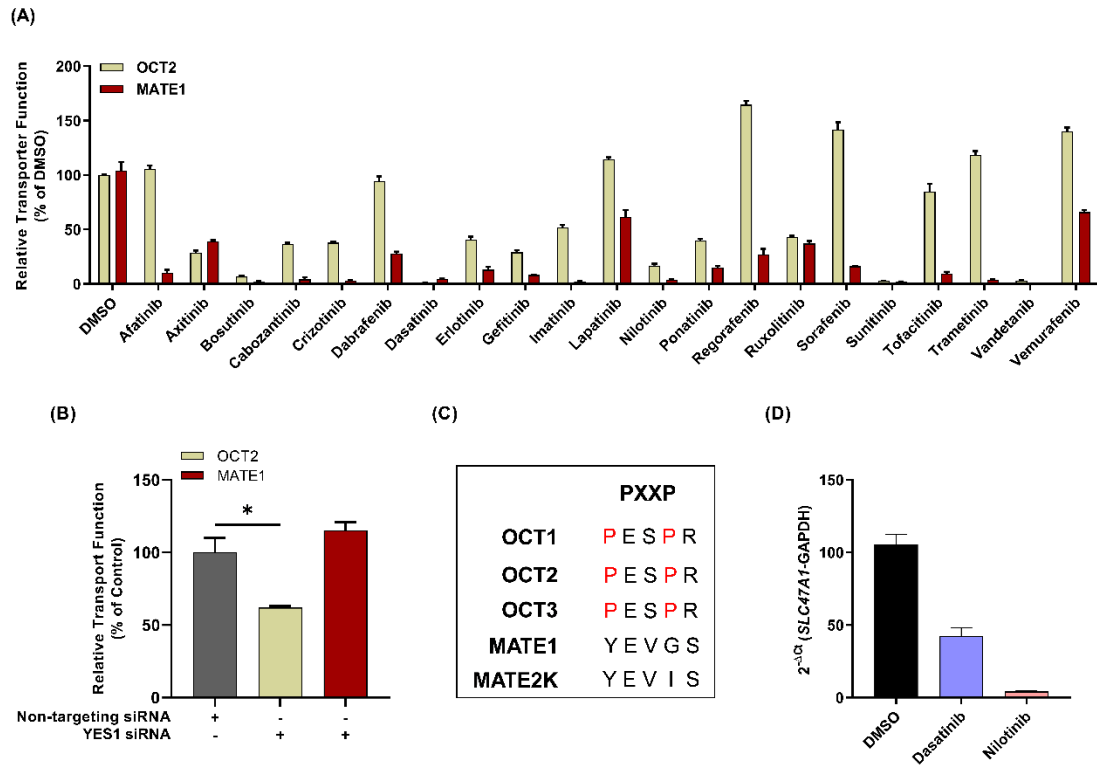
Figure 12: *In silico* analysis of mechanisms underlying MATE1 inhibition by TKIs



***In silico* analysis of mechanisms underlying MATE1 inhibition by TKIs. (A)** The workflow of pharmacophore and ML-QSAR modeling. **(B)** The accuracy for the test dataset for 20 ML-QSAR runs. **(C)** The Tanimoto similarity comparisons of TKIs. **(D)**

Probability distributions of active TKIs, inactive TKIs, allosteric modulators and competitive inhibitors using LDA. **(E)** Chemical space of the TKIs, allosteric modulators and approved drugs projected along the first two PC modes from PCA using t-SNE. **(F)** The clustering of the best binding poses for active, inactive, and neutral TKIs in a hMATE1 model.

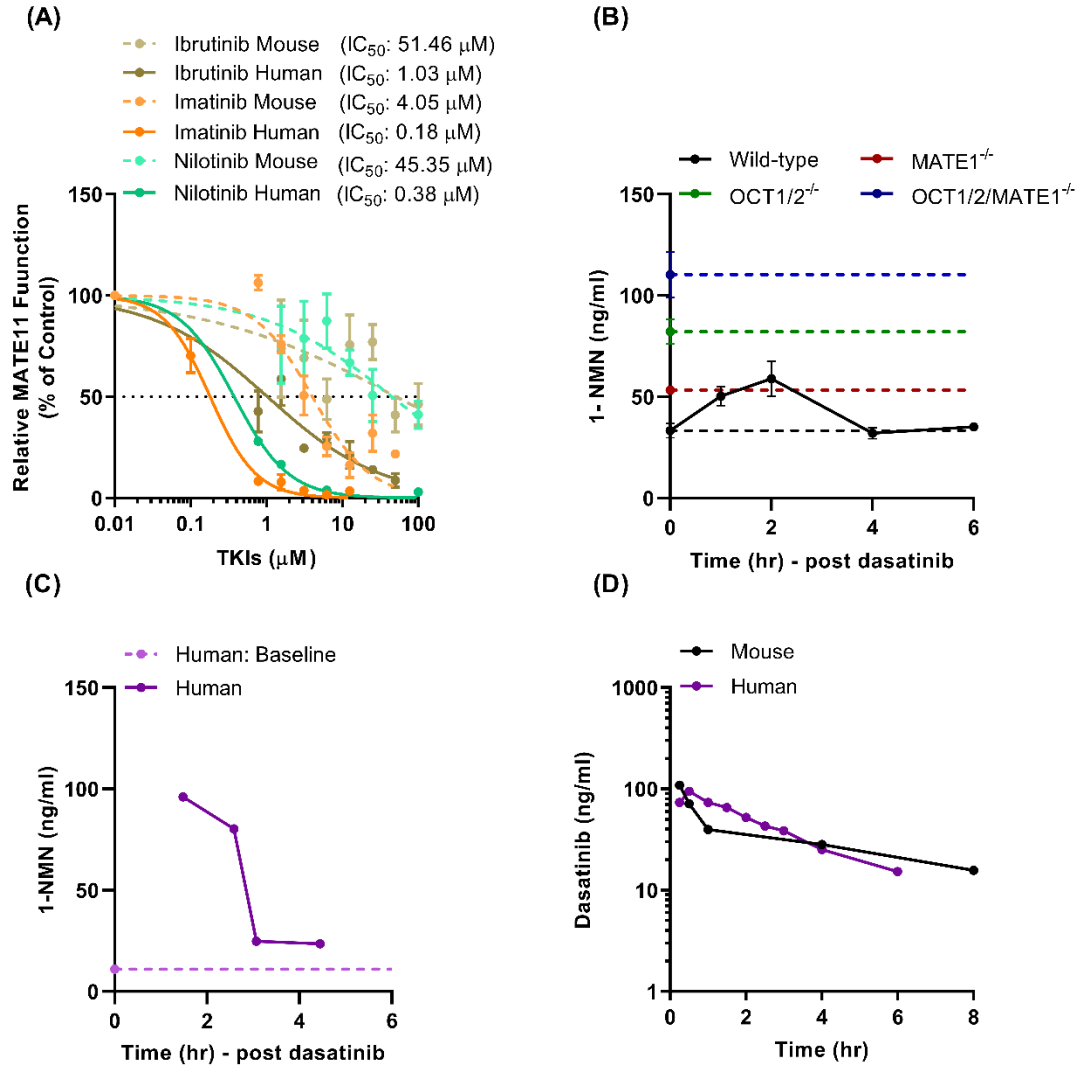
Figure 13: Influence of TKIs on MATE1 expression



Influence of TKIs on MATE1 expression. (A) Relative transporter function in HEK293 cells stably transfected with human OCT2 and MATE1 was evaluated by a substrate drug [^{14}C] TEA in the presence of FDA approved TKIs (10 μM). The graph represents relative transport activity of indicated substrate drug compared to DMSO. (B) siRNA (25 nM)-mediated knockdown of YES1 kinase and its effects on HEK293 cells overexpressing human OCT2 and MATE1 using uptake assays with [^{14}C] TEA. The treatment condition for each bar is mentioned below the graph. Data are shown as mean \pm SEM (* $P < 0.05$). (C) Protein sequence of OCT1, OCT2, OCT3, MATE1 (residue 277) and MATE2K was aligned by a multiple sequence alignment program (MAFFT). (D) Effect of select TKIs

on the expression of MATE1 gene as measured by RT-PCR (results are reported as a difference with the respective control containing empty vector).

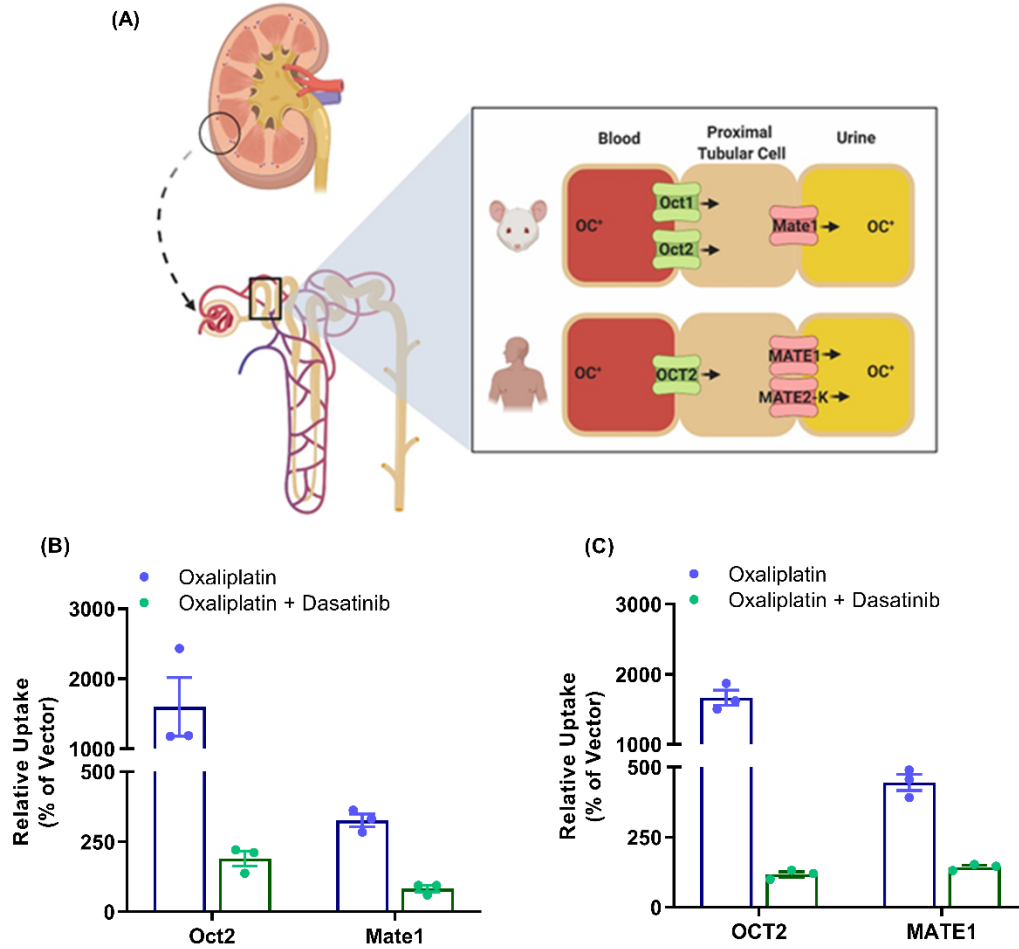
Figure 14: Characteristics of MATE1 inhibition by TKIs



Characteristics of MATE1 inhibition by TKIs. (A) Comparison of IC_{50} of several TKIs in HEK293 cells overexpressing mouse or human MATE1. (B) Influence of mouse genotype and TKI treatment on levels of the MATE1 biomarker, N-methynicotinamide (1-NMN) in plasma. Dashed lines represent baseline levels of 1-NMN in wild-type,

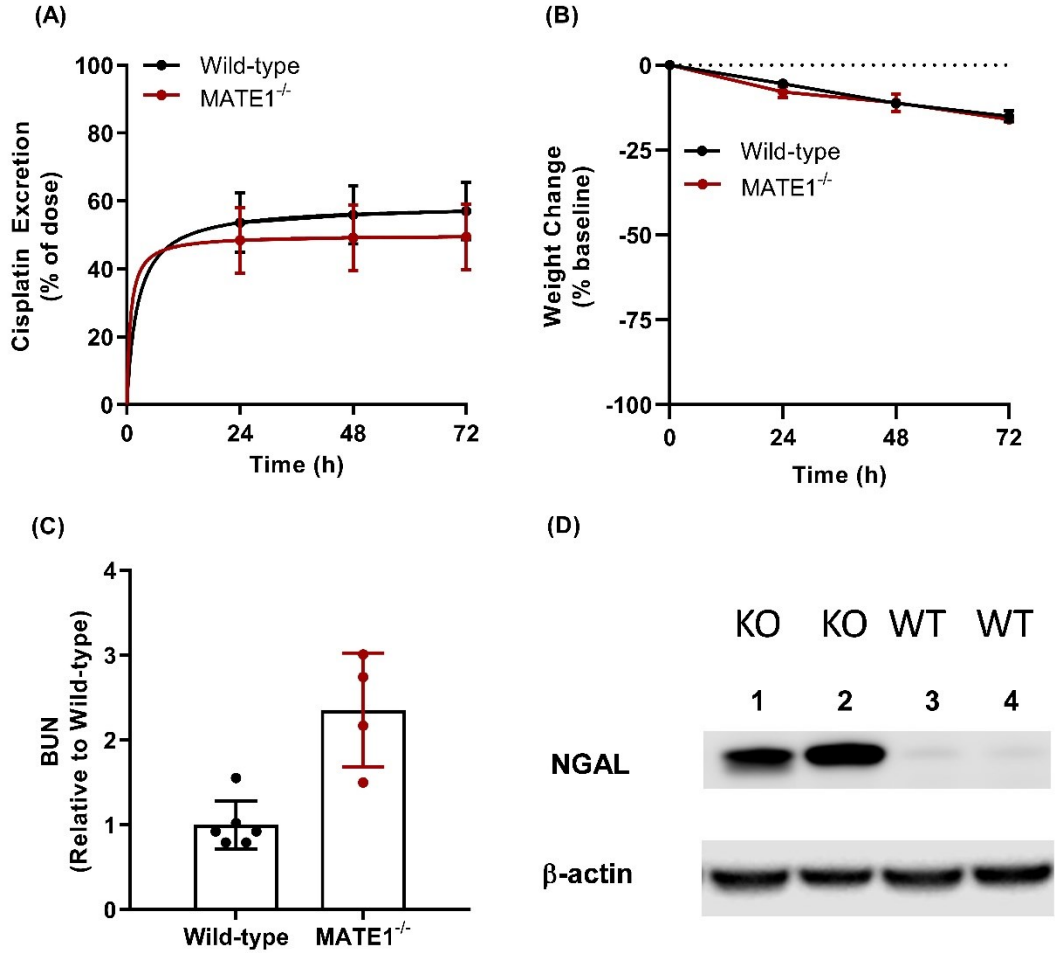
OCT1/2-, MATE1-, and OCT1/2/MATE1-deficient mice (n = 5 each), and solid lines represent concentration-time profiles of 1-NMN in wild-type mice after a single oral dose of dasatinib (15 mg/kg) ($p < 0.05$ treated vs. baseline 1-NMN level in wild-type mice). All values represent mean \pm SEM. **(C)** Plasma concentration-time profile of 1-NMN in a human patient after a single oral dose (p.o.) of dasatinib (100 mg). Dashed line represents baseline 1-NMN level in plasma. **(D)** Plasma concentration time profile of dasatinib in mice (15 mg/kg; p.o.) and a human patient (100 mg; p.o.).

Figure 15: Renal transport of oxaliplatin in mice and humans



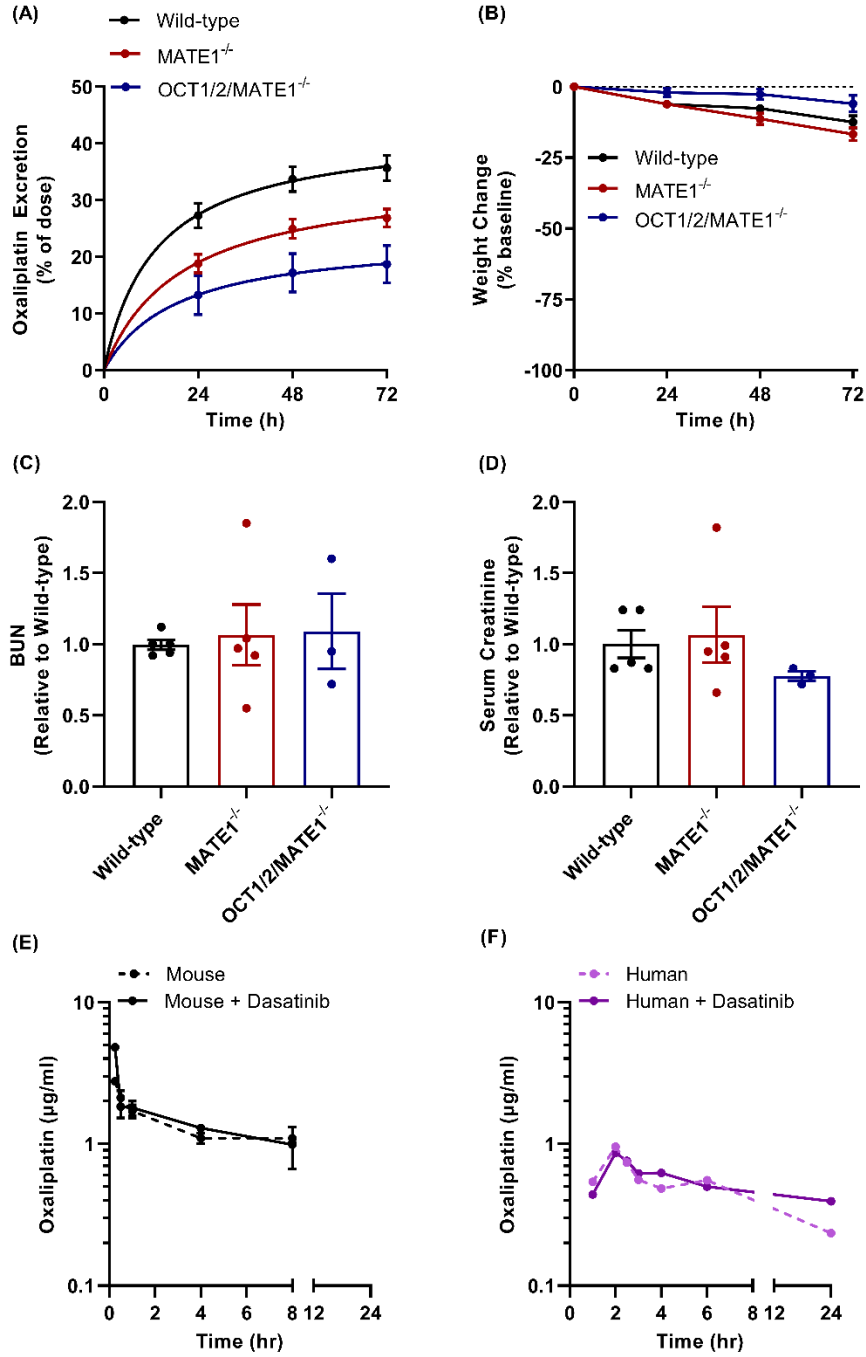
Renal transport of oxaliplatin in mice and humans. (A) Scheme depicting vectorial transport of organic cations (OC⁺) in the kidney of mice and humans. Transport activity of oxaliplatin (50 μ M) was assessed in HEK293 cells overexpressing mouse (B) and human (C) OCT2, or MATE1 transporters in the presence or absence of dasatinib (10 μ M).

Figure 16: Influence of MATE1 deficiency on cisplatin disposition



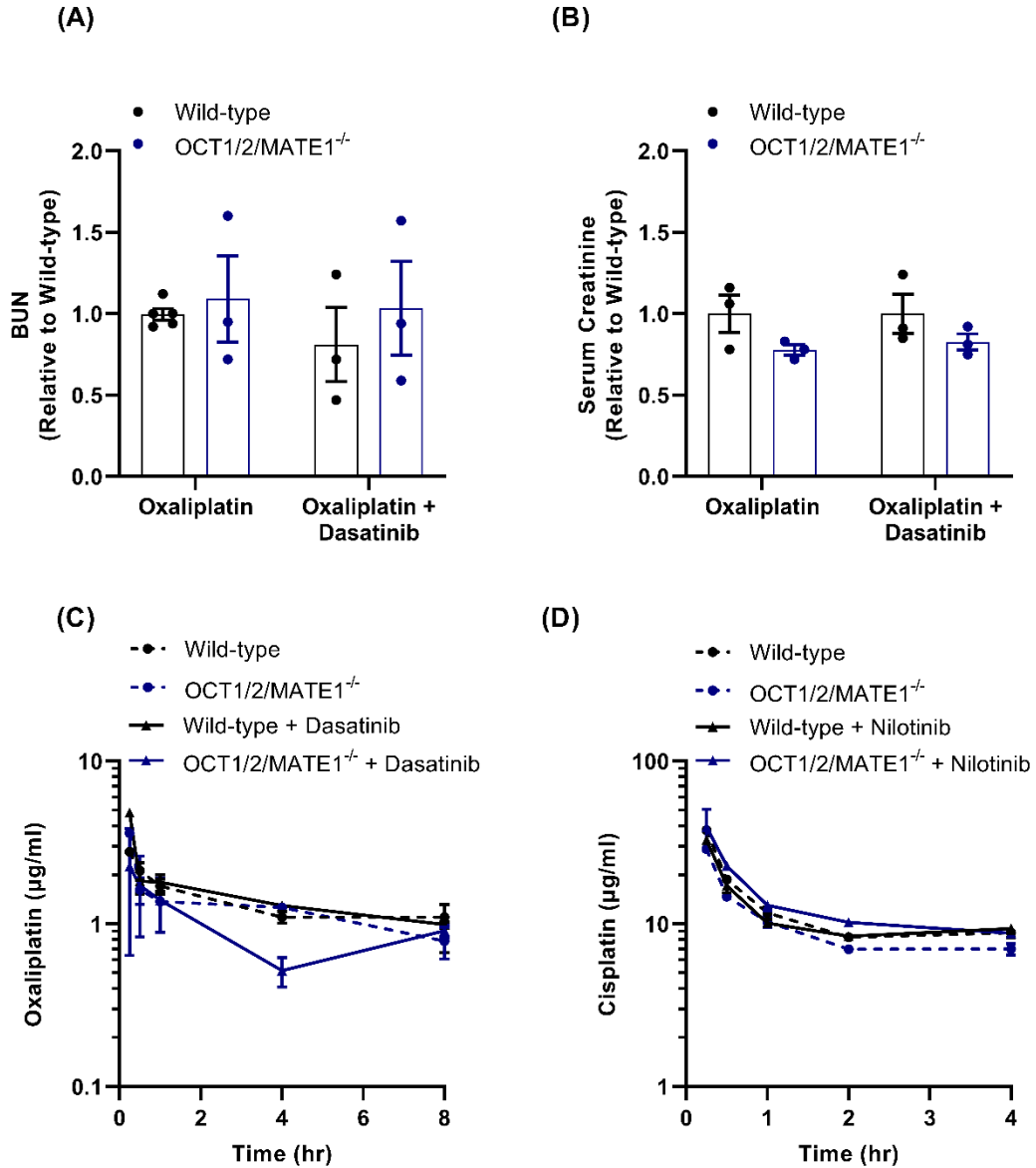
Influence of MATE1 deficiency on cisplatin disposition. Urinary excretion (A), weight loss (B), BUN (C), and the kidney damage marker NGAL (D) were analyzed in wild-type mice and MATE1-deficient mice (n=5 each) following the administration of a single dose of cisplatin (15 mg/kg, i.p.). Data represent mean ± SEM.

Figure 17: Influence of MATE1 inhibition on oxaliplatin disposition



Influence of MATE1 inhibition on oxaliplatin disposition. Urinary excretion (**A**) weight loss (**B**), blood urea nitrogen (BUN) (**C**), and serum creatinine (**D**) were assessed in wild-type, MATE1-deficient, and OCT1/2/MATE1-deficient mice (n = 5 each) following a single dose of oxaliplatin (10 mg/kg, i.p.). Data represent mean \pm SEM. Plasma concentration time profile of oxaliplatin in mice (10 mg/kg; i.p.) (**E**) and a human patient (85 mg/m²; i.v. infusion) (**F**) in the presence and absence of pre-treatment with dasatinib at the dose of 15 mg/kg in mice, and 100 mg in a human patient.

Figure 18: Influence of TKI pre-treatment on oxaliplatin and cisplatin disposition



Influence of TKI pre-treatment on oxaliplatin and cisplatin disposition. (A) BUN and **(B)** serum creatinine were assessed in wild-type mice and OCT1/2/MATE1-deficient mice (n=3 each) following the administration of a single dose of oxaliplatin (10 mg/kg,

i.p.) with and without dasatinib pre-treatment (15 mg/kg, p.o.). Data represent mean \pm SEM. Plasma concentration time profile of oxaliplatin (10 mg/kg, i.p.) with or without dasatinib pre-treatment (15 mg/kg, p.o.) **(C)** and cisplatin (15 mg/kg, i.p.) with or without nilotinib pre-treatment (10 mg/kg, p.o.) **(D)**.

Table 2: Plasma pharmacokinetic parameters of cisplatin and oxaliplatin in mice and a human patient with cancer*

Treatment	Species	C _{max} (µg/ml)	AUC (h×µg/ml)
Cisplatin	Mouse		
Wild-type		45.4 ± 2.04	43.2 ± 2.08
Wild-type + Nilotinib		37.1 ± 1.57	37.6 ± 1.57
OCT1/2/MATE1 ^{-/-}		40.2 ± 2.37	39.3 ± 1.26
OCT1/2/MATE1 ^{-/-} + Nilotinib		30.6 ± 2.77	32.2 ± 1.20
Oxaliplatin	Mouse		
Wild-type		2.76 ± 0.04	10.7 ± 1.00
Wild-type + Dasatinib		4.80 ± 0.01	12.2 ± 0.71
OCT1/2/MATE1 ^{-/-}		3.61 ± 0.18	10.5 ± 0.01
OCT1/2/MATE1 ^{-/-} + Dasatinib		3.86 ± 0.01	7.53 ± 0.90
Oxaliplatin	Human		
Oxaliplatin		0.96	11.3
Oxaliplatin + Dasatinib		0.87	11.6

*Cisplatin (15 mg/kg i.p.) and oxaliplatin (10 mg/kg, i.p.) were administered to male wild-type and OCT1/2/MATE1-deficient mice (n=5 each) with and without pretreatment with nilotinib (10 mg/kg, p.o.) or dasatinib (15 mg/kg, p.o.), respectively. The human patient received oxaliplatin as an i.v. infusion at a dose of 85 mg/m² with and without dasatinib pre-treatment (100 mg, p.o.).

3.5 Conclusions

In the present study, we identified MATE1 as a transporter that is sensitive to potent inhibition by a remarkably large number of small molecule drugs in the class of TKIs, and demonstrated through functional validation studies using genetic and pharmacological approaches that the observed inhibitory properties are potentially related to an effect on transcription. In addition, we found that some of these TKIs can inhibit renal MATE1 function *in vivo* as evidenced from their ability to modulate urinary excretion of the prototypical substrate, oxaliplatin, as well as systemic levels of the endogenous biomarker, NMN. These findings provide novel insight into the regulation of MATE1 and suggest that caution is warranted with polypharmacy regimes involving the use of certain MATE1 substrates given in combination with TKIs. This is particularly relevant in view of the fact that a large proportion of approved prescription drugs are organic cations, and that the membrane transport of many of these agents depends on facilitated carriers such as MATE1.²⁶⁷

3.6 Acknowledgments

We would like to thank Drs. Ji Young Kim and Kevin M. Huang (The Ohio State University, Columbus, OH) for assistance with the nephrotoxicity analyses, and Dr. Yan Shu (University of Maryland, Baltimore, MD) for providing MATE1-deficient mice on a C57BL/6J background.

Chapter 4. Involvement of Membrane Transporters and Dofetilide-induced Proarrhythmia

4.1. Development and Validation of a UPLC-MS/MS Analytical Method for Dofetilide

****Disclaimer****

The following chapter contains excerpts from an article published and copyrighted by

Journal of Pharmaceutical and Biomedical Analysis ²⁶⁸

4.1.1 Abstract

A novel method using UPLC with tandem mass-spectrometric detection (UPLC-MS/MS) with positive electrospray ionization was developed for the detection of the antiarrhythmic drug, dofetilide, in mouse plasma and urine. Protein precipitation was performed on 10 μ L of plasma and 2 μ L of urine samples using dofetilide-D4 as an internal standard, and separation of the analyte was accomplished on a C18 analytical column with the flow of 0.40 mL/min. Subsequently, the method was successfully applied to determine the pharmacokinetic parameters of dofetilide following oral and intravenous administration. The calibration curve was linear over the selected concentration range ($R^2 \geq 0.99$), with a lower limit of quantitation of 5 ng/mL. The intra-day and inter-day precisions, and accuracies obtained from a 5-day validation ranged from 3.00-7.10%, 3.80-7.20%, and 93.0-106% for plasma, and 3.50-9.00%, 3.70-10.0%,

87.0-106% for urine, while the recovery of dofetilide was 93.7% and 97.4% in plasma and urine, respectively. The observed pharmacokinetic profiles revealed that absorption is the rate-limiting step in dofetilide distribution and elimination. Pharmacokinetic studies illustrate that the absolute bioavailability of dofetilide in the FVB strain mice is 34.5%. The current developed method allows for accurate and precise quantification of dofetilide in micro-volumes of plasma and urine, and was found to be suitable for supporting *in vivo* pharmacokinetic studies.

4.1.2 Introduction

Dofetilide is a class III antiarrhythmic drug that inhibits the delayed rectifier potassium channel and is used to treat the recurrence of atrial fibrillation.²⁶⁹ This agent does not cause any negative inotropic, dromotropic, and chronotropic effects observed with other commonly prescribed antiarrhythmic drugs, such as amiodarone, dronedarone, or sotalol.²⁷⁰ However, the clinical use of dofetilide is associated with extensive inter-individual pharmacokinetic variability, in which mechanisms of variability remains to be elucidated. Furthermore, dofetilide has a narrow therapeutic window, and elevated plasma concentrations have been associated with QTc prolongation changes and increasing the risk of *torsade de pointes*, a potentially lethal cardiac arrhythmia.²⁷¹ Dofetilide undergoes extensive renal tubular secretion,²⁷² and the initial dofetilide dose is individualized based on an individual's creatinine clearance. Taken together, the initiation of dofetilide therapy requires inpatient hospice monitoring due to the variable response, and the potential risk of proarrhythmia. Despite the presence of its narrow

therapeutic index, mechanistic details of dofetilide elimination and the underlying causes of recurrent or drug-induced arrhythmias remain poorly understood.²⁷³ Prior studies have suggested that certain drug transporters play an important role in mediating drug-drug interactions through inhibition of renal tubular secretion of dofetilide and thus, elevating drug levels in systemic circulation that may exacerbate adverse events.^{274,275}

In parallel of a project to define the renal tubular secretion mechanisms involved in the elimination of dofetilide, we developed a new analytical method for dofetilide that is adaptable to micro-volumes of plasma and urine obtained through serial sampling in individual mice. In order to avoid the use of antisera required in previously used radioimmunoassays²⁷⁶⁻²⁷⁸ and improve on the specificity of methods based on HPLC with fluorescence detection,²⁷⁹ our method utilizes UPLC technology with tandem mass-spectrometric detection (UPLC-MS/MS). The developed method was found to provide enhanced speed, resolution, and accuracy, and was successfully applied to a pharmacokinetic application of dofetilide in mice.

4.1.3 Materials and Methods

Chemical and reagents. Dofetilide was purchased from Selleck Chemicals (100% purity, Houston, TX, USA). An internal standard of dofetilide (dofetilide-D4) was purchased from Toronto Research Chemicals Inc. (>99% purity, North York, ON, Canada). HPLC-grade acetonitrile, methanol, and formic acid were obtained from Fisher Scientific (Fair Lawn, NJ, USA). Blank plasma and urine samples were obtained from

untreated inbred wild-type mice on an FVB strain (Taconic Biosciences, Cambridge City, IN, USA).

UPLC-MS/MS conditions. The analysis was performed on a Vanquish UHPLC system, a TSQ Quantiva triple quadrupole mass spectrometer from Thermo Fisher Scientific, and Thermo Trace Finder General Quan system software (version 3.3). Chromatographic separation was accomplished on an Accucore Vanquish C18 column (2.1 mm x 100 mm, dp = 1.5 μ m, Thermo Fisher Scientific) shielded by an XBridge®BEH C18 guard column (dp = 5 μ m) by injecting sample volumes of 5 μ L. The temperature of the auto-sampler rack and the column was maintained at 4°C and 40°C, respectively. The mobile phase A contained water with 0.1% (v/v) formic acid; whereas mobile phase B contained a mixture of acetonitrile and methanol (1:3) with 0.1% (v/v) formic acid. Gradient elution (5 min) was as follows: 0 - 0.5 min, 10% of mobile phase B; 0.5 - 3.0 min, 95% mobile phase B; 3.0 - 4.0 min, 95% mobile phase B; 4.0 - 4.1 min, 10% mobile phase B; and 4.1 - 5.0 min, 10% mobile phase B. The flow rate was maintained at 0.4 mL/ min. The positive voltage applied to the ESI capillary in mass spectrometer assay was 3500 V, and the capillary temperature was 342°C with a vaporizer temperature of 358°C. The collision gas argon was used at a pressure of 1.5 mTorr. The precursor molecular ions, as well as product ions for confirmation and detection, are shown in **Table 1**.

Working solution, calibration and quality control sample. Stock solutions of dofetilide were prepared by dissolving 10 mg of dofetilide with 10 mL methanol, and working solutions were prepared by diluting the stock with methanol. The calibration

standard concentrations ranged from 5 to 1000 ng/mL. The lower limit of quantitation (LLOQ), low (QC 1), medium (QC 2), and high-quality controls (QC 3) were prepared at dofetilide concentrations of 5, 25, 75, and 750 ng/mL, respectively. A stock solution of the internal standard dofetilide-D4 was prepared at a concentration of 100 ng/mL in a mixture of acetonitrile: water (3:1, v/v). All the solutions were stored at -20°C and brought to room temperature immediately prior to use.

Method validation

Calibration curve, accuracy, and precision. The method validation was carried out according to recommendations outlined in the United States Food and Drug Administration (FDA), and the European Medicines Agency (EMA) guidelines.^{280,281} To evaluate the linearity of the dofetilide concentration-response relationships, a regression model was used by plotting data from the calibration curves as measured by the peak area ratios of analytes to IS. In the calibration curves, seven concentrations (5, 10, 50, 100, 250, 500, and 1000 ng/mL) were measured, and weighting of $1/\text{area}^2$ was used in every case. The coefficient of variance (CV) for each concentration was <15%, and <20% for the LLOQ. The intra-day precision, inter-day precision, and accuracy of LLOQ and QC samples were measured in quintuplicate at each concentration on 5 different days.^{282,283}

Selectivity, dilution, and recovery. Plasma samples from 6 different untreated mice were used to confirm selectivity, to evaluate the accuracy of sample dilution, plasma containing dofetilide at a concentration of 500 ng/mL was diluted 1:10 (v/v) in blank mouse plasma, and results within $\pm 15\%$ of nominal values were considered

sufficiently accurate. The extraction recoveries of dofetilide were calculated by comparing the peak area of QC samples with those of reference QC samples in blank plasma. The matrix effects were measured by continuous post-column infusion of the analytes in plasma from untreated mice.^{283,284}

Freeze-thaw, bench, short-term stability. The influence of freeze-thawing cycles from -80°C to room temperature on the stability of analytes was measured by analyzing plasma QC samples at low, medium, and high concentrations during three consecutive cycles. The bench stability was evaluated by leaving the QC samples in the autosampler at 4°C for a period of 24 hours, followed by re-analysis. Short-term stability was assessed for the QC samples at room temperature for 8 h.

***In vivo* pharmacokinetics studies.** *In vivo* experiments were performed in male mice from an inbred FVB strain (25-30 g) aged 8-10 weeks. All studies were approved by the University Laboratory Animal Resources (ULAR) Animal Care and Use Committee at The Ohio State University (2015A00000101-R1). Animals had free access to a standard diet and water, and were housed in a temperature- and light-controlled environment. Prior to drug administration, dofetilide was dissolved in a mixture of a sterile saline and HCl solution (399:1) with the pH adjusted to 7.4. Mice were randomly divided into two experimental groups of equal size (n=5), and received dofetilide by oral gavage at the dose of 5 mg/kg or intravenously at a dose of 2.5 mg/kg.

For pharmacokinetic studies, whole blood samples of 30 µL were collected in heparinized capillary tubes from each mouse at 5 min, 15 min, 30 min, 1 h, 3 h, and 6 h post administration of dofetilide. The samples were centrifuged at 11,000 rpm for 5 min,

and the plasma (supernatant) was placed immediately on dry ice and then stored at -80°C . Samples collected between 5 and 30 min were obtained from the submandibular vein using a 5 mm Goldenrod™ sterile animal lancet. For samples at 1 h and 3 h, mice were anesthetized under 2% isoflurane and whole blood was taken from the retro-orbital venous plexus using heparinized capillary tubes. A final sample was obtained at 6 h by cardiac puncture using a syringe and needle. This protocol was followed and adapted according to Leblanc, *et al* (2018).²⁸⁵

In case of metabolic studies, a group FBV male wild-type mice ($n=5$) were placed in Nalgene single mouse metabolic cages 3-days prior the intravenous administration of dofetilide at a dose of 2.5 mg/kg. Animals had free access to a standard diet and water, and were housed in a temperature- and light-controlled environment. Urine samples were collected in sterile 1.5 ml Eppendorf tubes at 8 h, 24 h, 48 h, and 72 h post administration of dofetilide and stored at -80°C .

Sample preparation. Prior to analysis, frozen plasma and urine samples were thawed at room temperature. Dofetilide was extracted by protein precipitation; in brief, an aliquot of 10 μL of plasma was transferred into a 0.5 mL Eppendorf tube, followed by the addition of 20 μL of methanol, and mixed with 50 μL of the internal standard, dofetilide-D4, at a concentration of 100 ng/mL in acetonitrile for 5 min. The tubes were then centrifuged at 13,000 rpm for 5 min at 4°C . Supernatants of the mixture (60 μL) and Milli-Q water (25 μL) were added to autosampler vials and vortex-mixed. Subsequently, 5 μL of the above mixture was injected into the UPLC-MS/MS system for drug quantification.

Since dofetilide is extensively eliminated through the kidneys, the accumulation in the urine samples was highly concentrated. Thus, in case of preparing urine samples, a similar procedure was followed where 2 μL of urine (versus 10 μL of plasma) were used and samples were further diluted (1:5) in 8 μL of Milli-Q water. Despite the micro-volume of urine, dofetilide was still detectable within the linear concentration range.

Pharmacokinetic data analysis. A non-compartmental analysis using Phoenix WinNonlin® version 8.0 (Certara, USA) was used to determine the pharmacokinetic parameters of dofetilide in mice receiving an oral and intravenous dose. From the slope of the log plasma concentration vs time curve, the elimination rate constant (K_{el}) was calculated following the least squares method. The terminal half-life ($T_{1/2}$) was calculated by $0.693/K_{el}$. The linear trapezoidal rule was followed to estimate the area under the plasma concentration-time curve (AUC). Peak plasma concentration (C_{max}), and time to reach peak plasma concentration (T_{max}) were determined by visual inspection of the data from the log concentration vs time curve. The absolute bioavailability (F_{abs}) was calculated by $F_{abs} = 100 \times (AUC_{po} \times D_{iv}) / (AUC_{iv} \times D_{po})$, where D_{iv} and D_{po} are the absolute doses after intravenous and oral administration of dofetilide, respectively.

Urinary excretion of dofetilide was determined based on the concentration in diluted urine measured by UPLC-MS/MS at each individual time points, collected urine volume, normalized to body weight, and expressed as a percentage to the total amount of dofetilide administered per animal.

4.1.4 Results

4.1.4.1 UPLC-MS/MS spectrometry and specificity

Mass-spectra results of dofetilide and dofetilide-D4 generated as protonated molecular ions $[M + H]^+$ are shown in **Table 3** and **Figure 19**. To obtain the highest intensity of fragmentation, mass-spectra parameters were optimized, and the collision-induced dissociation energy was enhanced. Both dofetilide and dofetilide-D4 showed a retention time of 2.16 min under optimal separation conditions. Representative chromatograms for untreated, treated, and spiked plasma and urine samples are shown in **Figure 20**. The lack of interference in the blank plasma and urine samples supports the specificity of the method.

4.1.4.2 Linearity, accuracy, precision, and selectivity

Dofetilide calibration curves were demonstrated to be linear in the concentration range of 5 to 1000 ng/mL ($R^2 \geq 0.99$). The signal to noise ratios for dofetilide at 5 ng/mL was >1000-fold in blank plasma and urine samples. Calibration curves of dofetilide in plasma and urine, assessed by performing back-calculated concentrations, showed <15% deviation from nominal values at all concentrations, and the deviation was <20% for the LLOQ. The results from a 5-day validation study are presented in **Table 4**. Intra- and inter-day accuracy values of dofetilide in plasma and urine ranged 93.0-106%, and 87.0-106%, respectively. The intra- and inter-assay precision values for the LLOQ, QCs, and diluted QC samples were 4.30-5.00%, 3.00-7.20%, and 3.80-5.80% in plasma, and 7.60-10.5%, 3.50-10.0%, 3.50-3.60% in urine, respectively. Selectivity was evaluated by

analyzing plasma samples from 6 different untreated mice. The interfering peak areas were less than 10% for the LLOQ analyte in plasma.

4.1.4.3 Recovery, matrix effect, and stability

The recovery and matrix effect of dofetilide in plasma and urine were measured at 25, 75, and 750 ng/mL. Both dofetilide in plasma and urine QCs samples showed >90% recovery. By comparing the response signal with those of standard solutions, matrix effects of dofetilide in plasma and urine were determined (**Table 5**). However, in the post-column infusion process, no matrix effects were observed. The stability data obtained during method validation are shown in **Table 6** and demonstrate that the exposure of plasma or urine samples to room temperature for a period of up to 8 hours is not associated with significant degradation of dofetilide (<15% deviation from nominal concentrations). Plasma and urine samples in the autosampler were also found to be stable at 4°C for up to 24 h.

4.1.4.4 Pharmacokinetic studies

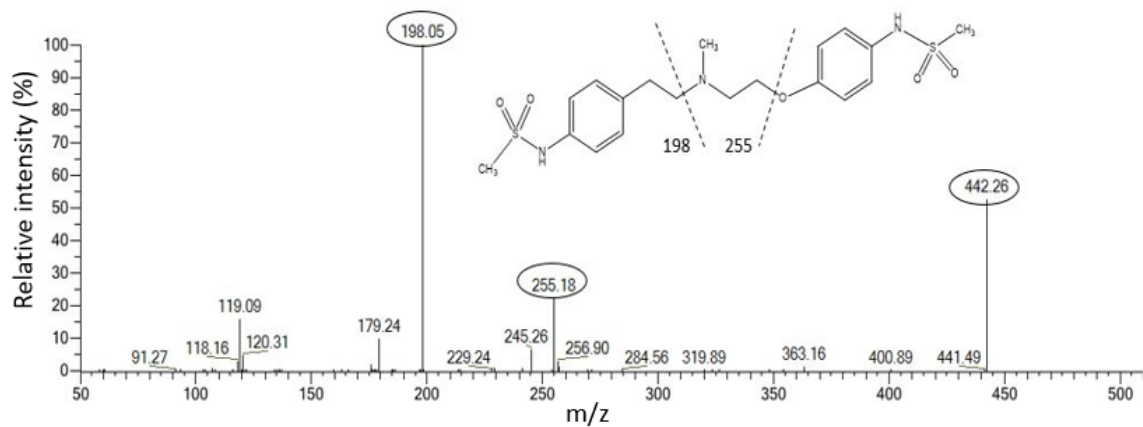
The developed analytical method was subsequently applied to establish the concentration-time profile of dofetilide. The observed mean plasma concentration-time curves after oral (5 mg/kg) and intravenous (2.5 mg/kg) administration of dofetilide are shown in **Figure 21**, and pharmacokinetic parameters derived from a non-compartmental analysis are shown in **Table 7**. The concentration-time profiles associated with oral administration of dofetilide exhibit typical flip-flop kinetics, indicating that dofetilide

distribution and elimination is rate-limited by absorption. The analysis of dofetilide excretion in urine by administering a single-dose (2.5 mg/kg; i.v.) is shown in **Figure 21**.

Table 3: Precursor molecular/product ion for quantification, confirmation, and detection parameters for each analyte

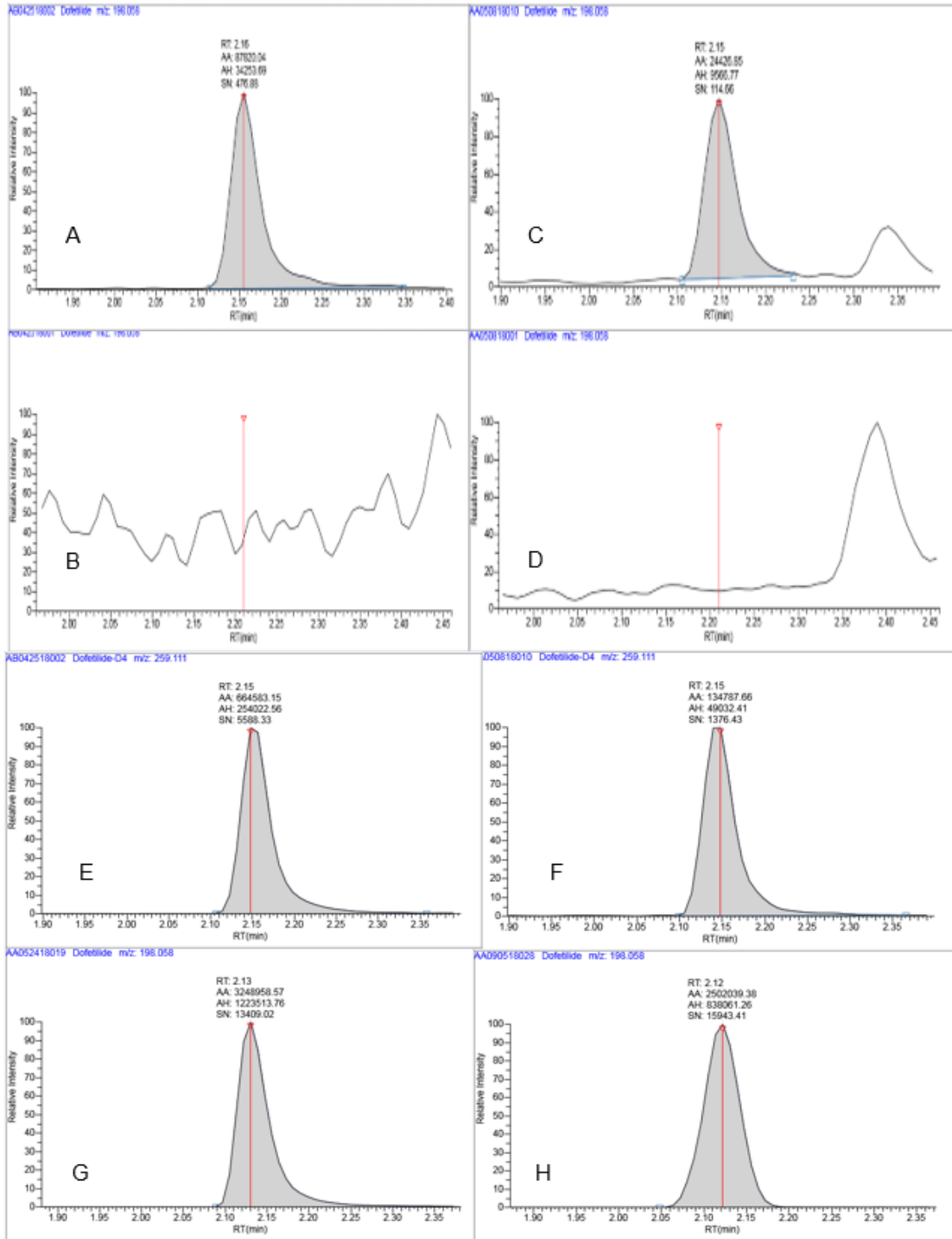
Analyte	Polarity	Precursor (m/z)	Product (m/z)	Confirmation (m/z)	Collision Energy (V)	RF Lens (V)
Dofetilide	Positive	442.26	198.05	255.04	26.38	86
Dofetilide - D4	Positive	446.23	259.18	N/A	21.43	88

Figure 19: MS/MS chromatograms and proposed fragmentation pathways of dofetilide



MS/MS chromatograms and proposed fragmentation pathways of dofetilide.

Figure 20: Representative chromatograms of dofetilide analytes



Representative chromatograms of dofetilide analytes. Representative chromatograms spiked with (A) a concentration of 5 ng/mL dofetilide in plasma, (B) blank plasma, (C) a concentration of 5 ng/mL dofetilide in urine, (D) blank urine, (E) a concentration of 100 ng/mL dofetilide-D4 in plasma, (F) a concentration of 100 ng/mL dofetilide-D4 in urine, (G) a dofetilide plasma sample in 5 min after oral administration, (H) a dofetilide urine samples in 24 h after oral administration.

Table 4: Assay performance data for the quantitation of dofetilide in mouse plasma and urine

	Concentration (ng/ml)	Intra-assay (%)	Inter-assay (%)	Accuracy (%)
In plasma				
LLOQ	5	4.28	4.98	93.83
QC 1	25	3	3.82	92.49
QC 2	75	7.1	7.18	103.31
QC 3	750	5.03	4.87	105.94
Dilution (1:10)	500	3.84	5.78	108.36
In urine				
LLOQ	5	7.57	10.46	107.29
QC 1	25	3.56	3.68	87.26
QC 2	75	3.54	4.51	105.26
QC 3	750	9.13	10.34	106.26
Dilution (1:10)	500	3.55	3.5	108.34

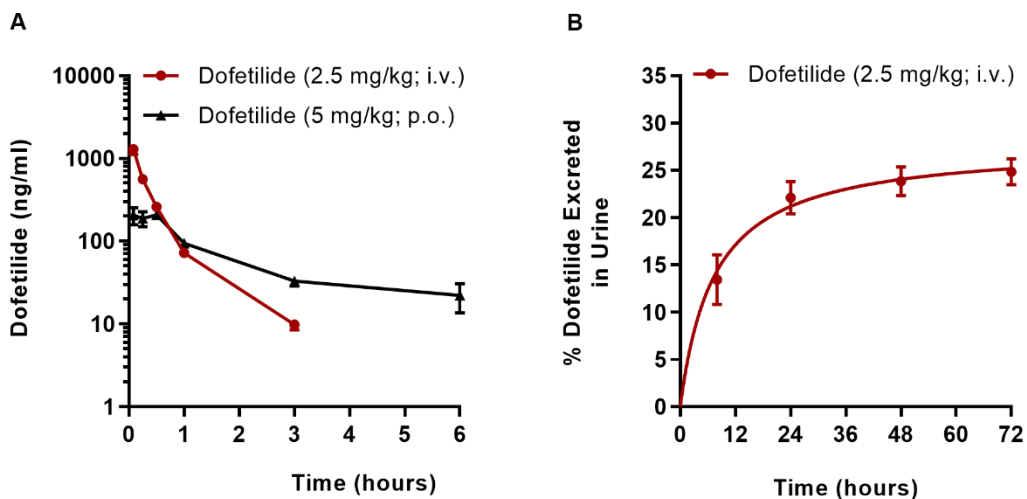
Table 5: Recovery and matrix effect of dofetilide and its metabolites in mouse plasma

Concentration (ng/mL)	Dofetilide in plasma		Dofetilide in urine	
	Absolute Recovery (%)	Matrix Effect (%)	Absolute Recovery (%)	Matrix Effect (%)
25	92.7 ± 3.01	-0.29 ± 8.76	93.2 ± 16.9	2.99 ± 9.75
75	91.3 ± 5.02	-1.44 ± 5.07	97.9 ± 11.6	1.38 ± 3.92
750	97.1 ± 8.73	-0.06 ± 14.5	110 ± 4.98	-3.21 ± 2.33

Table 6: Short-term stability of dofetilide and its metabolites in mouse plasma and urine

Concentration (ng/ml)	Dofetilide in plasma		Dofetilide in urine	
	CV (%)	Accuracy (%)	CV (%)	Accuracy (%)
25	3.38	106	6.06	107
75	1.52	113	3.60	112
750	1.38	111	0.85	114

Figure 21: Concentration of dofetilide in plasma and urine



Concentration of dofetilide in plasma and urine. (A) Mean plasma concentration-time profiles of dofetilide after an oral (5 mg/kg) and intravenous (2.5 mg/kg) administration in FVB male mice (mean \pm SEM, n=5). (B) Urinary excretion-time profile of dofetilide after an intravenous (2.5 mg/kg) administration in FVB male mice (mean \pm SEM, n=5).

Table 7: Pharmacokinetics parameters of dofetilide oral and IV administration in mice

Parameter	Dofetilide (5 mg/kg; p.o.)	Dofetilide (2.5 mg/kg; i.v)
C _{max} (ng/mL)	245 ± 73.9	1296 ± 397
T _{1/2} (h)	1.46 ± 0.53	0.75 ± 0.42
AUC _{last} (ng*h/mL)	329 ± 41.4	475 ± 123
T _{max} (h)	0.29 ± 0.24	
F (%)	34.5	

4.1.5 Discussion

The elimination of dofetilide is predominantly mediated by glomerular filtration and tubular secretion, yet the mechanism by which this occurs remains poorly understood. Since clinical drug interactions with dofetilide pose increased risk for patients developing proarrhythmia, drug-drug interaction studies are further warranted to fully establish patient covariates such as renal transport function, genetic polymorphisms, and concomitant use of other medications which negatively impact the narrow therapeutic window of dofetilide. Such studies require analyzing plasma and urine samples in rodent animals by administering single and multiple doses of dofetilide along with other contraindicated drugs. Therefore, to elucidate the mechanism(s) contributing to pharmacokinetic variability, a rapid and accurate analytical method was developed to quantify dofetilide concentrations in both mice plasma and urine.

Several analytical methods were previously developed to measure plasma concentrations of dofetilide in different animal species using radioimmunoassays,^{276,286} and HPLC with fluorescence detection technique.²⁷⁹ However, in spite of having lower LOQ of 1.7 ng/mL and 2.5 ng/mL for dofetilide quantification by Kaddar et. al. 2013²⁷⁹ and Walker et. al. 1991,²⁷⁶ respectively, the drawbacks of these techniques were limited to using high plasma (400 μ L) in guinea pig²⁷⁹, and urine volume (100 μ L).^{276,277} Both of these analytical methods^{279,286} require high sample retention time of 43 and 44 min, respectively. In addition, some analytical method also requires the usage of radioactive biohazard conducting radioimmunoassays that involve in using the selective antibody for each analyte to be measured.^{276,286} As a result, analyzing plasma and urine samples could

be expensive, and likely to cause cross-reactivity among antibodies which could lower the specificity of an assay.

In contrast, our method uses UPLC technology with tandem mass-spectrometric detection (UPLC-MS/MS) for the first time which requires less run time (5 min), provides accurate and cost-effective analysis of dofetilide using very low sample volume (2-10 μ L). This method also reduces the usage of radioactive chemicals and immunological reagents in analyzing plasma and urine samples.

In this analytical method, chromatographic separation of dofetilide was performed in a gradient elution mode having water with 0.1% (v/v) formic acid as a mobile phase A, and a mixture of acetonitrile and methanol (1:3) with 0.1% (v/v) formic acid as a mobile phase B. A mixture of acetonitrile-methanol (3:1, v/v) was used for an effective protein precipitation in plasma which illustrates a high linearity, intra-day, and inter-day within the concentration range of 5-1000 ng/mL. This method also exhibits a good recovery (>90%), intra-day and inter-day accuracy, and precision in both plasma and urine.

Pharmacokinetic analysis of dofetilide (5 mg/kg, oral; 2.5 mg/kg, intravenous) demonstrated that absorption is the rate-limiting step in dofetilide distribution and elimination. This phenomenon is also known as flip-flop kinetics, an exception to the usual case ($k_{el} > k_a$), in which rate of elimination (k_{el}) is greater than the rate of absorption (k_a),^{287,288} thus, an increase in oral half-life (1.46 ± 0.50 h) compared to intravenous half-life (0.75 ± 0.40 h) was observed. Our pharmacokinetic studies illustrate that the absolute bioavailability of dofetilide is 34.5% in the FVB strain mice.

Furthermore, the 72-hour urinary excretion profile shows that 25.3% of dofetilide (2.5 mg/kg) dose is eliminated through urine post intravenous administration.

4.1.6 Conclusion

A sensitive UPLC-MS/MS method was developed and validated for the quantification of dofetilide in plasma and urine from mice. The analysis requires micro-volume aliquots of 2-10 μ L, yet retains adequate sensitivity (LLOQ, 5 ng/mL), resolution, and speed (run time, 5 min). The developed method was also found to be sufficiently accurate and precise, independent of the matrix, to support pharmacokinetic studies in mice undergoing serial sampling. The results from preclinical pharmacokinetics study illustrate that absolute bioavailability of dofetilide is 34.5% FVB strain mice. The method is currently being implemented in studies that focus on the role of renal tubular solute carriers in the urinary excretion of dofetilide as a critical determinant of drug clearance. This analytical method is also being applied to investigate the transporter-mediated drug-drug interactions and evaluate the changes in pharmacokinetic parameters using contraindicated drugs of dofetilide such as cimetidine, verapamil, and ketoconazole.

4.1.7 Acknowledgments

The authors would like to gratefully acknowledge colleagues in Experimental Cancer Pharmacology Laboratory at The Ohio State University, OH. The project was supported by the National Institutes of Health (NIH) [grant number R01CA215802].

4.2 Contribution of MATE1 to Dofetilide-induced Proarrhythmia

4.2.1 Abstract

Dofetilide is a rapid delayed rectifier potassium current (I_{Kr}) inhibitor used to prevent the recurrence of atrial fibrillation and flutter. The clinical use of this drug is associated with increases in QTc interval, which can exacerbate cardiac arrhythmias. The mechanisms involved in dofetilide's renal tubular secretion and its uptake into cardiomyocytes remain unknown. Our *in vitro* studies demonstrated that dofetilide is a substrate of MATE1. Deficiency of MATE1 was associated with increased plasma concentrations of dofetilide and with a significantly reduced urinary excretion (3-fold in females and 5-fold in males, respectively). Dofetilide accumulation in *ex vivo* cardiomyocytes was increased by 2-fold in MATE1-deficient females, and pre-incubation with the MATE1 inhibitor, e.g. cimetidine, significantly reduced dofetilide uptake in wild-type cardiomyocytes. Neonatal mice having deficiency of MATE1 demonstrated significant increase in QTc prolongation compared with wild-type. In addition, we found that CYP3A does not involve in the metabolism of dofetilide. Several contraindicated drugs listed in the dofetilide prescribing information, including bictegravir, cimetidine, ketoconazole, verapamil increased dofetilide plasma exposure in wild-type mice by >1.6-fold. A physiologically-based pharmacokinetic (PBPK) model of dofetilide was developed by incorporating data from *in vitro*, preclinical, and clinical pharmacokinetic studies in healthy volunteers. The model reasonably predicted changes in dofetilide exposure after co-administration of cimetidine (65.5% predicted versus 58% observed

increase) and ketoconazole (41.1% predicted versus 41% observed increase) as well as reduced renal clearance with cimetidine (38.92% predicted versus 43.7% observed). These findings provide a novel insight that renal tubular secretion of dofetilide is mediated by MATE1 and is sensitive to inhibition by widely used prescription drugs. Furthermore, deficiency of MATE1 not only reduces urinary excretion of dofetilide but also increases accumulation in the heart which may contribute to individual variation in response.

4.2.2 Introduction

Atrial fibrillation (AFib) is one of the most commonly encountered cardiac arrhythmia in clinical practice globally.²⁸⁹ Data suggests that an estimated 2.7 - 6.1 million people in the United States had atrial fibrillation between 1990 and 2013.²⁹⁰ The prevalence of atrial fibrillation is predicted to affect about 12 million people in the USA and 17 million people in Europe by 2050, and people over the age of 65 are particularly prone to experience atrial fibrillation.^{291,292} Some predictive models and preventative interventions have been proposed to identify patients based on age, race, blood pressure, smoking, diabetes, and prior history of myocardial infarction, but primary prevention strategies for AFib have yet to be established.^{293,294} Due to atrial fibrillation, the rate of hospitalization, morbidity, and financial burden is increasing each year in the USA.²⁹⁵⁻²⁹⁸ A retrospective analysis of national incremental cost for atrial fibrillation demonstrated an estimated of \$6.0 billion in between 2004 and 2006.²⁹⁹

Dofetilide, a class III antiarrhythmic drug, is widely used for the treatment of AFib and flutter, by acting on a rapid delayed rectifier potassium current (I_{kr}) and inhibition of the efflux of potassium.²⁶⁹ Dofetilide does not cause any negative inotropic, dromotropic, and chronotropic effects observed with other commonly prescribed antiarrhythmic drugs, such as amiodarone, dronedarone, or sotalol.²⁷⁰ Furthermore, due to the lack of serious adverse effects and relatively low morbidity rate as compared with other antiarrhythmic drugs, dofetilide has become standard of care in the treatment of atrial fibrillation. However, the clinical use of dofetilide is associated with extensive inter-individual pharmacokinetic variability, and mechanisms underlying this variability remain to be elucidated. Furthermore, dofetilide has a relatively narrow therapeutic window, and elevated plasma concentrations have been associated with QTc prolongation and increase the risk of *torsade de pointes* (TdP), a potentially lethal cardiac arrhythmia.²⁷¹ It has been reported that females are exposed to higher dofetilide plasma concentrations (14-22%) than males,²⁷² and the rate of discontinuation and dose reduction due to QTc prolongation is higher in females.³⁰⁰ Dofetilide undergoes extensive renal tubular secretion,²⁷² and the initial dofetilide dose is individualized based on an individual's creatinine clearance. Taken together, the initiation of dofetilide therapy requires inpatient monitoring due to the variable response and the potential risk of proarrhythmia. Despite the presence of a narrow therapeutic index, mechanistic details of dofetilide elimination and the underlying causes of recurrent or drug-induced arrhythmias remain poorly understood.²⁷³ Prior studies have suggested on the basis of pharmacokinetic drug-drug interactions that certain renal transporters play a role in the

tubular secretion of dofetilide and consequently, elevating drug levels in the systemic circulation may exacerbate the adverse events.^{274,275}

Multidrug and toxin extrusion protein (MATE1, *SLC47A1*) is predominantly expressed in the brush border membrane of renal proximal tubular cells and canalicular membrane of hepatocytes.^{46,301} In addition, MATE1 is expressed at detectable levels in skeletal muscle, adrenal gland, testes, and the heart.^{46,302} Several prior studies have shown that MATE1 plays an important role in the distribution and elimination of endogenous and exogenous cationic compounds,³⁰³ and functional variation or polymorphism of MATE1 can affect the renal clearance of such compounds, including metformin and cimetidine.^{14,47,68,304} In addition, there is evidence that suggests that inhibition of MATE1 could increase the area under the plasma concentration-time curve (AUC) of certain drugs.³⁰⁵ Since anti-coagulant, and/or beta-blocker therapy is commonly used in conjunction with dofetilide as a preferred prophylactic treatment,³⁰⁶ potential drug-drug interactions may occur due to inhibition of MATE1 transport function. This in turn may influence renal clearance of dofetilide, and suggest that inter-individual variability in the expression of MATE1 may influence dofetilide plasma concentrations and the development of proarrhythmia. Therefore, elucidation of the mechanisms by which dofetilide is eliminated is urgently needed in order to derive preventative and/or intervention strategies that could effectively mitigate the occurrence of QTc prolongation and incidence of recurrent arrhythmia without affecting the efficacy of dofetilide.

Physiologically-based pharmacokinetics (PBPK) model provides a comprehensive representation of an organism's physiology that allow to predict organs that are most

relevant to absorption, distribution, metabolism, and excretion of drugs due to their physiological/pharmacological function.^{307,308} PBPK models also incorporate inter-individual variability, thus, provide the ability to predict disposition characteristics of dofetilide and need for dose adjustments in special populations,^{309–311} but this has not been previously attempted with dofetilide. Here, we investigate the contribution of MATE1 to the disposition of dofetilide, and develop physiologically-based pharmacokinetics (PBPK) model to predict transporter mediated drug-drug interactions (DDIs) in human.

4.2.3 Materials and Methods

Chemical and Reagents. Parental human embryonic kidney (HEK293), and chinese hamster ovary (CHO) cells were obtained from American Type Culture Collection (ATCC; Manassas, VA, USA). The cDNAs for the mouse and human plasmids of OCT1, OCT2, OCT3, OCTN1, OAT1, OAT3, or MATE1 were obtained from Origene (Rockville, MD, USA), and the reconstructed cDNAs were subcloned into an empty vector containing pcDNA5/FRT. The vector was transfected into HEK293 cells using the Flp-In system (Invitrogen, Waltham, MA, USA) and selected for expression using geneticin (G418). Cells were cultured in DMEM supplemented with 10% FBS and grown in a humidified incubator containing 5% CO₂ at 37°C. Contraindicated drugs of dofetilide were obtained from Sigma-Aldrich (St. Louis, MO, USA) or Selleckchem (Houston, TX, USA). Dofetilide radiolabeled compound were obtained from American Radiolabeled Chemicals (St. Louis, MO, USA).

Cellular accumulation. Uptake experiments in human AC-16 cardiomyocytes, HEK293 cells overexpressing OCT1, OCT2, OCT3, OCTN1, or MATE1, and CHO cells overexpressing OAT1 and OAT3 were performed with radiolabeled [³H] dofetilide using standard methods.^{216,217} The cell culture and uptake conditions for cells expressing mMATE1 or hMATE1 were described previously.^{207,215} All results were normalized to uptake values in cells transfected with an empty vector or DMSO-treated groups. In brief, cells were seeded in 12- or 24-well plates in phenol red-free DMEM containing 10% FBS, and were incubated at 37°C for 24 h. After removal of the culture medium and rinsing with PBS, cells were preincubated with either DMSO or inhibitors for 15 min followed by addition of indicated substrate for 15 min. Uptake studies were generally done with [¹⁴C] TEA (2 μM) or [³H] dofetilide (1 μM) in the presence or absence of inhibitors for a period of 15 min, unless stated otherwise. The uptake experiment was terminated by washing three times with ice-cold PBS. Cells were lysed in 1N NaOH at 4°C overnight, and then the solution was neutralized with 2M HCl. Total protein was measured using a Pierce BCA Protein Assay Kit (Thermo Scientific, Waltham, MA), and total protein content was quantified using a microplate spectrophotometer. Intracellular drug concentrations were determined in the remaining cell lysate by liquid scintillation counting using a scintillation counter.

The transcellular transport assay of [³H] dofetilide or [¹⁴C] metformin (1 μM) were performed in monolayers of single-transfected MDCK cells overexpressing human OCT2 or MATE1, and double-transfected human OCT2/MATE1 as previously

described.^{312,313} Transcellular transport was quantified by measuring the amount of dofetilide appearing in the apical compartment after 60 min of incubation.

***Ex vivo* cardiomyocytes uptake.** Cardiomyocytes from wild-type and MATE1-deficient mice were isolated as previously described^{314,315} and conducted the *ex vivo* cardiomyocyte uptake assay of dofetilide. Briefly, hearts from wild-type and MATE1-deficient mice were quickly removed and perfused on a Langendorff's apparatus at 37°C. After ~5 min perfusion with nominally Ca²⁺-free tyrode solution (containing (in mM): 140 NaCl, 5.4 KCl 0.5 MgCl₂, 10 Hepes and 5.6 glucose; pH 7.3), the perfusate was then switched to tyrode solution containing Liberase Blendzymes (Roche, Applied Science, IN, USA) for digestion of the connective tissue. After ~20 min digestion, cardiomyocytes were isolated from dissected and triturated heart and stabilized in BSA containing tyrode solution.

Isolated cardiomyocytes were then plated in 12 wells plate containing Ca²⁺ and Mg²⁺ free Hank's balanced salt solution. Cells were preincubated with either DMSO or cimetidine (25 µM) for 15 min followed by addition of [³H] dofetilide (2 µM) for 30 min. The uptake experiment was terminated by washing three times with ice-cold PBS. Cells were lysed in 1N NaOH at 4°C overnight, and then the solution was neutralized with 2M HCl. Total protein was measured using a Pierce BCA Protein Assay Kit (Thermo Scientific, Waltham, MA). Intracellular drug concentration of dofetilide was measured in the remaining cell lysate by liquid scintillation counting using a scintillation counter.

Gene expression analysis. RNA was isolated from wild-type adult and neonatal mouse heart and kidney (30 mg) as well as cardiomyocyte cells isolated from wild-type

and MATE1-deficient mice. Tissues and cardiomyocytes were homogenized and then extracted RNA using EZNA Total RNA Kit extraction kit (Cat# R6834-02, Omega Bio-tek, Norcross, GA). cDNA was generated from 2 µg of RNA using qScript XLT cDNA Supermix (Cat# 95161-100, Quantabio, Beverly, MA). Real-time reverse transcriptase PCR (RT-PCR) was performed with TaqMan primer (Mm00840361_m1, Thermo Fisher Scientific, Waltham, MA) and TaqMan Fast reagents. Reactions were carried out in triplicate, and normalized to Gapdh (Mm99999915_g1, Thermo Fisher Scientific, Waltham, MA).

Protein analysis. Isolated heart from wild-type and MATE1-deficient mice were extracted and lysed using sonication. Pierce Bicinchoninic Acid (BCA) Protein Assay Kit (Thermo Fisher Scientific, Waltham, MA) was used to determine protein concentrations. Next, an equal amount of protein was separated on a Bis-Tris 4-12% SDS-polyacrylamide gel with MOPS buffer according to the instructions from manufacturer (Life Technologies, Grand Island, NY) and transferred to PVDF membranes. Western blot analysis was performed using antibodies against mouse MATE1 (Cat # 20898-1-AP) obtained from Proteintech Group, Inc (Rosemont, IL), GAPDH (Cat # 2118), and HRP-conjugated secondary anti-rabbit (Cat # 7074) obtained from Cell Signaling Technology (Danvers, MA). Proteins were visualized by chemiluminescence using the SignalFire ECL Reagent (Cell Signaling Technology, Danvers, MA) or SuperSignal West Femto Maximum Sensitivity Substrate (Invitrogen, Carlsbad, CA) using film.

Electrocardiographic recordings (ECG). Continuous ECG recordings (PL3504 PowerLab 4/35, ADInstruments) were obtained from wild-type and MATE1-deficient

neonatal mice (1 day old) according to previously described method.^{316,317} Briefly, baseline ECG was recorded for 5 min, neonatal mice were received a single intraperitoneal dose of dofetilide (0.5 mg/kg) dissolved in sterile saline containing DMSO (20:1), and ECG recording continued for 20 min as described previously.³¹⁸ ECG recordings were analyzed using the LabChart 7.3 software (ADInstruments). QT interval was measured before and after the administration of dofetilide from the beginning of the QRS complex to the isoelectric baseline for T waves.³¹⁷ Heart rate-corrected QT (QTc) intervals were then obtained using the formula $QTc = QT/(RR/100)^{1/2}$.³¹⁹

Animal Models. All animals were housed in a temperature-controlled environment with a 12-hour light cycle, given standard diet and water *ad libitum*, and handled according to the Animal Care and Use Committee of The Ohio State University, under an approved protocol (2015A00000101-R2). All experiments were performed with male and female mice from inbred wild-type strain (FVB) or with age- and sex-matched (8-15 weeks) genetically engineered mice with deficiency of all CYP3A isoforms (CYP3A^{-/-}), OCT1/2-deficient mice (OCT1/2^{-/-}), MATE1-deficient mice (MATE1^{-/-}), and OCT1/2 and MATE1-deficient mice (OCT1/2/MATE1^{-/-}). Dr. Yan Shu (University of Maryland, Baltimore, Maryland USA) provided the MATE1-deficient mice (backcrossed to an FVB background). The loss of MATE1 increased the systemic exposure and accumulation in the heart, liver, and kidneys of cationic-type substrates.^{42,320} OCT1/2 and MATE1-deficient mice were generated by backcrossing to FVB wild-type (male and females) and subsequently, OCT1/2 and MATE1 heterozygotes bred together. The deletion of OCT1/2 and MATE1 were verified at the level of DNA by PCR.³²¹

Pharmacokinetic studies. For pharmacokinetic studies, plasma and tissue samples were collected from both male and female wild-type FVB mice (8-15 weeks old), and age-matched OCT1/2-deficient (OCT1/2^{-/-}), MATE1-deficient (MATE1^{-/-}), and mice deficient for OCT1, OCT2, and MATE1 (OCT1/2/MATE1^{-/-}) following an established protocol.²⁸⁵ Dofetilide was administered as a single oral (5 mg/kg) and intravenous (2.5 mg/kg) dose dissolved in sterile saline-1M HCl (399:1) with pH adjusted to 7.4. All the contraindicated drugs of dofetilide e.g. bicitegravir (5 mg/ml), cimetidine (20 mg/ml), ketoconazole (10 mg/ml), trimethoprim (20 mg/ml), and verapamil (2 mg/ml) were dissolved in PEG400, and were given orally 30 min prior to the administration of dofetilide. In order to determine the plasma concentration of dofetilide in the presence or absence of contraindicated drugs serial whole blood samples (0.083, 0.25, 0.5, 1, 3, and 6 h) were collected from the submandibular vein (3x), retro-orbital sinus vein (2x) and cardiac puncture at the terminal time-point. Blood samples were centrifuged at 13,000 rpm for 5 min, and the plasma supernatants collected and stored at -80°C until analysis. Dofetilide concentration in heart was measured in wild-type and MATE1-deficient mice at 15 min after a single intravenous administration of dofetilide (2.5 mg/kg) via caudal vein.

To measure dofetilide concentration in urine, both male and female wild-type and age-matched OCT1/2^{-/-}, MATE1^{-/-}, and OCT1/2/MATE1^{-/-} mice were placed in Nalgene single mouse metabolic cages 3-days prior the intravenous administration of dofetilide at a dose of 2.5 mg/kg. Animals had free access to a standard diet and water, and were housed in a temperature- and light-controlled environment. Urine samples were collected

in sterile 1.5 ml Eppendorf tubes at 24 h, 48 h, and 72 h post administration of dofetilide and stored at -80°C until analysis. Plasma, urine, and tissue samples were analysis by a validated method based on reversed-phase liquid chromatography coupled to tandem mass-spectrometric detection (LC-MS/MS).³²²

Pharmacokinetic parameters were calculated by non-compartmental analysis using Phoenix WinNonlin version 8.2 (Certara, USA). Peak plasma concentration (C_{\max}) was determined by visual inspection of the data from the concentration-time curves. The linear trapezoidal rule was used to obtain the area under the plasma concentration-time curve (AUC) over the sample collection interval. The relative heart exposure of dofetilide was calculated by determining the dofetilide concentration in the heart (ng/mg tissue), corrected for contaminating blood, and dividing by the corresponding dofetilide concentration in plasma (ng/mL) at 15 min time-point.

For TEA experiments, cimetidine (100 mg/kg) was given orally in wild-type and MATE1-deficient mice 30 min prior to the intravenous administration of [^{14}C] TEA (0.2 mg/kg) via caudal vein. Plasma samples were then collected after 15 min and measured TEA concentration by scintillation counter.

Dofetilide SimCYP physiologically based pharmacokinetic (PBPK) model.

Input parameters. PBPK model of dofetilide was developed using a physiologically-based PBPK software, SimCYP® (Sheffield, UK, Version 19). Simulations were carried out in software's built-in healthy volunteer virtual population from the ages of 20-50 years. Data from in vitro dofetilide uptake, inhibition of transport

function, and observed pharmacokinetic and drug-drug interactions data in healthy subjects were used to develop the model (**Table 12**). To simulate the effect of inhibitors (e.g. cimetidine, ketoconazole) on dofetilide pharmacokinetic profile, inhibitor models from software's drug library were directly used. The absorption of dofetilide was simulated using the first order absorption model with an absorption rate constant (k_a) estimated from the plasma concentration-time profiles.²⁷⁷ The volume of distribution at steady-state was estimated using the plasma concentration-time profiles. The multicompartment mechanistic kidney model (EGD) was used to incorporate the glomerular filtration and active renal secretion of dofetilide.³²³ Active secretion of dofetilide was modeled measuring V_{max} and K_m values for OCT2 and MATE1. Relative activity factor (RAF) value was set to 1 and 0.25 for OCT2 and MATE1, respectively.

PBPK Modeling Strategy. Dofetilide PBPK model was developed following top-down approach. The multicompartment mechanistic kidney model was used to incorporate the glomerular filtration and active renal secretion of dofetilide.³²³ The modeling strategy employed in this project was the following: 1) The active secretion of dofetilide was defined to be via OCT2 and MATE1 on the basolateral and apical membrane of the proximal tubular cells, respectively. 2) Dofetilide PBPK model was developed using *in vitro* and clinical data. 3) The model was optimized by using dofetilide plasma concentration-time profiles from healthy volunteers. 4) The model was tested by using dofetilide dose given orally (0.5 mg, twice per day, BID), and intravenous infusion (0.5 mg) over 90 min, and the results were compared with clinical studies. 5)

Prediction of dofetilide drug-drug interactions with cimetidine and ketoconazole were carried out using software's drug library and compared with clinical studies.

Dofetilide Clinical Data. Plasma concentration-time profiles data after oral administration of dofetilide at a dose of 0.5 mg, BID, and an intravenous infusion 0.5 mg over 90 min in healthy volunteers were used from a published article to build the model.²⁷⁷ To evaluate the model predicted DDI with cimetidine and ketoconazole, DDI study reports by US FDA clinical pharmacology and biopharmaceutics review(s) were used.³²⁴

PBPK DDI simulations. The drug-drug interactions between dofetilide and inhibitors was assumed to occur at the level of the basolateral uptake transporter OCT2 and apical efflux transporter MATE1. The K_i and $f_{u,inc}$ values were obtained from *in vitro* experiments. In the simulations, cimetidine was administered orally at a dose of 400 mg BID for 3 days while ketoconazole was given orally at a dose of 400 mg QD for 7 days. Inhibitors were administered from day 1 along with dofetilide through day 3 and day 7 for cimetidine and ketoconazole, respectively. To evaluate the effect of the interaction between dofetilide and inhibitors, results were calculated and compared with observed and predicted AUC_{0-last} and C_{max} data.

4.2.4 Results and Discussion

4.2.4.1 Identification of MATE1 as a high-affinity carrier of dofetilide

Dofetilide is a basic compound that is partially ionized under normal physiological conditions (pH 7.4).²⁸⁶ The moderately lipophilic dofetilide is slightly

cationic,²⁷⁷ and its extensive elimination through kidney have triggered our efforts to connect uptake of dofetilide to organic cation-type transporters. To identify an uptake transporter of dofetilide, we initially performed a screen in cells overexpressing organic cation transporters (OCT1, OCT2, OCT3, OCTN1), organic anion transporters (OAT1, OAT3), and multidrug and toxin extrusion protein (MATE1) that are known to be involved in the transport of cationic xenobiotics. The results of this screen indicated that dofetilide was most efficiently transported by MATE1 (4.3-fold compared to vector control; **Figure 22A**), and this process was time-dependent and saturable where K_m and V_{max} values for transport activity are $6.72 \pm 1.71 \mu\text{M}$, and $544.40 \pm 55.70 \text{ pmol/mg protein/min}$, respectively (**Figure 22C, D**). The transport assay of dofetilide was also carried out in cells overexpressing mouse orthologue of OCT2, OCTN1, and MATE1 (**Figure 28A**). However, HEK293 cells overexpressing human MATE1 treated with cimetidine ($25 \mu\text{M}$), a known OCT2 and MATE1 inhibitor, significantly reduced the uptake of dofetilide and TEA (**Figure 22B**).

A transporter inhibition assay was performed to examine this hypothesis using [¹⁴C] labeled TEA and metformin, known substrates for OCT2 and MATE1, while dofetilide was tested as an inhibitor (concentration range: 1-50 μM) in HEK293 cells stably transfected with human (h) MATE1. The difference in intracellular accumulation of [¹⁴C] TEA and metformin between overexpressing cell lines (HEK293-hMATE1) and vector control (VC) cells were measured. We found that dofetilide caused concentration-dependent inhibition of both [¹⁴C] TEA and metformin uptake in HEK293 cells

overexpressing hMATE1 which suggest potent interactions of dofetilide in a manner that is independent of test substrates (**Figure 28D**).

Previous studies have also demonstrated that MATE1 is highly expressed in the heart.^{14,325} Thus, we hypothesize that inhibition or deficiency of MATE1 could lead to a change in the extent of dofetilide retention in cardiomyocytes and alter its pharmacodynamics profile. To test this hypothesis, cardiomyocytes from wild-type and MATE1^{-/-} were isolated using a Langendorff perfusion system,³²⁶ and isolated cardiomyocytes were pre-treated in the presence or absence of cimetidine, followed by [³H] dofetilide accumulation studies. This analysis indicated that uptake of dofetilide is time dependent, and deficiency of MATE1 facilitates dofetilide accumulation in *ex vivo* cardiomyocytes (**Figure 22F**). Moreover, cardiomyocytes pre-treated with cimetidine substantially altered the accumulation of dofetilide in both wild-type and MATE1-deficient mice suggesting the inhibition of uptake transporter(s) (**Figure 22G**). We also confirmed that MATE1 gene and protein are expressed in the mice heart (**Figure 22E, 28E**) which is consistent with previously reported studies,^{14,325} and MATE1-deficient mice did not have any intrinsically abnormal pathological or biochemical changes.³²⁷

In line with dofetilide *ex vivo* cardiomyocytes accumulation in MATE1-deficient mice, we found that accumulation of dofetilide in whole heart tissue is higher in mice having deficiency of MATE1 compared to wild-type mice (**Figure 22I**). We also verified that TEA can also accumulate in the heart, and this accumulation can be reversed with the treatment of cimetidine (**Figure 22J**). This finding suggests that deficiency of MATE1 could lead to increase the accumulation of any cationic compounds, independent of

dofetilide, in the whole heart. Next, we conducted an *in vitro* uptake experiment using AC-16 human cardiomyocytes cells pre-treated in the presence or absence of cimetidine, followed by the uptake of [³H] dofetilide and [¹⁴C] TEA (**Figure 22H**). These similar observations provided further support to our hypothesis that dofetilide is a transport substrate of MATE1, and genetic or pharmacologic inhibition of MATE1 potentiates the cellular accumulation of dofetilide.

4.2.4.2 MATE1 deficiency exacerbates dofetilide-induced proarrhythmia

Since MATE1 inhibition has been shown to facilitate dofetilide accumulation in the heart, and previous studies have reported a positive correlation between plasma concentrations of dofetilide and its ability to induce QTc prolongation.³²⁸ Therefore, we sought to investigate whether inhibition of MATE1 would trigger the onset of QTc prolongation. In prior study evaluating the changes in electrocardiogram (ECG) with response to selective K⁺ channel blockers between neonatal and adult mice, it was concluded that changes in mouse ECG due to K⁺ channel blockers depend on age where dofetilide-sensitive *I_{Kr}* is dominant in day 1 neonatal mice.³¹⁸ Hence, we evaluated ECG in 1-day old wild-type and MATE1-deficient neonatal mice following a single intraperitoneal injection of dofetilide.

Significant increase in QTc prolongation was observed in neonatal mice with a genetic deletion of MATE1 following the treatment with dofetilide. Importantly, all MATE1-deficient mice were found to develop second degree heart blocks (Mobitz I and II) compared to wild-type mice treated with dofetilide suggesting that MATE1 transporter

has potential utility as a modulator of I_{Kr} blockage (**Figure 23A-B, D-F**). We also verified that MATE1 is expressed in neonatal mice heart and kidney (**Figure 23C**). These experiments shed light on the initiating mechanism responsible for QTc prolongation, and provide proof-of-principle that genetic or pharmacologic inhibition of MATE1 could enhance dofetilide-induced proarrhythmia such as TdP.

Although results from our study suggest that inhibition of MATE1, an efflux transporter, exacerbates I_{Kr} blockage, thus further investigations are required in order to identify specific influx transporter(s) that are involved in the transport of dofetilide into cardiomyocytes. Here, we propose dofetilide transport mechanisms in cardiomyocytes (**Figure 23G**): (A) normal dofetilide transport in cardiomyocytes by influx (*SLCs*) and efflux transporter(s) (MATE1); (B) reduced dofetilide efficacy due to genetic (polymorphism) or pharmacologic (perpetrator) inhibition of influx transporters; (C) dofetilide-induced toxicity due to inhibition of MATE1 leading to accumulating dofetilide in the cardiomyocytes.

4.2.4.3 Inhibition of MATE1 attenuates renal elimination of dofetilide

Previous studies have indicated that certain known inhibitors of renal cation secretion such as cimetidine, verapamil, and trimethoprim significantly increase the plasma concentration of dofetilide by 53-93%.³²⁹ Therefore, we originally hypothesized that dofetilide might be a transported substrate of OCT2, which is predominantly expressed on the basolateral side of proximal tubular cells. Furthermore, compounds or drugs that are transported by OCT2 are also likely to be a substrate for MATE1, which is

highly expressed on the apical side of tubular cells, and works in concert with OCT2 to move substrates from the circulation to the urine. Identification of the exact transporter(s) involved in this process may provide insights into the mechanism of drug-drug interaction and the development of preventative strategies for dofetilide induced proarrhythmia. Although our preliminary uptake assay of dofetilide was conducted in non-polarized HEK293 cells overexpressing OCT2 and MATE1 which might not be an ideal *in vitro* model system in order to evaluate the contribution of transporters that are expressed in opposite side (e.g. basal and apical) under normal physiological condition. Thus, it is important to establish that the transport of dofetilide is not compromised by using a different model system.

In order to evaluate the joint contribution of OCT2 and MATE1 to dofetilide transport in a more physiologically-relevant *in vitro* model system, we considered apical to basolateral drug flux in differentiated Madin-Darby canine kidney (MDCK) cells as a potential alternative model to HEK293 cells. MDCK cells originate from dog kidney epithelial cells,^{330,331} which differentiate to form a polarized monolayer. MDCK has become a *de facto* standard model for studies of pharmaceutical drug transport in kidneys and other tissues with the expression of different transporters.³³² This model was developed based on the idea that for a molecule to cross membrane through two or more successive transporter-mediated processes, it first needs to get into the cell through influx transporters on the basolateral side, and then be pumped out by efflux transporters on the apical side. To elucidate the transport mechanism of dofetilide, we conducted a basolateral to apical drug flux assay in differentiated MDCK cells using [¹⁴C]-labeled

metformin, as a known substrate for both OCT2 and MATE1, or [³H]-labeled dofetilide were added to the basal chamber of the trans-well plate at a concentration of 1 μM, and aliquots from the apical chamber were taken after an hour. Our preliminary data with this transfected MDCK cell line model showed that dofetilide is a dual substrate, and requires both OCT2 and MATE1 to be transported from the basal to apical membrane (**Figure 24A, B**).

Based on these *in vitro* findings, we hypothesize that inhibition of MATE1 *in vivo* could potentially lead to decreased urinary excretion and a concomitant increase in dofetilide plasma concentration. In order to understand the role of MATE1 in distribution and elimination of dofetilide, we performed *in vivo* pharmacokinetics studies in female mice on an FVB background that were either wild-type, OCT1/2^{-/-}, MATE1^{-/-}, or OCT1/2/MATE1^{-/-}. In a mass balance study, we found that deficiency of MATE1 and OCT1/2/MATE1 significantly reduced the renal elimination of dofetilide compared with wild-type and OCT1/2^{-/-} mice (**Figure 24C**) which were also consistent in male mice (**Figure 30C**). In order to examine if deficiency of these transporters play a role in elevating dofetilide plasma concentrations, we also performed plasma pharmacokinetics analyses after oral (5 mg/kg) (**Figure 24D, E**) and intravenous (2.5 mg/kg) (**Figure 30A, B, Table 9**) administration of dofetilide. The results of these studies revealed no significant increase in dofetilide plasma concentration among OCT1/2 and MATE1 transporters deficient mice except OCT1/2/MATE1^{-/-} mice after having a single oral administration of dofetilide. These observations suggest that there might be (i) shunting of dofetilide to alternative routes of elimination in the absence of MATE1, (ii) alternate

distribution profiles operational that compensate for the MATE1 loss in the kidney, (iii) additional basolateral transporters that regulate dofetilide movement from the circulation to tubular cells, and (iv) a simultaneous dependence of OCT2 and MATE1 impairment on circulating dofetilide concentrations.^{12,46}

4.2.4.4 Contraindicated drugs of dofetilide inhibit MATE1 function

Previously reported studies demonstrated that co-administration of several contraindicated drugs increases the plasma concentration of dofetilide, and this interaction has been mechanistically ascribed to the inhibition of CYP3A4 enzyme as well as to renal elimination, presumably involving the organic cation transport system.^{333–336} Among the known contraindicated drugs, cimetidine, dolutegravir, megestrol, and prochlorperazine are known to interfere with the renal cation transport system and elevate the plasma concentration of several other co-administered organic cations.^{274,337,338} Therefore, we hypothesize that such contraindicated drugs might inhibit the function of OCT2 and/or MATE1 and due to their high expression in the kidney, diminish their ability of fluxing cationic compounds such as dofetilide. To test this hypothesis, we considered performing *in vitro* inhibition assay to measure the relative MATE1 function of dofetilide with all the contraindicated drugs. We found that most of the contraindicated drugs inhibited cellular uptake of dofetilide by MATE1, and that cimetidine, verapamil, vandetanib, megestrol, trimethoprim, ketoconazole, and itraconazole inhibited MATE1 by >75%. Only vemurafenib, a BRAF inhibitor, was found to have no influence on MATE1 function, and it is likely that this agent is contraindicated because of its intrinsic severe nephrotoxicity

properties, which can cause delayed elimination of dofetilide independently of MATE1 (Figure 25A, B).^{339,340}

We next examined *in vivo* drug-drug interaction (DDI) study to assess if the addition of these contraindicated drugs elevates dofetilide plasma concentration. Our preliminary pharmacokinetics (PK) study revealed that plasma concentration of dofetilide in females was moderately elevated compared to males (Figure 24E, Table 10), and this observation is consistent in line with clinical settings where females tend to have higher dofetilide plasma concentration than males.²⁷² Therefore, subsequent PK studies were focused exclusively on female mice. We first sought to perform this *in vivo* assay in FVB wild-type male mice by oral administration (p.o.) of cimetidine (100 mg/kg) or ketoconazole (50 mg/kg). The doses were given 30 minutes prior to dofetilide (5 mg/kg, p.o.). The effect of PEG400, used as a formulation excipient of cimetidine and ketoconazole, was also evaluated to confirm that this vehicle does not influence the absorption of dofetilide. Plasma exposure (C_{max}) and area under the curve (AUC) of dofetilide in the presence or absence of PEG400, cimetidine, or ketoconazole were significantly higher in mice treated with cimetidine and ketoconazole, but not PEG400 (Figure 25C, D).

Next, we evaluated the influence of several listed contraindicated drugs, for example, bictegravir, cimetidine, ketoconazole, trimethoprim, and verapamil on dofetilide plasma exposure to unequivocally demonstrate that this elevated plasma exposure is exclusively dependent on the inhibition of OCT1/2 and, or MATE1 transporters. To test this hypothesis, we performed DDI studies in wild-type, OCT1/2^{-/-},

and MATE1^{-/-} mice with dofetilide in the presence and absence of pre-treated contraindicated drugs. These studies demonstrated that all contraindicated drugs significantly increased dofetilide plasma and AUC level except trimethoprim compared with wild-type mice (**Figure 29, Table 8**). We also extended this DDI studies of dofetilide with ketoconazole and verapamil in males to see if these interactions are independent regardless of gender. Surprisingly, unlike females, treatment with verapamil in males did not influence plasma levels of dofetilide, while effect of ketoconazole was consistent with females in elevating dofetilide plasma exposure (**Figure 30D-E, Table 10**). This discrepancy on the effect of contraindicated drugs between gender could potentially be due to the difference in transporter(s) expression in the kidney where expression of MATE1 is higher in males compared to females (**Figure 28C**).

4.2.4.5 Influence of CYP3A in the disposition of dofetilide

According to dofetilide product information, and data from the past based on *in vitro* microsomal incubation studies reported that dofetilide is metabolized by CYP3A4, and inhibition of this enzyme could potentially increase dofetilide plasma level.^{341,342} To explicitly determine the contribution of CYP3A to the pharmacokinetics of dofetilide, we next performed PK and mass balance studies in CYP3A^{-/-} mice. No significant alteration has been observed in plasma and urine concentration after an oral and intravenous administration of dofetilide in CYP3A^{-/-} mice compared to wild-type mice (**Figure 26A-D**). To further validate our hypothesis that CYP3A4 does not have any influence in the metabolism of dofetilide, we next performed DDI studies with ketoconazole, a known

inhibitor of CYP3A4, in CYP3A^{-/-} mice. Both wild-type and CYP3A^{-/-} mice treated with ketoconazole demonstrated increased dofetilide plasma exposure. This study suggests that increase in dofetilide plasma exposure with the treatment of ketoconazole is not due to CYP3A inhibition rather related to the inhibition of OCT1/2 and, or MATE1 transporters.

4.2.4.6 Dofetilide PBPK Model predicts transporter-mediated DDI

At present, physiologically-based pharmacokinetic (PBPK) modeling approaches are commonly applied for predicting drug effects in human.³⁰⁹⁻³¹¹ PBPK is a powerful tool to quantitatively predict DDIs based on drug-dependent physicochemical and pharmacokinetic parameters along with drug-independent physiological systems parameters.^{307,308} Furthermore, the US Food and Drug Administration (FDA), the European Medicines Agency (EMA), and the Japanese Pharmaceuticals and Medical Devices Agency (PMDA) have issued DDI guidance, which highlights the use of integrated mechanistic approaches including PBPK models.^{343,344}

Based on these considerations, we developed a PBPK model for dofetilide following top-down approach. Dofetilide PBPK model reproduced the observed C_{max} , AUC_{0-last} , and renal clearance providing a single oral dose of 0.5 mg and 0.5 mg IV infusion for 90 min. Simulated PK profiles were compared with data from clinical trial in which single-agent PK data were available. The simulated mean plasma concentration-time profiles with observed data overlaid are shown in **Figure 27A-B**. The prediction

error (PE) between observed and predicted dofetilide PK parameters were within 50% of our cut-off limit (**Table 11**).

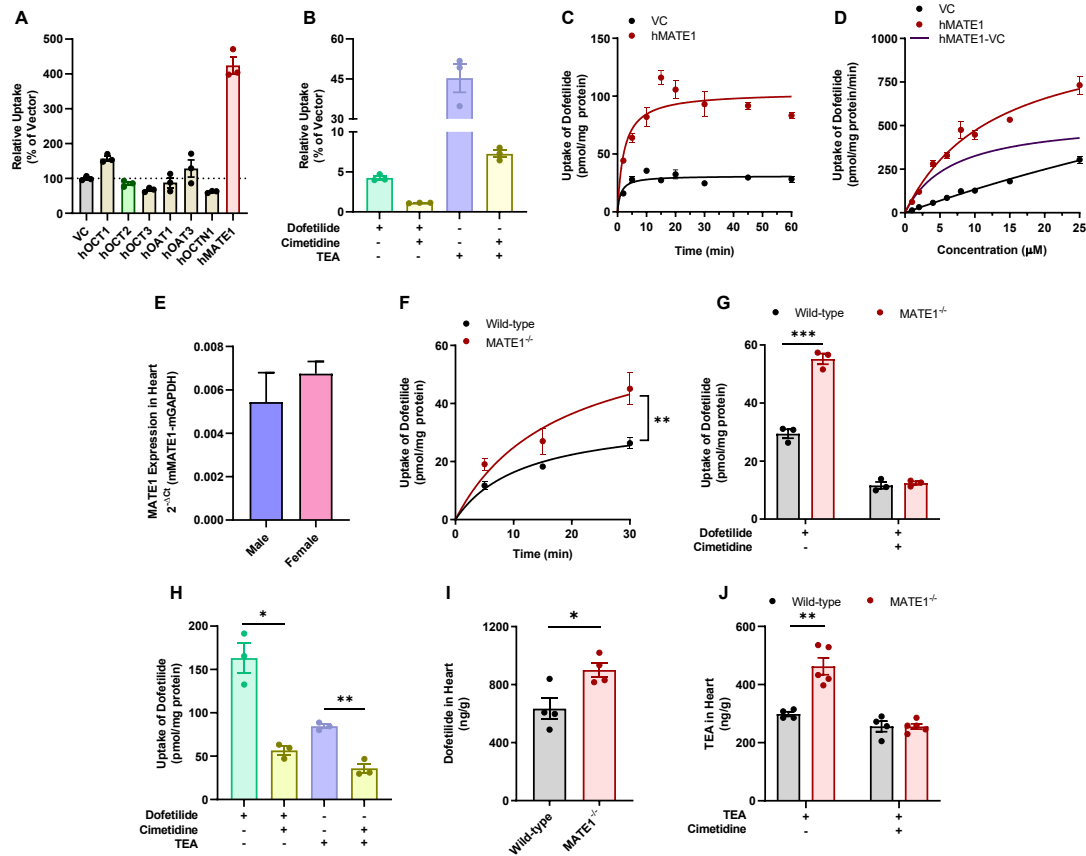
Next, in order to predict transporter-mediated DDI with cimetidine and ketoconazole, clinical DDI trial of dofetilide 0.5 mg BID with cimetidine 400 mg BID, and ketoconazole 400 mg QD was simulated according to the clinical trial design in healthy subjects. Simulated PK profiles for DDI with cimetidine and ketoconazole were then compared with observed data, as shown in **Figure 27C-D**. The percent increase in C_{max} , and AUC between predicted and observed cimetidine DDI with dofetilide were 40.14% and 52.2%, and 65.5% and 58%, respectively. Furthermore, coadministration of cimetidine also shown to reduce renal clearance of dofetilide where percent change in predicted and observed values were 38.92% and 43.7%, respectively (**Table 11**).

For ketoconazole DDI, PBPK model accurately predicted the percent increase in dofetilide AUC (41.1%) compare with observed in human. The corresponding predicted versus observed increase in C_{max} for dofetilide was 28.9% and 53%, respectively. Since ketoconazole also inhibits OCT2 and MATE1, a reduction in renal clearance was also predicted by our developed model. However, no observed clinical data on renal clearance with ketoconazole has been found for dofetilide to compare with predicted result. Overall, the PBPK model predicted the exposure change in dofetilide reasonably well when it was co-administered with cimetidine or ketoconazole.

4.2.5 Acknowledgments

We would like to thank Dr. Yan Shu (University of Maryland, Baltimore, MD) for providing MATE1-deficient mice on a C57BL/6J background. We would like to thank Dr. Przemyslaw Radwanski and Alec Millar for their assistance with ECG experiments in neonatal mice. We would like to thank Xiaoming Cui, Ryan M. Pelis, and Heidi J. Einolf (Novartis Institute for Biomedical Research, East Hanover, NJ) for their support in developing dofetilide PBPK model.

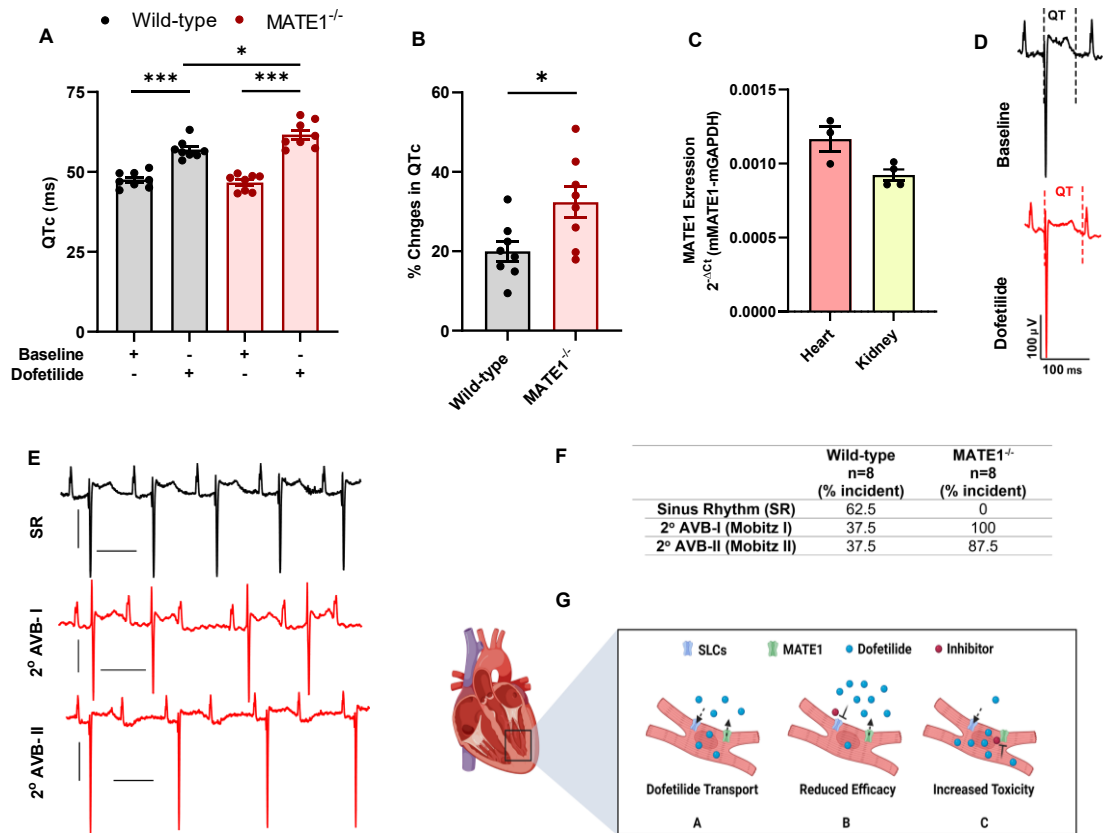
Figure 22. Inhibition of MATE1 enhances dofetilide accumulation in the heart



Inhibition of MATE1 enhances dofetilide accumulation in the heart. (A) Transport of [³H] dofetilide (1 μM) in cells overexpressing the human homolog of OCT1, OCT2, OCT3, OAT1, OAT3, OCTN1, or MATE1. Relative uptake is expressed as percentage change compared with empty vector controls (n = 3). (B) Relative uptake of [³H] dofetilide and [¹⁴C] TEA in HEK293 cells overexpressing human MATE1 in the presence and absence of cimetidine (25 μM). (C) Time dependent uptake (2-60 min) of [³H] dofetilide (1 μM) in HEK293 cells stably transfected with vector (VC) and MATE1. (D) Transport kinetics of [³H] dofetilide in cells overexpression of human MATE1. The

Michaelis-Menten constant (K_m) and the maximal uptake rate (V_{max}) values for the kinetics of dofetilide (1-25 μ M) was determined after an incubation time of 2 min. K_m and V_{max} values for transport activity are $6.72 \pm 1.71 \mu$ M, and 544.40 ± 55.70 pmol/mg protein/min, respectively. **(E)** Gene expression of MATE1 in the heart isolated from untreated wild-type male and female mice (n = 4 per group). **(F)** Time dependent uptake of [3 H] dofetilide (2 μ M) in *ex vivo* cardiomyocytes isolated from wild-type or MATE1-deficient female mice (n = 4-6 per group). **(G)** *Ex vivo* concentrations of [3 H] dofetilide (2 μ M) in cardiomyocytes isolated from female wild-type or MATE1-deficient mice (n = 3 per group) for 30 min in the presence or absence of cimetidine (25 μ M) cotreatment. **(H)** Uptake of 2 μ M [3 H] dofetilide and [14 C] TEA in AC16 human cardiomyocyte cell line (n = 3) for 20 min in the presence or absence of cimetidine (25 μ M) pretreatment (15 min). **(I)** Concentration of dofetilide in whole heart tissue from male wild-type or MATE1-deficient mice following a single intravenous injection of dofetilide via caudal vein at a dose of 2.5 mg/kg (n = 4 per group) after 15 min. **(J)** Wild-type and MATE1-deficient male mice (n = 4 to 5 per group) were treated with cimetidine (100 mg/kg) 30 min before an intravenous administration of [14 C] TEA (0.2 mg/kg). Heart samples were collected at 15 min after TEA treatment. All experimental values are presented as mean \pm SEM. Statistical analysis was performed using an unpaired two-sided Student's t test with Welch's correction: *P < 0.05, **P < 0.01, ***P < 0.001, compared to wild-type values.

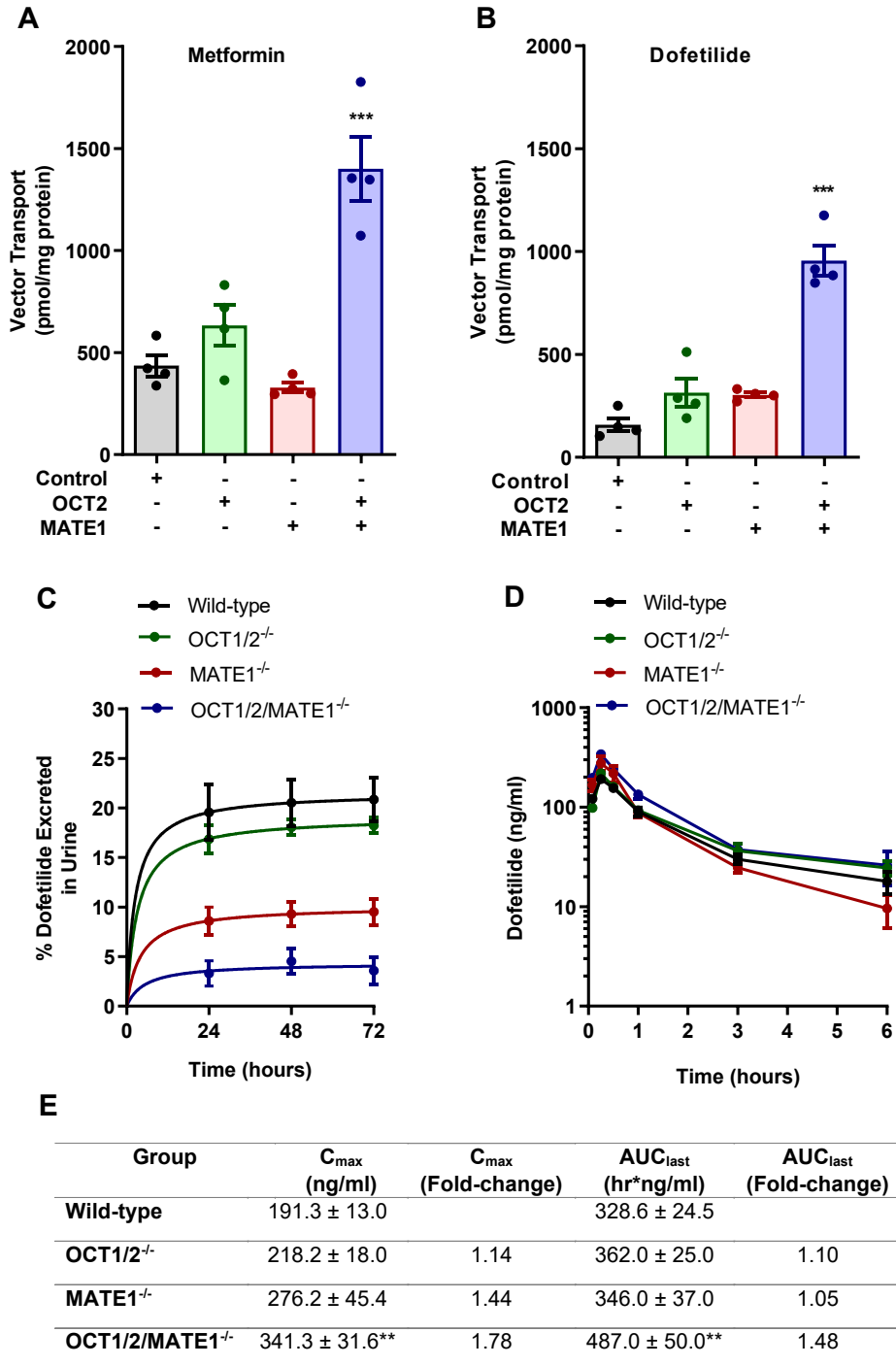
Figure 23. MATE1 deficiency exacerbates dofetilide-induced proarrhythmia



MATE1 deficiency exacerbates dofetilide-induced proarrhythmia. (A) Changes in QTc level in wild-type or MATE1-deficient neonatal mice (day 1) following a single intraperitoneal injection of dofetilide at a dose of 0.5 mg/kg (n = 8 per group) after 15 min. All experimental values are presented as mean ± SEM. Statistical analysis was performed using an unpaired two-sided Student's t test with Welch's correction: *P < 0.05, ***P < 0.001, compared to baseline values. (B) Evaluation of QTc changes in wild-

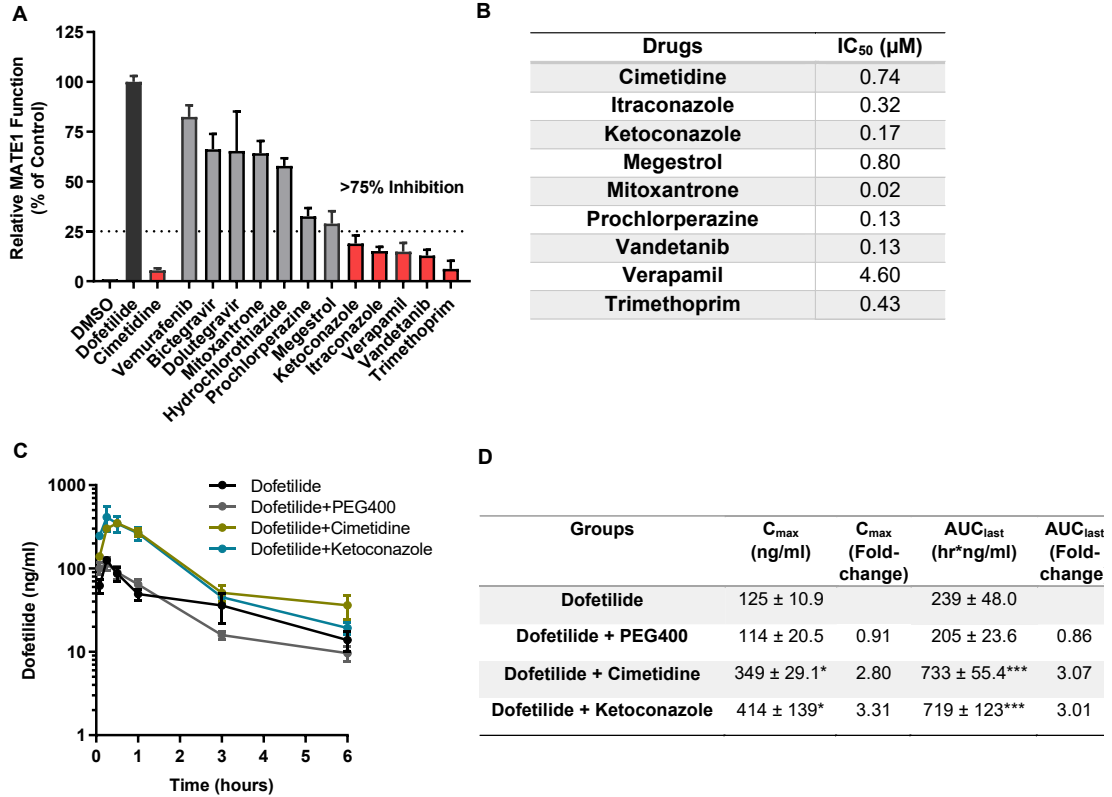
type or MATE1-deficient neonatal mice (day 1). Data are presented as percentage changes in QTc from baseline after dofetilide treatment at 15 min. Statistical analysis was performed using an unpaired two-sided Student's t test with Welch's correction: *P < 0.05 compared to wild-type values. **(C)** Gene expression of MATE1 in the heart (n = 3) and kidney (n = 4) isolated from untreated wild-type neonatal mice (day 1). **(D)** *in vivo* surface ECG illustrates changes in QTc after dofetilide treatment in wild-type neonatal mice. **(E)** Dofetilide-induced second-degree AV blocks in MATE1-deficient neonatal mice. **(F)** Incidents of second-degree AV blocks (Mobitz I and Mobitz II) in wild-type and MATE1-deficient neonatal mice (n = 8 per group) after the treatment of dofetilide. **(G)** Schematic diagram illustrating the proposed mechanism of dofetilide-induced proarrhythmia due to inhibition of MATE1 transporter leading to accumulating dofetilide in the cardiomyocytes.

Figure 24. Inhibition of MATE1 attenuates renal elimination of dofetilide



Inhibition of MATE1 attenuates renal elimination of dofetilide. Characterization of transcellular, basal to apical, transport of [¹⁴C] metformin **(A)** [³H] dofetilide **(B)** in single transfected MDCK-VC, MDCK-OCT2, MDCK-MATE1, and double-transfected MDCK-OCT2-MATE1 cell lines. Transcellular transport was quantified by measuring the amount of dofetilide appearing in the apical compartment after 60 min of incubation. Statistical analysis was performed using an unpaired two-sided Student's t test with Welch's correction: ***P < 0.001 vs. MDCK-VC. **(C)** Urinary excretion of dofetilide in wild-type, OCT1/2-deficient, MATE1-deficient, and OCT1/2/MATE1-deficient female mice (n = 5) following a single intravenous dose of dofetilide (2.5 mg/kg) via caudal vein. **(D)** Plasma concentration time profile of dofetilide in wild-type, OCT1/2-deficient, MATE1-deficient, and OCT1/2/MATE1-deficient female mice (n = 5) receiving a single oral dose of dofetilide (5 mg/kg). **(E)** Pharmacokinetic parameters of dofetilide after a single oral dose of administration. Statistical analysis was performed using one-way ANOVA with Dunnett's post hoc test: **P < 0.01, compared with wild-type mice. All data presented represent the mean ± SEM.

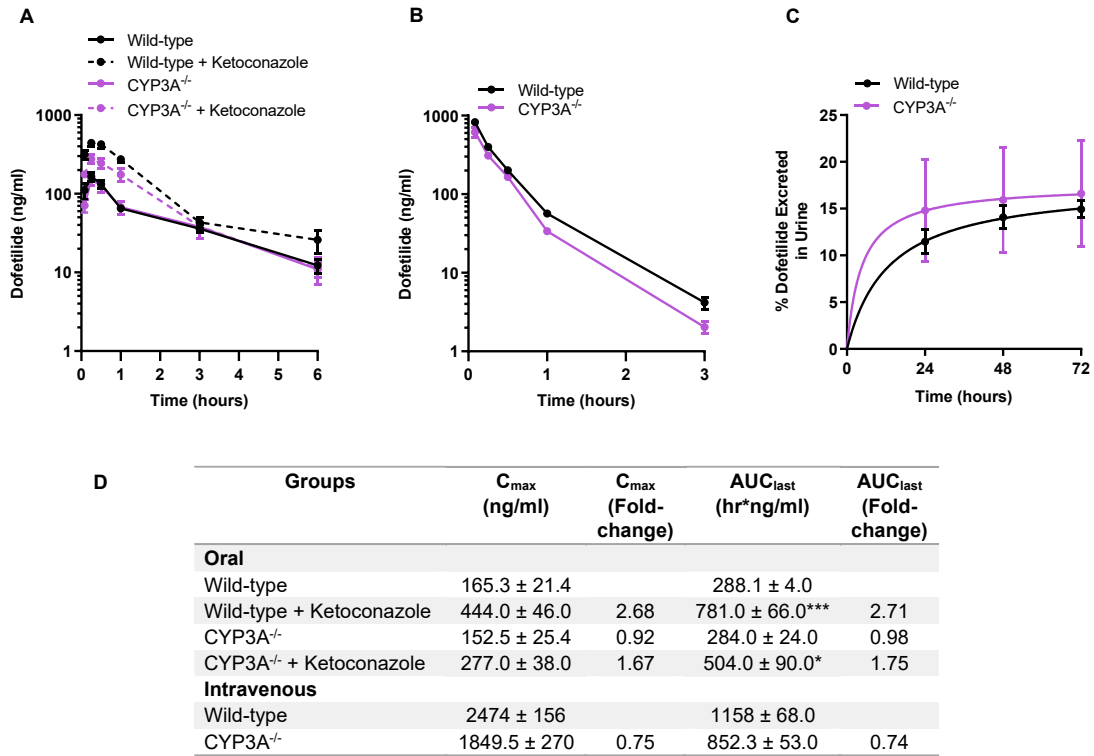
Figure 25. Contraindicated drugs of dofetilide restrain MATE1 function



Contraindicated drugs of dofetilide restrain MATE1 function. (A) FDA-listed contraindicated drugs of dofetilide were assessed at a concentration of 25 μM in HEK293 cells overexpressing human MATE1. [³H] Dofetilide (1 μM) and cimetidine were used as positive control substrate or inhibitor, respectively. Data are represented as percentage MATE1 activity as compared with DMSO group (n = 3 per group). **(B)** IC₅₀ values of different contraindicated drugs. **(C)** Plasma concentration-time curves profile of dofetilide in wild-type male mice pretreated for 30 min receiving vehicle (PEG400), cimetidine (100 mg/kg), and ketoconazole (50 mg/kg) (n = 5 per group). **(D)**

Pharmacokinetic parameters of dofetilide in wild-type male mice in the presence or absence of the administration of vehicle or contraindicated drugs. All data presented represent the mean \pm SEM. Statistical analysis was performed using one-way ANOVA with Dunnett's post hoc test: *P < 0.05, ***P < 0.001, compared with dofetilide alone treatment group.

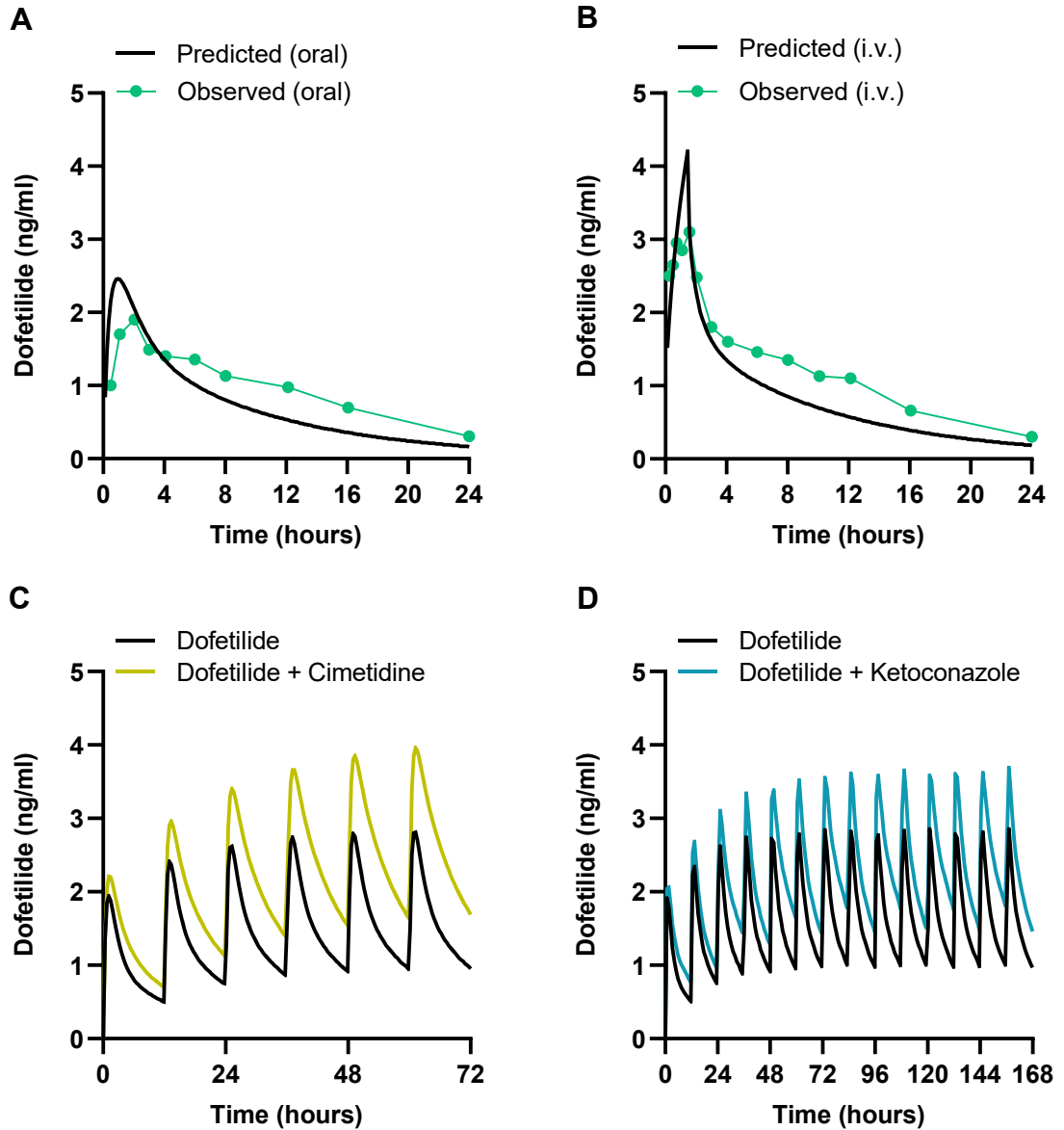
Figure 26. CYP3A does not influence in the disposition of dofetilide



CYP3A does not influence in the disposition of dofetilide. (A) Plasma concentration-time profile of dofetilide (5 mg/kg, p.o.) in wild-type or CYP3A-deficient male mice pre-treated for 30 min with ketoconazole (100 mg/kg) (n = 5 per group). (B) Plasma concentration-time curves profile of dofetilide receiving an intravenous dose of 2.5 mg/kg in wild-type or CYP3A-deficient male mice (n = 5). (C) Urinary excretion of dofetilide in wild-type and CYP3A-deficient male mice (n = 5) following a single dose of dofetilide (2.5 mg/kg, i.v.). (D) Pharmacokinetic parameters of dofetilide in wild-type and CYP3A-deficient male mice. Statistical analysis was performed using one-way

ANOVA with Dunnett's post hoc test: *P < 0.05, ***P < 0.001 compared with wild-type mice treated by vehicle group. All data presented represent the mean \pm SEM.

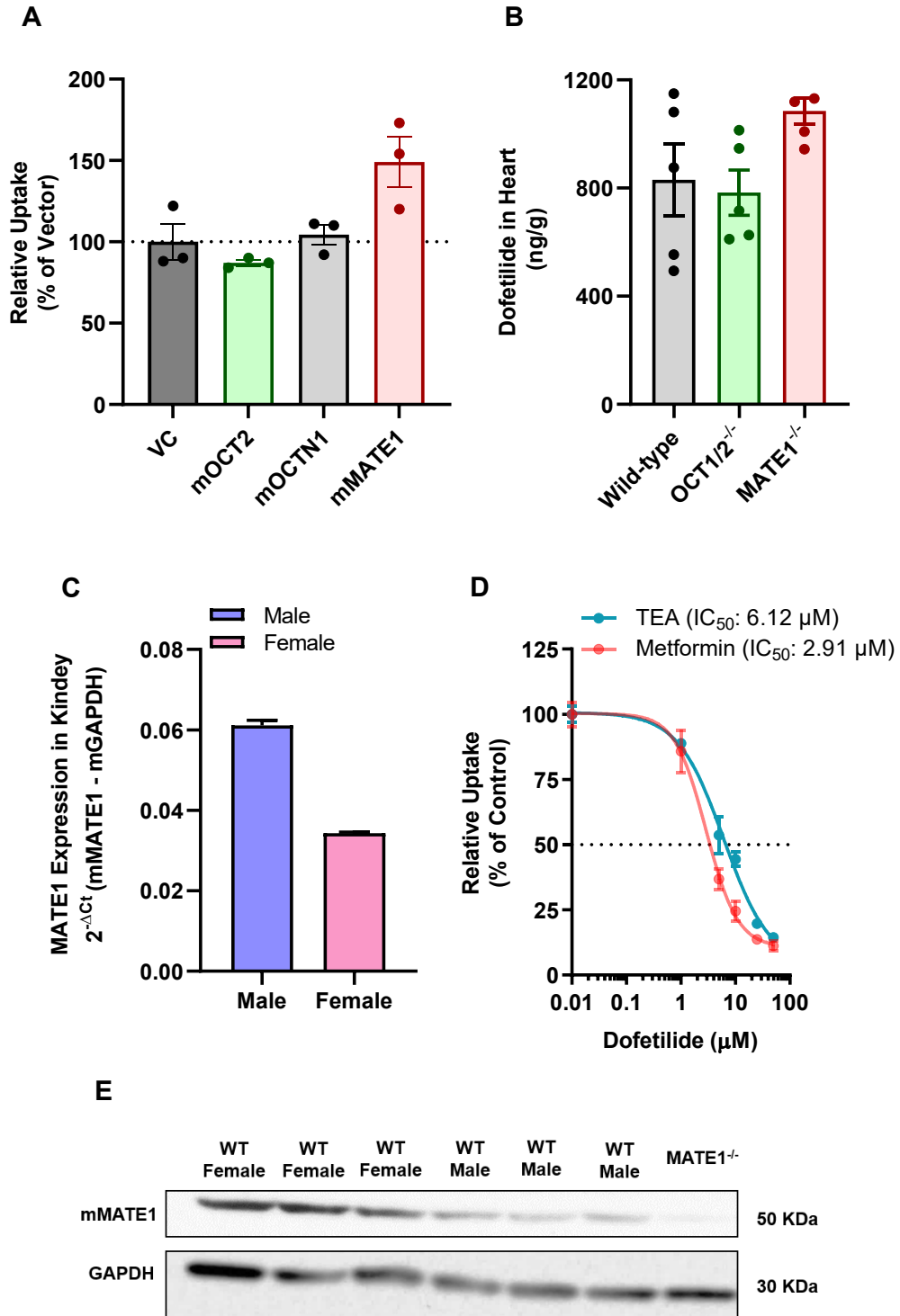
Figure 27. Physiologically based pharmacokinetics (PBPK) model predicts transporter-mediated drug-drug interactions of dofetilide



Physiologically based pharmacokinetics (PBPK) model predicts transporter-mediated drug-drug interactions of dofetilide. Observed and predicted plasma

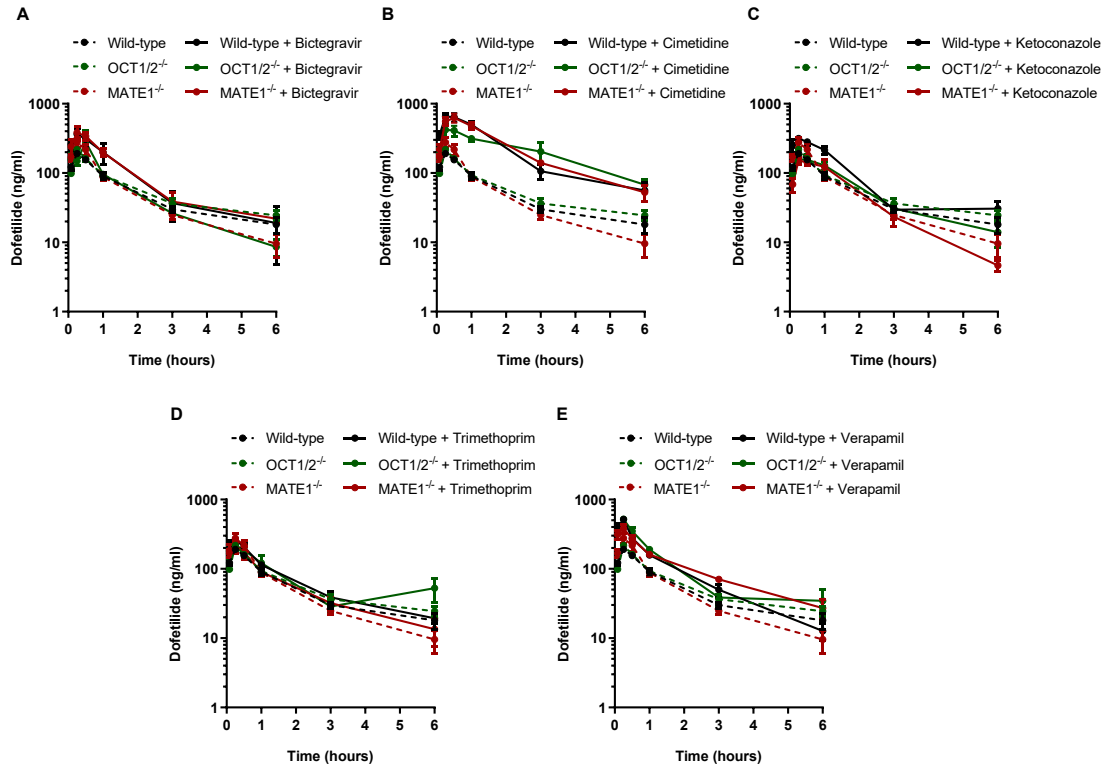
concentration-time profile of dofetilide after oral administration **(A)** of a single dose of 0.5 mg, and intravenous infusion **(B)** at a single dose of 0.5 mg for 90 min in adult healthy volunteers. Predicted plasma concentration-time profiles of dofetilide receiving oral administration of multiple doses of 0.5 mg, BID with and without cimetidine (400 mg, BID) **(C)** and ketoconazole (400 mg, QD) **(D)** in healthy volunteers. The observed dofetilide plasma concentration-time profile graph was recreated from Smith *et al* 1992, and DDI data was extracted from US FDA drug approval package.^{277,324}

Figure 28. Influence of MATE1 in the disposition of dofetilide



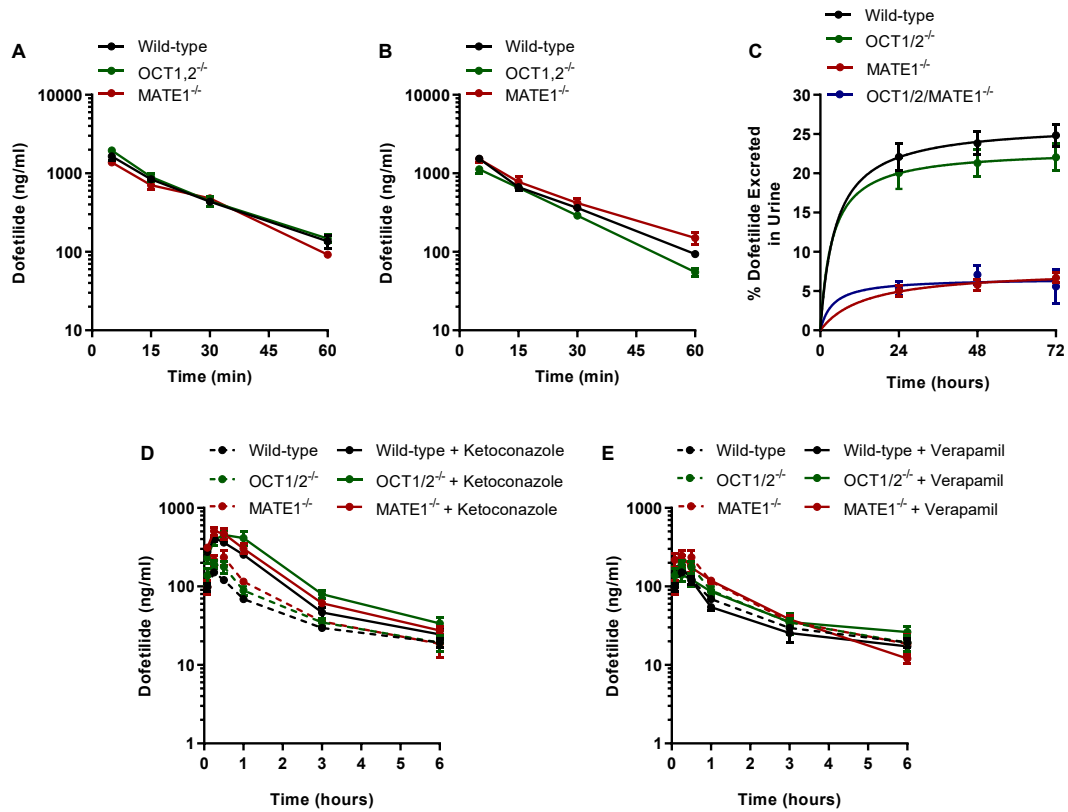
Influence of MATE1 in the disposition of dofetilide. **(A)** Transport of [³H] dofetilide (1 μM) in cells overexpressing the mouse homolog of OCT2, OCT3, OCTN1, or MATE1. Relative uptake is expressed as percentage change compared with empty vector controls (n = 3). **(B)** Concentration of dofetilide in whole heart tissue from male wild-type, OCT1/2-deficient, and MATE1-deficient mice following a single intravenous injection of dofetilide via caudal vein at a dose of 2.5 mg/kg (n = 4-5 per group) after 15 min. **(C)** Gene expression of MATE1 in the kidney isolated from untreated wild-type adult (12-15 weeks old) and neonatal mice (day 1) (n = 4 per group). **(D)** Uptake of [¹⁴C] TEA (2 μM) and [¹⁴C] metformin (5 μM) was evaluated in HEK293 cells overexpressing hMATE1 after preincubation with dofetilide at various concentrations (1-50 μM) for 15 min, followed by the co-incubation with TEA and metformin for 15 min. Data represent the mean ± SEM and are expressed as a percentage over vector control. **(E)** Protein expression of MATE1 in the heart isolated from adult wild-type and MATE1^{-/-} mice (n=3).

Figure 29. Drug-drug interactions increase dofetilide plasma exposure



Drug-drug interactions increase dofetilide plasma exposure. Plasma concentration time profile of dofetilide in wild-type, OCT1/2-deficient, and MATE1-deficient female mice (n = 5 to 29 per group) receiving a single oral dose of dofetilide (5 mg/kg) 30 min after the administration of bictegravir (30 mg/kg) (A), cimetidine (100 mg/kg) (B), ketoconazole (50 mg/kg) (C), trimethoprim (100 mg/kg) (D), and verapamil (10 mg/kg) (E).

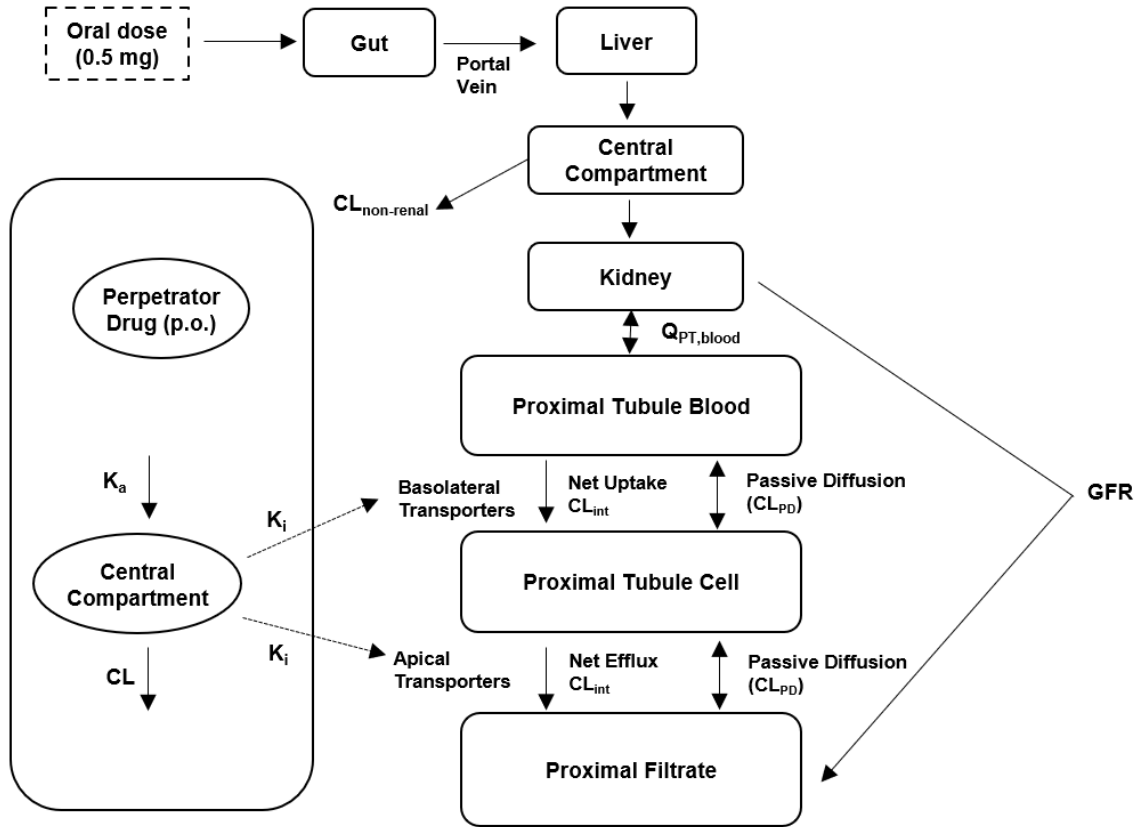
Figure 30. Plasma exposure and renal elimination of dofetilide



Plasma exposure and renal elimination of dofetilide. Plasma concentration time profile of dofetilide in wild-type, OCT1/2-deficient, and MATE1-deficient female (**A**) and male (**B**) mice (n = 5 per group) receiving a single intravenous dose of dofetilide (2.5 mg/kg) via caudal vein. (**C**) Urinary excretion of dofetilide in wild-type, OCT1/2-deficient, MATE1-deficient, and OCT1/2/MATE1-deficient male mice (n = 5) following an intravenous dose of dofetilide (2.5 mg/kg). Plasma concentration time profile of dofetilide in wild-type, OCT1/2-deficient, and MATE1-deficient male mice (n = 5 to 38

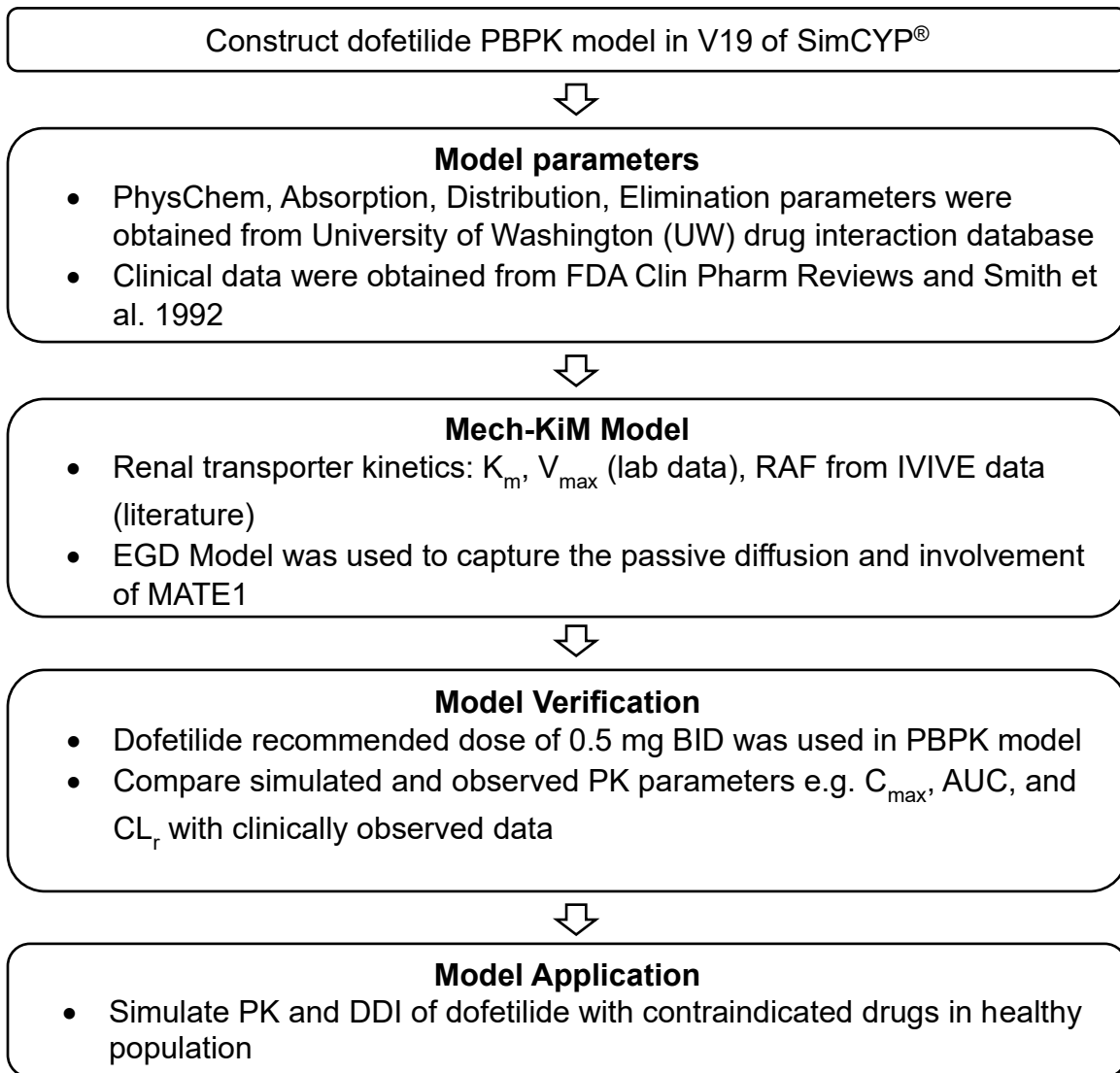
per group) receiving an oral dose of dofetilide (5 mg/kg) 30 min after the administration of ketoconazole (50 mg/kg) **(D)**, and verapamil (10 mg/kg) **(E)**.

Figure 31. Structure of the physiologically based pharmacokinetic (PBPK) model for dofetilide



Structure of the physiologically based pharmacokinetic (PBPK) model for dofetilide.

Figure 32. Workflow of dofetilide physiologically based pharmacokinetic (PBPK) model



Workflow for the development of dofetilide physiologically based pharmacokinetic (PBPK) model

Table 8. Influence of contraindicated drugs on the pharmacokinetic parameters of dofetilide in female mice

Group (Female)	C_{max} (ng/ml)	C_{max} (Fold- change)	AUC_{last} (hr*ng/ml)	AUC_{last} (Fold- change)
Dofetilide (5 mg/kg)				
Wild-type	191.3 ± 13.0		328.6 ± 24.5	
OCT1/2 ^{-/-}	218.2 ± 18.0	1.14	362.0 ± 25.0	1.10
MATE1 ^{-/-}	276.2 ± 45.4	1.44	346.0 ± 37.0	1.05
Bictegravir (30 mg/kg)				
Wild-type + Bictegravir	365.0 ± 72.0*	1.91	595.0 ± 194*	1.81
OCT1/2 ^{-/-} + Bictegravir	281.5 ± 132	1.47	354.0 ± 46.4	1.08
MATE1 ^{-/-} + Bictegravir	383.0 ± 86.4*	2.00	614.2 ± 77.0*	1.87
Cimetidine (100 mg/kg)				
Wild-type + Cimetidine	656.0 ± 81.3***	3.43	1395 ± 183***	4.25
OCT1/2 ^{-/-} + Cimetidine	420.2 ± 89.4**	2.20	1267 ± 150***	3.86
MATE1 ^{-/-} + Cimetidine	625.0 ± 92.2***	3.27	1403 ± 89.5***	4.27
Ketoconazole (50 mg/kg)				
Wild-type + Ketoconazole	314.5 ± 34.0*	1.64	588.2 ± 64.0**	1.79
OCT1/2 ^{-/-} + Ketoconazole	475.3 ± 61.5**	2.48	1089 ± 128***	3.31
MATE1 ^{-/-} + Ketoconazole	455.0 ± 32.0***	2.38	938.0 ± 181***	2.85
Trimethoprim (100 mg/kg)				
Wild-type + Trimethoprim	264.0 ± 27.0	1.38	428.0 ± 25.4	1.3
OCT1/2 ^{-/-} + Trimethoprim	220.0 ± 38.0	1.15	440.0 ± 76.0	1.34
MATE1 ^{-/-} + Trimethoprim	212.0 ± 45.0	1.11	345.0 ± 29.3	1.05
Verapamil (10 mg/kg)				
Wild-type + Verapamil	517.5 ± 47.0***	2.71	602.0 ± 35.0*	1.83
OCT1/2 ^{-/-} + Verapamil	519.1 ± 42.4***	2.71	669.0 ± 42.0**	2.04
MATE1 ^{-/-} + Verapamil	384.2 ± 58.0**	2.01	638.0 ± 26.5**	1.94

Data represent mean \pm SEM. *P < 0.05, **P < 0.01, ***P < 0.001.

Abbreviations: C_{max}, peak plasma concentration; AUC_{last}, area under the plasma concentration-time curve to the last measurable concentration.

Table 9. Pharmacokinetic parameters of dofetilide after giving an intravenous dose (2.5 mg/kg) in mice

Group	C_{max} (ng/ml)	C_{max} (Fold-change)	AUC_{last} (hr*ng/ml)	AUC_{last} (Fold-change)
Female				
Wild-type	1642 ± 170		673.2 ± 28.0	
OCT1/2 ^{-/-}	1960 ± 126	1.29	756.0 ± 47.0	1.19
MATE1 ^{-/-}	1521 ± 149	0.93	635.0 ± 61.0	0.94
Male				
Wild-type	1535 ± 131		587.4 ± 29.4	
OCT1/2 ^{-/-}	1123 ± 113	0.81	461.0 ± 23.0	0.76
MATE1 ^{-/-}	1379 ± 112	0.90	603.0 ± 28.5	1.03

Abbreviations: C_{max}, peak plasma concentration; AUC_{last}, area under the plasma concentration-time curve to the last measurable concentration.

Table 10. Influence of contraindicated drugs on the pharmacokinetic parameters of dofetilide in male mice

Group (Male)	C_{max} (ng/ml)	C_{max} (Fold- change)	AUC_{last} (hr*ng/ml)	AUC_{last} (Fold- change)
Dofetilide (5 mg/kg)				
Wild-type	151.2 ± 8.80		278.2 ± 12.3	
OCT1/2 ^{-/-}	191.0 ± 23.4	1.26	351.0 ± 36.0	1.26
MATE1 ^{-/-}	235.0 ± 50.0*	1.55	406.6 ± 32.6**	1.46
Ketoconazole (50 mg/kg)				
Wild-type + Ketoconazole	415.3 ± 43.0***	2.75	728.0 ± 55.4***	2.62
OCT1/2 ^{-/-} + Ketoconazole	453.0 ± 65.0***	3.00	1048 ± 142***	3.77
MATE1 ^{-/-} + Ketoconazole	508.5 ± 62.2***	3.36	894 ± 92.0***	3.21
Verapamil (10 mg/kg)				
Wild-type + Verapamil	181.4 ± 32.0	1.20	259.0 ± 18.3	0.93
OCT1/2 ^{-/-} + Verapamil	148.3 ± 32.0	0.98	328.3 ± 52.0	1.18
MATE1 ^{-/-} + Verapamil	246.0 ± 38.4	1.63	406.0 ± 38.0	1.46

Data represent mean ± SEM. *P < 0.05, **P < 0.01, ***P < 0.001.

Abbreviations: C_{max}, peak plasma concentration; AUC_{last}, area under the plasma concentration-time curve to the last measurable concentration.

Table 11. Observed and predicted pharmacokinetic parameters of dofetilide with the presence and absence of cimetidine and ketoconazole

	Mean C _{max} ± SD (CV%) (ng/mL)		Mean AUC _{0-last} ± SD (CV%) (ng*h/mL)		Mean CL ± SD (CV%) (L/h)	
	Predicted	Observed	Predicted	Observed	Predicted	Observed
Dofetilide (0.5 mg, p.o.)	2.48 ± 0.58 (23) PE = +32.66%	1.87 ± 0.65	18.01 ± 3.38 (19) PE = +2.91%	17.5 ± 3.2	28.77 ± 6.05 (21) PE = +30.77%	22.00
Dofetilide (0.5 mg i.v. infusion over 90 min)	4.28 ± 0.52 (12) PE = +38.06%	3.1 ± 0.50	20.37 ± 3.92 (19) PE = -3.92%	21.2 ± 4.5	25.37 ± 4.94 (19) PE = +40.48%	18.06
DDI with Cimetidine 400 mg BID (p.o.)						
Dofetilide (0.5 mg BID, p.o.)	2.84 ± 0.53 (19) PE = +25.7%	2.26	19.59 ± 3.66 (19) PE = +12.6%	17.4	26.41 ± 5.36 (20) PE = +28.2%	20.6
Dofetilide + Cimetidine (400 mg BID, p.o.)	3.98 ± 0.70 (18) PE = +15.7%	3.44	32.42 ± 6.76 (21) PE = +17.9%	27.5	16.13 ± 3.79 (23) PE = +39.1%	11.6
% Change	40.14% ↑	52.2% ↑	65.50% ↑	58.00% ↑	38.92% ↓	43.7% ↓
DDI with Ketoconazole 400 mg QD (p.o.)						

Dofetilide (0.5 mg BID, p.o.)	2.87 ± 0.52 (18) PE = +27.0%	2.26	19.88 ± 3.69 (19) PE = +14.3%	17.4	26.01 ± 5.20 (20) PE = +26.3%	20.6
Dofetilide + Ketoconazole (400 mg QD, p.o.)	3.70 ± 0.73 (20)	-	28.05 ± 6.17 (22)	-	18.72 ± 4.68 (25)	-
% Change	28.9% ↑	53.0% ↑	41.1% ↑	41.0% ↑	28.0% ↓	-

Data represent mean ± SEM.

Abbreviations: p.o., given orally; BID, twice per day; QD, four times a day, C_{max}, peak plasma concentration; AUC_{0-last}, area under the plasma concentration-time curve between time zero and the last measurable concentration; CL, clearance; PE, calculated prediction error (%) = [(predicted value - observed value)/observed value] x 100.

Table 12. Input parameters of dofetilide in PBPK model

Input parameters	Description	Units	Value	Reference
1. Physicochemical and binding properties				
MW	Molecular weight	g/mol	441.57	
Log P	Octanol-water partition	-	2.1	PubChem
Compound type	Acid, base or neutral	-	Monoprotic base	
pK _a	Acid dissociation constant	-	7.89	UWDIDB
B/P profile	Blood to plasma ratio dependent on drug concentration	-	1.048	Simcyp predicted
f _u	Fraction unbound in plasma	-	0.36	UWDIDB
2. Absorption				
Absorption model	First order absorption model			
f _a	Fraction available from dosage form	-	1	
CV f _a	Coefficient of variation f _a	%	30	Default
k _a	Absorption rate constant	1/h	0.9	UWDIDB
CV k _a	Coefficient of variation k _a	%	30	Default

Input parameters	Description	Units	Value	Reference
$f_{u_{gut}}$	Unbound fraction in enterocytes	-	0.039	Simcyp predicted
Q_{gut}	Nominal flow in gut model	L/h	4.068	Simcyp predicted
CV Q_{gut}	Coefficient of variation $Q(gut)$	%	30	Default
$P_{eff,man}$	Effective permeability in man	10^{-4} cm/s	12	Simcyp predicted
Permeability assay	Passive + active permeability		Physicochemical	
PSA	Polar surface area	Å^2	104.81	Drug central
HBD	Hydrogen bond donor		2	Drug central

3. Distribution

Distribution model	Full PBPK model			
Prediction method			Method 2	
Kp scalar	Tissue to plasma partition coefficient		0.61	Optimized
V_{ss}	Volume of distribution at steady-state	L/kg	2.8	Smith et al 1992
CV V_{ss}	Coefficient of variation V_{ss}	%	30	Default

4. Elimination

Elimination model	Enzyme kinetics			
CYP, recombinant			CYP3A4	Smith et al 1992

Input parameters	Description	Units	Value	Reference
CL _{int} (HLM)	<i>In vitro</i> clearance (human liver microsomes)	μL/min/mg protein	0.25	Smith et al 1992
f _{u,mic}	Fraction unbound <i>in vitro</i>		0.81	
CL _r	Renal clearance in 20-30yr healthy male	L/h	18.06	Smith et al 1992
5. Transport				
Organ/Tissue			Kidney	
Transporter			SLC22A2 (OCT2)	
Location			Basolateral	
Function			EGD model	
J _{max}		pmol/min/10 ⁶ cells	506.35	Measured
K _m	Michaelis-Menten constant	μM	347.2	Measured
System			User	
RAF/REF	Relative activity factor/relative expression factor		1	Optimized
CL _{PD} basal	Passive diffusion clearance	mL/min/10 ⁶ cells	0	

Input parameters	Description	Units	Value	Reference
Transporter			<i>SLC47A1</i> (MATE1)	
Location			Apical	
Function			Efflux	
CL _{int}	Intrinsic clearance	μL/min/10 ⁶ cells	22.2	Measured
System			User	
RAF/REF	Relative activity factor/relative expression factor		0.25	Optimized
CL _{PD} apical	Passive diffusion clearance	mL/min/10 ⁶ cells	0	

Drug central: <https://drugcentral.org/drugcard/942>

UWDIDB: University of Washington Drug Interaction Database

Chapter 5. Conclusion

Membrane transporters are key regulators of selective cellular permeability, and facilitate the passage of many endogenous metabolites and small-molecule xenobiotics across the plasma membrane. Therefore, membrane transporters play a pivotal role in maintaining normal physiology and pathophysiology, as well as therapeutic response to drugs. At the cellular level, transporter-mediated influx or efflux can lead to the emergence of drug sensitivity or resistant phenotypes in target cells, and as such affect therapeutic efficacy. On the other hand, transporter-mediated uptake in non-target tissues can result in drug-related toxicities, and several transporters involved in these processes have emerged as critical determinants of drug absorption, disposition, therapeutic efficacy, adverse drug reactions, and drug-drug interactions. Here, we highlighted the contribution of membrane transporters in chemotherapy-induced various toxicities and discuss novel strategies to improve therapeutic outcomes. We also provided insights into the recently updated FDA guidelines for *in vitro* drug interaction studies, with a particular focus on the class of TKIs as perpetrators of transporter-mediated drug interactions.

We first evaluated *in vitro* and *in vivo* functional regulation of OCT1, a most abundant cationic transporter expressed in the liver which plays a crucial role in the elimination and pharmacological activity of many prescription drugs. We identified a novel regulatory mechanism for OCT1 function that involves tyrosine phosphorylation by the kinase YES1, and that is highly sensitive to inhibition by multiple TKIs, including

dasatinib. We also identified a novel OCT1 specific biomarker isobutyryl L-carnitine (IBC) in plasma which could ultimately be utilized to guide the selection of optimal doses and schedule of potential perpetrators to be used in conjunction with OCT1 substrates.

Next, we evaluated the interactions with FDA-approved TKIs with MATE1 transporter which is highly expressed in the brush border membrane of proximal tubule cells. We identified MATE1 as a transporter that is sensitive to potent inhibition by a remarkably large number of TKIs, and demonstrated through functional validation studies using genetic and pharmacological approaches that the observed inhibitory properties are potentially related to an effect on transcription. These findings provide novel insight into the regulation of MATE1 and suggest that caution is warranted with polypharmacy regimes involving the use of certain MATE1 substrates given in combination with TKIs.

Finally, we characterized the transport mechanism of dofetilide, a class III anti-arrhythmic drug. We identified that dofetilide is a substrate of MATE1, and is sensitive to inhibition by widely used prescription drugs. In addition, we found that deficiency or inhibition of MATE1 not only reduces urinary excretion of dofetilide but also increases its accumulation in the heart which could potentially lead to cause QTc prolongation as well as individual variation in response. This finding will help understand the etiology of dofetilide-induced proarrhythmia, and provide a rationale for avoiding the use of MATE1 inhibitors in order to derive preventative and/or intervention strategies that could effectively mitigate the occurrence of QTc prolongation and incidence of recurrent arrhythmia without affecting the efficacy of dofetilide.

In the present study, we demonstrated that membrane transporters are important determinants governing the therapeutic response of many drugs. Disruption of these sensitive transport systems through changes in gene expressions, genetic variations or drug-drug interactions, has the potential to contribute to chemoresistance, endogenous toxin-mediated diseases, diminished therapeutic efficacy, and increased sensitivity to drug-induced organ damage. More comprehensive evaluation of drug-transporter interactions should become an integrated approach to human studies aimed at understanding basic pharmacokinetic properties of approved and investigational drugs, and it is anticipated that such studies will continue to make significant contributions to the design of clinical studies aimed at improving the safety and quality of patients' life.

The recently updated FDA guidelines provide inadequate recommendations for *in vitro* studies to identify substrates or inhibitors of drug transporters. The absence of detailed guidance on experimental methodology and study design, which are now left at the discretion of investigators, can contribute to the generation of false-negative data, as evidenced by the noted discrepancies between data contained in the prescribing information and those available in the published literature. It is our contention that the number of currently FDA-approved TKIs that is able to substantially affect the function of OCTs and/or MATEs is underestimated. Therefore, the translational and predictive power of FDA-approved drugs as modulators of transport function remains ambiguous and warrants further revision of the current guidelines.

Bibliography

1. Huang KM, Uddin ME, DiGiacomo D, Lustberg MB, Hu S, Sparreboom A. Role of SLC transporters in toxicity induced by anticancer drugs. *Expert Opin Drug Metab Toxicol.* 2020;16(6):493-506. doi:10.1080/17425255.2020.1755253
2. Uddin ME, Moseley A, Hu S, Sparreboom A. Contribution of membrane transporters to chemotherapy-induced cardiotoxicity. *Basic Clin Pharmacol Toxicol.* 2022;130 Suppl 1:36-47. doi:10.1111/bcpt.13635
3. Hediger MA, Clemencon B, Burrier RE, Bruford EA. The ABCs of membrane transporters in health and disease (SLC series): introduction. *Mol Aspects Med.* 2013;34(2-3):95-107. doi:10.1016/j.mam.2012.12.009
4. Hediger MA, Romero MF, Peng JB, Rolfs A, Takanaga H, Bruford EA. The ABCs of solute carriers: physiological, pathological and therapeutic implications of human membrane transport proteinsIntroduction. *Pflugers Arch.* 2004;447(5):465-468. doi:10.1007/s00424-003-1192-y
5. Koepsell H, Lips K, Volk C. Polyspecific organic cation transporters: Structure, function, physiological roles, and biopharmaceutical implications. *Pharmaceutical Research.* 2007;24(7):1227-1251. doi:10.1007/s11095-007-9254-z
6. Zhang L, Brett CM, Giacomini KM. Role of organic cation transporters in drug absorption and elimination. *Annu Rev Pharmacol Toxicol.* 1998;38:431-460. doi:10.1146/annurev.pharmtox.38.1.431
7. Grundemann D, Gorboulev V, Gambaryan S, Veyhl M, Koepsell H. Drug excretion mediated by a new prototype of polyspecific transporter. *Nature.* 1994;372(6506):549-552. doi:10.1038/372549a0
8. Koepsell H, Lips K, Volk C. Polyspecific organic cation transporters: structure, function, physiological roles, and biopharmaceutical implications. *Pharm Res.* 2007;24(7):1227-1251. doi:10.1007/s11095-007-9254-z
9. Zhang S, Lovejoy KS, Shima JE, et al. Organic cation transporters are determinants of oxaliplatin cytotoxicity. *Cancer research.* 2006;66(17):8847-8857. doi:10.1158/0008-5472.CAN-06-0769
10. Alnouti Y, Petrick JS, Klaassen CD. Tissue distribution and ontogeny of organic cation transporters in mice. *Drug Metab Dispos.* 2006;34(3):477-482. doi:10.1124/dmd.105.006932

11. Gorboulev V, Ulzheimer JC, Akhoundova A, et al. Cloning and characterization of two human polyspecific organic cation transporters. *DNA Cell Biol.* 1997;16(7):871-881. doi:10.1089/dna.1997.16.871
12. Hiasa M, Matsumoto T, Komatsu T, Moriyama Y. Wide variety of locations for rodent MATE1, a transporter protein that mediates the final excretion step for toxic organic cations. *Am J Physiol Cell Physiol.* 2006;291(4):C678-86. doi:10.1152/ajpcell.00090.2006
13. Ohta KY, Inoue K, Hayashi Y, Yuasa H. Molecular identification and functional characterization of rat multidrug and toxin extrusion type transporter 1 as an organic cation/H⁺ antiporter in the kidney. *Drug Metab Dispos.* 2006;34(11):1868-1874. doi:10.1124/dmd.106.010876
14. Yonezawa A, Inui K. Importance of the multidrug and toxin extrusion MATE/SLC47A family to pharmacokinetics, pharmacodynamics/toxicodynamics and pharmacogenomics. *Br J Pharmacol.* 2011;164(7):1817-1825. doi:10.1111/j.1476-5381.2011.01394.x
15. Okabe M, Unno M, Harigae H, et al. Characterization of the organic cation transporter SLC22A16: a doxorubicin importer. *Biochem Biophys Res Commun.* 2005;333(3):754-762. doi:10.1016/j.bbrc.2005.05.174
16. Koepsell H. Organic cation transporters in health and disease. *Pharmacological Reviews.* 2020;72(1):253-319. doi:10.1124/pr.118.015578
17. Nicolaou M, Andress EJ, Zolnerciks JK, Dixon PH, Williamson C, Linton KJ. Canalicular ABC transporters and liver disease. *J Pathol.* 2012;226(2):300-315. doi:10.1002/path.3019
18. Robey RW, Pluchino KM, Hall MD, Fojo AT, Bates SE, Gottesman MM. Revisiting the role of ABC transporters in multidrug-resistant cancer. *Nat Rev Cancer.* 2018;18(7):452-464. doi:10.1038/s41568-018-0005-8
19. International Transporter Consortium, Giacomini KM, Huang SM, et al. Membrane transporters in drug development. *Nat Rev Drug Discov.* 2010;9(3):215-236. doi:10.1038/nrd3028
20. Administration UF and D. In vitro drug interaction studies-cytochrome P450 enzyme-and transporter-mediated drug interactions. *Guidance for industry.* Published online 2020.
21. Chen L, Shu Y, Liang X, et al. OCT1 is a high-capacity thiamine transporter that regulates hepatic steatosis and is a target of metformin. *Proceedings of the*

National Academy of Sciences of the United States of America.
2014;111(27):9983-9988. doi:10.1073/pnas.1314939111

22. Denk GU, Soroka CJ, Mennone A, Koepsell H, Beuers U, Boyer JL. Down-regulation of the organic cation transporter 1 of rat liver in obstructive cholestasis. *Hepatology.* 2004;39(5):1382-1389. doi:10.1002/hep.20176
23. Nies AT, Koepsell H, Winter S, et al. Expression of organic cation transporters OCT1 (SLC22A1) and OCT3 (SLC22A3) is affected by genetic factors and cholestasis in human liver. *Hepatology.* 2009;50(4):1227-1240. doi:10.1002/hep.23103
24. Zamek-Gliszczyński MJ, Giacomini KM, Zhang L. Emerging Clinical Importance of Hepatic Organic Cation Transporter 1 (OCT1) in Drug Pharmacokinetics, Dynamics, Pharmacogenetic Variability, and Drug Interactions. *Clin Pharmacol Ther.* 2018;103(5):758-760. doi:10.1002/cpt.941
25. Shu Y, Sheardown SA, Brown C, et al. Effect of genetic variation in the organic cation transporter 1 (OCT1) on metformin action. *Journal of Clinical Investigation.* 2007;117(5):1422-1431. doi:10.1172/JCI30558
26. Lips KS, Volk C, Schmitt BM, et al. Polyspecific cation transporters mediate luminal release of acetylcholine from bronchial epithelium. *Am J Respir Cell Mol Biol.* 2005;33(1):79-88. doi:10.1165/rcmb.2004-0363OC
27. Lin CJ, Tai Y, Huang MT, et al. Cellular localization of the organic cation transporters, OCT1 and OCT2, in brain microvessel endothelial cells and its implication for MPTP transport across the blood-brain barrier and MPTP-induced dopaminergic toxicity in rodents. *J Neurochem.* 2010;114(3):717-727. doi:10.1111/j.1471-4159.2010.06801.x
28. Chen JJ, Li Z, Pan H, et al. Maintenance of serotonin in the intestinal mucosa and ganglia of mice that lack the high-affinity serotonin transporter: Abnormal intestinal motility and the expression of cation transporters. *J Neurosci.* 2001;21(16):6348-6361.
29. Karbach U, Kricke J, Meyer-Wentrup F, et al. Localization of organic cation transporters OCT1 and OCT2 in rat kidney. *American Journal of Physiology - Renal Physiology.* 2000;279(4 48-4). doi:10.1152/ajprenal.2000.279.4.f679
30. Sugawara-Yokoo M, Urakami Y, Koyama H, et al. Differential localization of organic cation transporters rOCT1 and rOCT2 in the basolateral membrane of rat kidney proximal tubules. *Histochem Cell Biol.* 2000;114(3):175-180. doi:10.1007/s004180000186

31. Wu X, Kekuda R, Huang W, et al. Identity of the organic cation transporter OCT3 as the extraneuronal monoamine transporter (uptake2) and evidence for the expression of the transporter in the brain. *J Biol Chem*. 1998;273(49):32776-32786. doi:10.1074/jbc.273.49.32776
32. Hayer-Zillgen M, Bruss M, Bonisch H. Expression and pharmacological profile of the human organic cation transporters hOCT1, hOCT2 and hOCT3. *Br J Pharmacol*. 2002;136(6):829-836. doi:10.1038/sj.bjp.0704785
33. Solbach TF, Grube M, Fromm MF, Zolk O. Organic cation transporter 3: Expression in failing and nonfailing human heart and functional characterization. *Journal of Cardiovascular Pharmacology*. 2011;58(4):409-417. doi:10.1097/FJC.0b013e3182270783
34. Tregouet DA, Konig IR, Erdmann J, et al. Genome-wide haplotype association study identifies the SLC22A3-LPAL2-LPA gene cluster as a risk locus for coronary artery disease. *Nat Genet*. 2009;41(3):283-285. doi:10.1038/ng.314
35. Chen L, Hong C, Chen EC, et al. Genetic and epigenetic regulation of the organic cation transporter 3, SLC22A3. *Pharmacogenomics Journal*. 2013;13(2):110-120. doi:10.1038/tpj.2011.60
36. Zhao Q, Wei H, Liu D, et al. PHACTR1 and SLC22A3 gene polymorphisms are associated with reduced coronary artery disease risk in the male Chinese Han population. *Oncotarget*. 2017;8(1):658-663. doi:10.18632/oncotarget.13506
37. Zwart R, Verhaagh S, Buitelaar M, Popp-Snijders C, Barlow DP. Impaired activity of the extraneuronal monoamine transporter system known as uptake-2 in *Orect3/Slc22a3*-deficient mice. *Mol Cell Biol*. 2001;21(13):4188-4196. doi:10.1128/MCB.21.13.4188-4196.2001
38. Solbach TF, Grube M, Fromm MF, Zolk O. Organic cation transporter 3: expression in failing and nonfailing human heart and functional characterization. *J Cardiovasc Pharmacol*. 2011;58(4):409-417. doi:10.1097/FJC.0b013e3182270783
39. Wu X, Prasad PD, Leibach FH, Ganapathy V. cDNA sequence, transport function, and genomic organization of human OCTN2, a new member of the organic cation transporter family. *Biochem Biophys Res Commun*. 1998;246(3):589-595. doi:10.1006/bbrc.1998.8669
40. Grundemann D, Harlfinger S, Golz S, et al. Discovery of the ergothioneine transporter. *Proc Natl Acad Sci U S A*. 2005;102(14):5256-5261. doi:10.1073/pnas.0408624102

41. Nakamura T, Nakanishi T, Haruta T, Shirasaka Y, Keogh JP, Tamai I. Transport of ipratropium, an anti-chronic obstructive pulmonary disease drug, is mediated by organic cation/carnitine transporters in human bronchial epithelial cells: implications for carrier-mediated pulmonary absorption. *Mol Pharm.* 2010;7(1):187-195. doi:10.1021/mp900206j
42. Grube M, Ameling S, Noutsias M, et al. Selective regulation of cardiac organic cation transporter novel type 2 (OCTN2) in dilated cardiomyopathy. *Am J Pathol.* 2011;178(6):2547-2559. doi:10.1016/j.ajpath.2011.02.020
43. Tachikawa M, Takeda Y, Tomi M, Hosoya K. Involvement of OCTN2 in the transport of acetyl-L-carnitine across the inner blood-retinal barrier. *Invest Ophthalmol Vis Sci.* 2010;51(1):430-436. doi:10.1167/iovs.09-4080
44. Nancy Nien-Jeh Jong. The role of the organic cation/carnitine transporters in the uptake and neurotoxicity of oxaliplatin. Published online 2012.
45. Shekhawat PS, Sonne S, Matern D, Ganapathy V. Embryonic lethality in mice due to carnitine transporter OCTN2 defect and placental carnitine deficiency. *Placenta.* 2018;69:71-73. doi:10.1016/j.placenta.2018.06.312
46. Otsuka M, Matsumoto T, Morimoto R, Arioka S, Omote H, Moriyama Y. A human transporter protein that mediates the final excretion step for toxic organic cations. *Proc Natl Acad Sci U S A.* 2005;102(50):17923-17928. doi:10.1073/pnas.0506483102
47. Tsuda M, Terada T, Mizuno T, Katsura T, Shimakura J, Inui K. Targeted disruption of the multidrug and toxin extrusion 1 (mate1) gene in mice reduces renal secretion of metformin. *Mol Pharmacol.* 2009;75(6):1280-1286. doi:10.1124/mol.109.056242
48. Go RS, Adjei AA. Review of the comparative pharmacology and clinical activity of cisplatin and carboplatin. *J Clin Oncol.* 1999;17(1):409-422. doi:10.1200/JCO.1999.17.1.409
49. Planting AS, van der Burg ME, de Boer-Dennert M, Stoter G, Verweij J. Phase I/II study of a short course of weekly cisplatin in patients with advanced solid tumours. *Br J Cancer.* 1993;68(4):789-792. doi:10.1038/bjc.1993.429
50. Jassem J, Gyergyay F, Kerpel-Fronius S, et al. Combination of daily 4-h infusion of 5-fluorouracil and cisplatin in the treatment of advanced head and neck squamous-cell carcinoma: a South-East European Oncology Group study. *Cancer Chemother Pharmacol.* 1993;31(6):489-494. doi:10.1007/bf00685041

51. Meijer S, Mulder NH, Sleijfer DT, et al. Nephrotoxicity of cis-diamminedichloride platinum (CDDP) during remission-induction and maintenance chemotherapy of testicular carcinoma. *Cancer Chemother Pharmacol*. 1982;8(1):27-30. doi:10.1007/bf00292867
52. Safirstein R, Winston J, Goldstein M, Moel D, Dikman S, Guttenplan J. Cisplatin nephrotoxicity. *Am J Kidney Dis*. 1986;8(5):356-367. doi:10.1016/s0272-6386(86)80111-1
53. Weiner MW, Jacobs C. Mechanism of cisplatin nephrotoxicity. *Fed Proc*. 1983;42(13):2974-2978.
54. Meijer S, Sleijfer DT, Mulder NH, Donker AJ. Cisplatin-induced nephrotoxicity. *Neth J Med*. 1982;25(8):262-269.
55. de Jongh FE, Gallo JM, Shen M, Verweij J, Sparreboom A. Population pharmacokinetics of cisplatin in adult cancer patients. *Cancer Chemother Pharmacol*. 2004;54(2):105-112. doi:10.1007/s00280-004-0790-5
56. Johnsson A, Hoglund P, Grubb A, Cavallin-Stahl E. Cisplatin pharmacokinetics and pharmacodynamics in patients with squamous-cell carcinoma of the head/neck or esophagus. *Cancer Chemother Pharmacol*. 1996;39(1-2):25-33. doi:10.1007/s002800050534
57. Stewart DJ, Mikhael NZ, Nanji AA, et al. Renal and hepatic concentrations of platinum: relationship to cisplatin time, dose, and nephrotoxicity. *J Clin Oncol*. 1985;3(9):1251-1256. doi:10.1200/JCO.1985.3.9.1251
58. Zhang P, Chen JQ, Huang WQ, et al. Renal Medulla is More Sensitive to Cisplatin than Cortex Revealed by Untargeted Mass Spectrometry-Based Metabolomics in Rats. *Sci Rep*. 2017;7:44804. doi:10.1038/srep44804
59. Volarevic V, Djokovic B, Jankovic MG, et al. Molecular mechanisms of cisplatin-induced nephrotoxicity: a balance on the knife edge between renoprotection and tumor toxicity. *J Biomed Sci*. 2019;26(1):25. doi:10.1186/s12929-019-0518-9
60. Price PM, Safirstein RL, Megyesi J. Protection of renal cells from cisplatin toxicity by cell cycle inhibitors. *Am J Physiol Renal Physiol*. 2004;286(2):F378-84. doi:10.1152/ajprenal.00192.2003
61. Hayati F, Hossainzadeh M, Shayanpour S, Abedi-Gheshlaghi Z, Beladi Mousavi SS. Prevention of cisplatin nephrotoxicity. *J Nephroarmacol*. 2016;5(1):57-60.
62. Pabla N, Dong Z. Cisplatin nephrotoxicity: mechanisms and renoprotective strategies. *Kidney Int*. 2008;73(9):994-1007. doi:10.1038/sj.ki.5002786

63. Filipski KK, Mathijssen RH, Mikkelsen TS, Schinkel AH, Sparreboom A. Contribution of organic cation transporter 2 (OCT2) to cisplatin-induced nephrotoxicity. *Clin Pharmacol Ther.* 2009;86(4):396-402. doi:10.1038/clpt.2009.139
64. Filipski KK, Loos WJ, Verweij J, Sparreboom A. Interaction of Cisplatin with the human organic cation transporter 2. *Clin Cancer Res.* 2008;14(12):3875-3880. doi:10.1158/1078-0432.CCR-07-4793
65. Song IS, Shin HJ, Shin JG. Genetic variants of organic cation transporter 2 (OCT2) significantly reduce metformin uptake in oocytes. *Xenobiotica.* 2008;38(9):1252-1262. doi:10.1080/00498250802130039
66. Song IS, Shin HJ, Shim EJ, et al. Genetic variants of the organic cation transporter 2 influence the disposition of metformin. *Clin Pharmacol Ther.* 2008;84(5):559-562. doi:10.1038/clpt.2008.61
67. Nematbakhsh M, Ebrahimian S, Tooyserkani M, Eshraghi-Jazi F, Talebi A, Ashrafi F. Gender difference in Cisplatin-induced nephrotoxicity in a rat model: greater intensity of damage in male than female. *Nephrourol Mon.* 2013;5(3):818-821. doi:10.5812/numonthly.10128
68. Nakamura T, Yonezawa A, Hashimoto S, Katsura T, Inui K. Disruption of multidrug and toxin extrusion MATE1 potentiates cisplatin-induced nephrotoxicity. *Biochem Pharmacol.* 2010;80(11):1762-1767. doi:10.1016/j.bcp.2010.08.019
69. Katsuda H, Yamashita M, Katsura H, et al. Protecting cisplatin-induced nephrotoxicity with cimetidine does not affect antitumor activity. *Biol Pharm Bull.* 2010;33(11):1867-1871. doi:10.1248/bpb.33.1867
70. Tanihara Y, Masuda S, Katsura T, Inui K. Protective effect of concomitant administration of imatinib on cisplatin-induced nephrotoxicity focusing on renal organic cation transporter OCT2. *Biochem Pharmacol.* 2009;78(9):1263-1271. doi:10.1016/j.bcp.2009.06.014
71. Ciarimboli G, Deuster D, Knief A, et al. Organic cation transporter 2 mediates cisplatin-induced oto- and nephrotoxicity and is a target for protective interventions. *Am J Pathol.* 2010;176(3):1169-1180. doi:10.2353/ajpath.2010.090610
72. Townsend DM, Marto JA, Deng M, Macdonald TJ, Hanigan MH. High pressure liquid chromatography and mass spectrometry characterization of the nephrotoxic biotransformation products of Cisplatin. *Drug Metab Dispos.* 2003;31(6):705-713. doi:10.1124/dmd.31.6.705

73. Sprowl JA, Lancaster CS, Pabla N, et al. Cisplatin-induced renal injury is independently mediated by OCT2 and p53. *Clin Cancer Res.* 2014;20(15):4026-4035. doi:10.1158/1078-0432.CCR-14-0319
74. Hu S, Leblanc AF, Gibson AA, et al. Identification of OAT1/OAT3 as Contributors to Cisplatin Toxicity. *Clin Transl Sci.* 2017;10(5):412-420. doi:10.1111/cts.12480
75. Sprowl JA, Mathijssen RH, Sparreboom A. Can erlotinib ameliorate cisplatin-induced toxicities? *J Clin Oncol.* 2013;31(27):3442-3443. doi:10.1200/JCO.2013.50.8184
76. Yonezawa A, Masuda S, Yokoo S, Katsura T, Inui K. Cisplatin and oxaliplatin, but not carboplatin and nedaplatin, are substrates for human organic cation transporters (SLC22A1-3 and multidrug and toxin extrusion family). *J Pharmacol Exp Ther.* 2006;319(2):879-886. doi:10.1124/jpet.106.110346
77. Yokoo S, Yonezawa A, Masuda S, Fukatsu A, Katsura T, Inui K. Differential contribution of organic cation transporters, OCT2 and MATE1, in platinum agent-induced nephrotoxicity. *Biochem Pharmacol.* 2007;74(3):477-487. doi:10.1016/j.bcp.2007.03.004
78. Hucke A, Park GY, Bauer OB, et al. Interaction of the New Monofunctional Anticancer Agent Phenanthriplatin With Transporters for Organic Cations. *Front Chem.* 2018;6:180. doi:10.3389/fchem.2018.00180
79. Aleksa K, Halachmi N, Ito S, Koren G. Renal ontogeny of ifosfamide nephrotoxicity. *J Lab Clin Med.* 2004;144(6):285-293. doi:10.1016/j.lab.2004.09.002
80. Ciarimboli G, Holle SK, Vollenbrocker B, et al. New clues for nephrotoxicity induced by ifosfamide: preferential renal uptake via the human organic cation transporter 2. *Mol Pharm.* 2011;8(1):270-279. doi:10.1021/mp100329u
81. Kunii E, Oguri T, Kasai D, et al. Organic cation transporter OCT6 mediates cisplatin uptake and resistance to cisplatin in lung cancer. *Cancer Chemotherapy and Pharmacology.* 2015;75(5):985-991. doi:10.1007/s00280-015-2723-x
82. Oguri T, Kunii E, Fukuda S, et al. Organic cation transporter 6 directly confers resistance to anticancer platinum drugs. *Biomed Rep.* 2016;5(5):639-643. doi:10.3892/br.2016.772
83. Cavaletti G. Peripheral neurotoxicity of platinum-based chemotherapy. *Nat Rev Cancer.* 2008;8(1):1p following 71; author reply 1p following 71. doi:10.1038/nrc2167-c1

84. Argyriou AA, Polychronopoulos P, Iconomou G, Chroni E, Kalofonos HP. A review on oxaliplatin-induced peripheral nerve damage. *Cancer Treat Rev.* 2008;34(4):368-377. doi:10.1016/j.ctrv.2008.01.003
85. McWhinney SR, Goldberg RM, McLeod HL. Platinum neurotoxicity pharmacogenetics. *Mol Cancer Ther.* 2009;8(1):10-16. doi:10.1158/1535-7163.MCT-08-0840
86. Pachman DR, Qin R, Seisler DK, et al. Clinical Course of Oxaliplatin-Induced Neuropathy: Results From the Randomized Phase III Trial N08CB (Alliance). *J Clin Oncol.* 2015;33(30):3416-3422. doi:10.1200/JCO.2014.58.8533
87. Di Cesare Mannelli L, Pacini A, Micheli L, Tani A, Zanardelli M, Ghelardini C. Glial role in oxaliplatin-induced neuropathic pain. *Exp Neurol.* 2014;261:22-33. doi:10.1016/j.expneurol.2014.06.016
88. Sprowl JA, Ciarimboli G, Lancaster CS, et al. Oxaliplatin-induced neurotoxicity is dependent on the organic cation transporter OCT2. *Proc Natl Acad Sci U S A.* 2013;110(27):11199-11204. doi:10.1073/pnas.1305321110
89. Sprowl JA, Ong SS, Gibson AA, et al. A phosphotyrosine switch regulates organic cation transporters. *Nature communications.* 2016;7:10880. doi:10.1038/ncomms10880
90. Jong NN, Nakanishi T, Liu JJ, Tamai I, McKeage MJ. Oxaliplatin transport mediated by organic cation/carnitine transporters OCTN1 and OCTN2 in overexpressing human embryonic kidney 293 cells and rat dorsal root ganglion neurons. *J Pharmacol Exp Ther.* 2011;338(2):537-547. doi:10.1124/jpet.111.181297
91. Nishida K, Takeuchi K, Hosoda A, et al. Ergothioneine ameliorates oxaliplatin-induced peripheral neuropathy in rats. *Life Sci.* 2018;207:516-524. doi:10.1016/j.lfs.2018.07.006
92. Fujita S, Hirota T, Sakiyama R, Baba M, Ieiri I. Identification of drug transporters contributing to oxaliplatin-induced peripheral neuropathy. *J Neurochem.* 2019;148(3):373-385. doi:10.1111/jnc.14607
93. Knight KR, Kraemer DF, Neuwelt EA. Ototoxicity in children receiving platinum chemotherapy: underestimating a commonly occurring toxicity that may influence academic and social development. *J Clin Oncol.* 2005;23(34):8588-8596. doi:10.1200/JCO.2004.00.5355

94. Coradini PP, Cigana L, Selistre SG, Rosito LS, Brunetto AL. Ototoxicity from cisplatin therapy in childhood cancer. *J Pediatr Hematol Oncol.* 2007;29(6):355-360. doi:10.1097/MPH.0b013e318059c220
95. Rybak LP, Mukherjea D, Jajoo S, Ramkumar V. Cisplatin ototoxicity and protection: clinical and experimental studies. *Tohoku J Exp Med.* 2009;219(3):177-186. doi:10.1620/tjem.219.177
96. Sheth S, Mukherjea D, Rybak LP, Ramkumar V. Mechanisms of Cisplatin-Induced Ototoxicity and Otoprotection. *Front Cell Neurosci.* 2017;11:338. doi:10.3389/fncel.2017.00338
97. Lanvers-Kaminsky C, Sprowl JA, Malath I, et al. Human OCT2 variant c.808G>T confers protection effect against cisplatin-induced ototoxicity. *Pharmacogenomics.* 2015;16(4):323-332. doi:10.2217/pgs.14.182
98. Leabman MK, Huang CC, Kawamoto M, et al. Polymorphisms in a human kidney xenobiotic transporter, OCT2, exhibit altered function. *Pharmacogenetics.* 2002;12(5):395-405. doi:10.1097/00008571-200207000-00007
99. Zolk O, Solbach TF, Konig J, Fromm MF. Functional characterization of the human organic cation transporter 2 variant p.270Ala>Ser. *Drug Metab Dispos.* 2009;37(6):1312-1318. doi:10.1124/dmd.108.023762
100. Zhang J, Zhou W. Ameliorative effects of SLC22A2 gene polymorphism 808 G/T and cimetidine on cisplatin-induced nephrotoxicity in Chinese cancer patients. *Food Chem Toxicol.* 2012;50(7):2289-2293. doi:10.1016/j.fct.2012.03.077
101. Iwata K, Aizawa K, Kamitsu S, et al. Effects of genetic variants in SLC22A2 organic cation transporter 2 and SLC47A1 multidrug and toxin extrusion 1 transporter on cisplatin-induced adverse events. *Clin Exp Nephrol.* 2012;16(6):843-851. doi:10.1007/s10157-012-0638-y
102. Hacker K, Maas R, Kornhuber J, Fromm MF, Zolk O. Substrate-Dependent Inhibition of the Human Organic Cation Transporter OCT2: A Comparison of Metformin with Experimental Substrates. *PLoS One.* 2015;10(9):e0136451. doi:10.1371/journal.pone.0136451
103. Fox E, Levin K, Zhu Y, et al. Pantoprazole, an Inhibitor of the Organic Cation Transporter 2, Does Not Ameliorate Cisplatin-Related Ototoxicity or Nephrotoxicity in Children and Adolescents with Newly Diagnosed Osteosarcoma Treated with Methotrexate, Doxorubicin, and Cisplatin. *Oncologist.* 2018;23(7):762-e79. doi:10.1634/theoncologist.2018-0037

104. Teft WA, Winquist E, Nichols AC, et al. Predictors of cisplatin-induced ototoxicity and survival in chemoradiation treated head and neck cancer patients. *Oral Oncol.* 2019;89:72-78. doi:10.1016/j.oraloncology.2018.12.010
105. Tkac I, Klimcakova L, Javorsky M, et al. Pharmacogenomic association between a variant in SLC47A1 gene and therapeutic response to metformin in type 2 diabetes. *Diabetes Obes Metab.* 2013;15(2):189-191. doi:10.1111/j.1463-1326.2012.01691.x
106. Bachur NR, Steele M, Meriwether WD, Hildebrand RC. Cellular Pharmacodynamics of Several Anthracycline Antibiotics. *Journal of Medicinal Chemistry.* 1976;19(5):651-654. doi:10.1021/jm00227a015
107. Dalmark M, Storm HH. A fickian diffusion transport process with features of transport catalysis: Doxorubicin transport in human red blood cells. *Journal of General Physiology.* 1981;78(4):349-364. doi:10.1085/jgp.78.4.349
108. Usansky JI, Liebert M, Wedemeyer G, Grossman HB, Wagner JG. The uptake and efflux of doxorubicin by a sensitive human bladder cancer cell line and its doxorubicin-resistant subline. *Sel Cancer Ther.* 1991;7(4):139-150. doi:10.1089/sct.1991.7.139
109. Huang KM, Uddin ME, DiGiacomo D, Lustberg MB, Hu S, Sparreboom A. Role of SLC transporters in toxicity induced by anticancer drugs. *Expert Opinion on Drug Metabolism and Toxicology.* 2020;16(6):493-506. doi:10.1080/17425255.2020.1755253
110. Lin L, Yee SW, Kim RB, Giacomini KM. SLC transporters as therapeutic targets: Emerging opportunities. *Nature Reviews Drug Discovery.* 2015;14(8):543-560. doi:10.1038/nrd4626
111. Schumacher T, Benndorf RA. ABC transport proteins in cardiovascular disease - A brief summary. *Molecules.* 2017;22(4). doi:10.3390/molecules22040589
112. Hausner EA, Elmore SA, Yang X. Overview of the components of cardiac metabolism. *Drug Metabolism and Disposition.* 2019;47(6):673-688. doi:10.1124/dmd.119.086611
113. Grube M, Ameling S, Noutsias M, et al. Selective regulation of cardiac organic cation transporter novel type 2 (OCTN2) in dilated cardiomyopathy. *Am J Pathol.* 2011;178(6):2547-2559. doi:10.1016/j.ajpath.2011.02.020
114. Lee N, Duan H, Hebert MF, Liang CJ, Rice KM, Wang J. Taste of a pill: Organic cation transporter-3 (OCT3) mediates metformin accumulation and secretion in

- salivary glands. *Journal of Biological Chemistry*. 2014;289(39):27055-27064. doi:10.1074/jbc.M114.570564
115. Uddin ME, Jin Y, Gibson AA, et al. Renal Tubular Secretion and Cardiac Distribution of Dofetilide is Dependent on MATE1 Function. *Circulation*. 2020;142(Suppl_3). doi:10.1161/circ.142.suppl_3.14035
 116. Chen Y, Li C, Yi Y, et al. Organic cation transporter 1 and 3 contribute to the high accumulation of dehydrocorydaline in the heart. *Drug Metabolism and Disposition*. 2020;48(10):1074-1083. doi:10.1124/dmd.120.000025
 117. Solbach TF, Grube M, Fromm MF, Zolk O. Organic cation transporter 3: Expression in failing and nonfailing human heart and functional characterization. *Journal of Cardiovascular Pharmacology*. 2011;58(4):409-417. doi:10.1097/FJC.0b013e3182270783
 118. Huang KM, Thomas MZ, Magdy T, et al. Targeting OCT3 attenuates doxorubicin-induced cardiac injury. *Proceedings of the National Academy of Sciences of the United States of America*. 2021;118(5). doi:10.1073/pnas.2020168118
 119. Paquette M, Bernard S, Baass A. SLC22A3 is associated with lipoprotein (a) concentration and cardiovascular disease in familial hypercholesterolemia. *Clinical Biochemistry*. 2019;66:44-48. doi:10.1016/j.clinbiochem.2019.02.008
 120. Al-Eitan LN, Almomani BA, Nassar AM, Elsaqa BZ, Saadeh NA. Metformin pharmacogenetics: Effects of SLC22A1, SLC22A2, and SLC22A3 polymorphisms on glycemic control and HbA1c levels. *Journal of Personalized Medicine*. 2019;9(1). doi:10.3390/jpm9010017
 121. Hucke A, Ciarimboli G. The Role of Transporters in the Toxicity of Chemotherapeutic Drugs: Focus on Transporters for Organic Cations. *Journal of Clinical Pharmacology*. Published online 2016:S157-S172. doi:10.1002/jcph.706
 122. Grube M, Köck K, Oswald S, et al. Organic anion transporting polypeptide 2B1 is a high-affinity transporter for atorvastatin and is expressed in the human heart. *Clinical Pharmacology and Therapeutics*. 2006;80(6):607-620. doi:10.1016/j.clpt.2006.09.010
 123. Bauer M, Matsuda A, Wulkersdorfer B, et al. Influence of OATPs on Hepatic Disposition of Erlotinib Measured With Positron Emission Tomography. *Clinical Pharmacology and Therapeutics*. 2018;104(1):139-147. doi:10.1002/cpt.888
 124. Medwid S, Li MMJ, Knauer MJ, et al. Fexofenadine and rosuvastatin pharmacokinetics in mice with targeted disruption of organic anion transporting

- polypeptide 2b1. *Drug Metabolism and Disposition*. 2019;47(8):832-842. doi:10.1124/dmd.119.087619
125. Chen M, Hu S, Li Y, et al. Role of OATP2B1 in drug absorption and drug-drug interactions. *Drug Metabolism and Disposition*. 2020;48(5):419-425. doi:10.1124/DMD.119.090316
 126. Durmus S, Naik J, Buil L, Wagenaar E, Van Tellingen O, Schinkel AH. In vivo disposition of doxorubicin is affected by mouse Oatp1a/1b and human OATP1A/1B transporters. *International Journal of Cancer*. 2014;135(7):1700-1710. doi:10.1002/ijc.28797
 127. Hertz DL, Caram MV, Kidwell KM, et al. Evidence for association of SNPs in ABCB1 and CBR3, but not RAC2, NCF4, SLC28A3 or TOP2B, with chronic cardiotoxicity in a cohort of breast cancer patients treated with anthracyclines. *Pharmacogenomics*. 2016;17(3):231-240. doi:10.2217/pgs.15.162
 128. Huang KM, Hu S, Sparreboom A. Drug transporters and anthracycline-induced cardiotoxicity. *Pharmacogenomics*. 2018;19(11):883-888. doi:10.2217/pgs-2018-0056
 129. Van Asperen J, Van Tellingen O, Tijssen F, Schinkel AH, Beijnen JH. Increased accumulation of doxorubicin and doxorubicinol in cardiac tissue of mice lacking mdr1a P-glycoprotein. *British Journal of Cancer*. 1999;79(1):108-113. doi:10.1038/sj.bjc.6690019
 130. Durmus S, Naik J, Buil L, Wagenaar E, Tellingen OV, Schinkel AH. In vivo disposition of doxorubicin is affected by mouse Oatp1a/1b and human OATP1A/1B transporters. *International Journal of Cancer*. 2014;135(7):1700-1710. doi:10.1002/ijc.28797
 131. Asperen JV, Tellingen OV, Tijssen F, Schinkel AH, Beijnen JH. Increased accumulation of doxorubicin and doxorubicinol in cardiac tissue of mice lacking mdr1a P-glycoprotein. *British Journal of Cancer*. 1999;79(1):108-113. doi:10.1038/sj.bjc.6690019
 132. Koltz JE, George SL, Marcucci G, et al. P-glycoprotein inhibition using valspodar (PSC-833) does not improve outcomes for patients younger than age 60 years with newly diagnosed acute myeloid leukemia: Cancer and Leukemia Group B study 19808. *Blood*. 2010;116(9):1413-1421. doi:10.1182/blood-2009-07-229492
 133. Zhang W, Deng J, Sunkara M, et al. Loss of multidrug resistance-associated protein 1 potentiates chronic doxorubicin-induced cardiac dysfunction in mice. *Journal of Pharmacology and Experimental Therapeutics*. 2015;355(2):280-287. doi:10.1124/jpet.115.225581

134. Semsei AF, Erdelyi DJ, Ungvari I, et al. ABCC1 polymorphisms in anthracycline-induced cardiotoxicity in childhood acute lymphoblastic leukaemia. *Cell Biology International*. 2012;36(1):79-86. doi:10.1042/cbi20110264
135. Zhang W, Clair DS, Butterfield A, Vore M. Loss of Mrp1 potentiates doxorubicin-induced cytotoxicity in neonatal mouse cardiomyocytes and cardiac fibroblasts. *Toxicological Sciences*. 2016;151(1):44-56. doi:10.1093/toxsci/kfw021
136. Sahoo S, Aurich MK, Jonsson JJ, Thiele I. Membrane transporters in a human genome-scale metabolic knowledgebase and their implications for disease. *Frontiers in Physiology*. 2014;5 MAR. doi:10.3389/fphys.2014.00091
137. Shao D, Tian R. Glucose transporters in cardiac metabolism and hypertrophy. *Comprehensive Physiology*. 2016;6(1):331-351. doi:10.1002/cphy.c150016
138. Agostino NM, Chinchilli VM, Lynch CJ, et al. Effect of the tyrosine kinase inhibitors (sunitinib, sorafenib, dasatinib, and imatinib) on blood glucose levels in diabetic and nondiabetic patients in general clinical practice. *Journal of Oncology Pharmacy Practice*. 2011;17(3):197-202. doi:10.1177/1078155210378913
139. Skrabs C, Pickl WF, Perkmann T, Jäger U, Gessl A. Rapid decline in insulin antibodies and glutamic acid decarboxylase autoantibodies with ibrutinib therapy of chronic lymphocytic leukaemia. *Journal of Clinical Pharmacy and Therapeutics*. 2018;43(1):145-149. doi:10.1111/jcpt.12602
140. Damaraju VL, Aminpour M, Kuzma M, et al. Tyrosine kinase inhibitors reduce glucose uptake by binding to an exofacial site on hGLUT-1: Effects on 18 F-FDG PET uptake . *Clinical and Translational Science*. Published online 2020. doi:10.1111/cts.12943
141. Hadova K, Mesarosova L, Kralova E, Doka G, Krenek P, Klimas J. The tyrosine kinase inhibitor crizotinib influences blood glucose and mRNA expression of GLUT4 and PPARs in the heart of rats with experimental diabetes. *Canadian Journal of Physiology and Pharmacology*. Published online 2020. doi:10.1139/cjpp-2020-0572
142. Thomas D, Karle C, Kiehn J. The Cardiac hERG/IKr Potassium Channel as Pharmacological Target: Structure, Function, Regulation, and Clinical Applications. *Current Pharmaceutical Design*. 2006;12(18):2271-2283. doi:10.2174/138161206777585102
143. Yang T, McBride BF, Leake BF, Kim RB, Roden DM. Modulation of drug block of the cardiac potassium channel KCNA5 by the drug transporters OCTN1 and MDR1. *British Journal of Pharmacology*. 2010;161(5):1023-1033. doi:10.1111/j.1476-5381.2010.00932.x

144. McBride BF, Yang T, Liu K, et al. The organic cation transporter, OCTN1, expressed in the human heart, potentiates antagonism of the HERG potassium channel. *Journal of Cardiovascular Pharmacology*. 2009;54(1):63-71. doi:10.1097/FJC.0b013e3181abc288
145. Krishnamurthy K, Vedam K, Kanagasabai R, Druhan LJ, Ilangovan G. Heat shock factor-1 knockout induces multidrug resistance gene, MDR1b, and enhances P-glycoprotein (ABCB1)-based drug extrusion in the heart. *Proceedings of the National Academy of Sciences of the United States of America*. 2012;109(23):9023-9028. doi:10.1073/pnas.1200731109
146. Sajid A, Lusvarghi S, Murakami M, et al. Reversing the direction of drug transport mediated by the human multidrug transporter P-glycoprotein. *Proceedings of the National Academy of Sciences of the United States of America*. 2020;117(47):29609-29617. doi:10.1073/pnas.2016270117
147. Burridge PW, Li YF, Matsa E, et al. Human induced pluripotent stem cell-derived cardiomyocytes recapitulate the predilection of breast cancer patients to doxorubicin-induced cardiotoxicity. *Nature Medicine*. 2016;22(5):547-556. doi:10.1038/nm.4087
148. MacArron R, Banks MN, Bojanic D, et al. Impact of high-throughput screening in biomedical research. *Nature Reviews Drug Discovery*. 2011;10(3):188-195. doi:10.1038/nrd3368
149. Carroll KJ, Makarewich CA, McAnally J, et al. A mouse model for adult cardiac-specific gene deletion with CRISPR/Cas9. *Proceedings of the National Academy of Sciences of the United States of America*. Published online 2016. doi:10.1073/pnas.1523918113
150. Silva-Platas C, Villegas CA, Oropeza-Almazán Y, et al. Ex vivo cardiotoxicity of antineoplastic casiopeinas is mediated through energetic dysfunction and triggered mitochondrial-dependent apoptosis. *Oxidative Medicine and Cellular Longevity*. 2018;2018. doi:10.1155/2018/8949450
151. Seraphim A, Westwood M, Bhuvana AN, et al. Advanced Imaging Modalities to Monitor for Cardiotoxicity. *Current Treatment Options in Oncology*. 2019;20(9). doi:10.1007/s11864-019-0672-z
152. Joshi S, Evangelisti A, Liao R, Alexander KM. Harnessing Cardiac Regeneration as a Potential Therapeutic Strategy for AL Cardiac Amyloidosis. *Curr Cardiol Rep*. 2020;22(1):1. doi:10.1007/s11886-020-1252-3

153. Biersmith MA, Tong MS, Guha A, Simonetti OP, Addison D. Multimodality Cardiac Imaging in the Era of Emerging Cancer Therapies. *J Am Heart Assoc.* 2020;9(2):e013755. doi:10.1161/JAHA.119.013755
154. Feldman HS, Hartvig P, Wiklund L, et al. Regional distribution of ¹¹C-labeled lidocaine, bupivacaine, and ropivacaine in the heart, lungs, and skeletal muscle of pigs studied with positron emission tomography. *Biopharmaceutics and Drug Disposition.* 1997;18(2):151-164. doi:10.1002/(SICI)1099-081X(199703)18:2<151::AID-BDD8>3.0.CO;2-H
155. Demir H, Tan YZ, Kozdag G, et al. Comparison of gated SPECT, echocardiography and cardiac magnetic resonance imaging for the assessment of left ventricular ejection fraction and volumes. *Annals of Saudi Medicine.* 2007;27(6):415-420. doi:10.5144/0256-4947.2007.415
156. Weber M, Hamm C. Role of B-type natriuretic peptide (BNP) and NT-PROBNP in clinical routine. *Heart.* 2006;92(6):843-849. doi:10.1136/hrt.2005.071233
157. Leerink JM, Verkleij SJ, Feijen EAM, et al. Biomarkers to diagnose ventricular dysfunction in childhood cancer survivors: A systematic review. *Heart.* 2019;105(3):210-216. doi:10.1136/heartjnl-2018-313634
158. Ibrahim NE, Januzzi JL. Established and Emerging Roles of Biomarkers in Heart Failure. *Circ Res.* 2018;123(5):614-629. doi:10.1161/CIRCRESAHA.118.312706
159. Rahman AM, Yusuf SW, Ewer MS. Anthracycline-induced cardiotoxicity and the cardiac-sparing effect of liposomal formulation. *Int J Nanomedicine.* 2007;2(4):567-583.
160. Page RL, O'bryant CL, Cheng D, et al. Drugs that may cause or exacerbate heart failure. *Circulation.* 2016;134(6):e32-e69. doi:10.1161/CIR.0000000000000426
161. Malki MA, Pearson ER. Drug–drug–gene interactions and adverse drug reactions. *Pharmacogenomics Journal.* 2020;20(3):355-366. doi:10.1038/s41397-019-0122-0
162. Uddin ME, Garrison DA, Kim K, et al. Influence of YES1 Kinase and Tyrosine Phosphorylation on the Activity of OCT1. *Front Pharmacol.* 2021;12:644342. doi:10.3389/fphar.2021.644342
163. Huang KM, Uddin ME, DiGiacomo D, Lustberg MB, Hu S, Sparreboom A. Role of SLC transporters in toxicity induced by anticancer drugs. *Expert Opinion on Drug Metabolism and Toxicology.* 2020;16(6):493-506. doi:10.1080/17425255.2020.1755253

164. Jonker JW, Wagenaar E, van Eijl S, Schinkel AH. Deficiency in the Organic Cation Transporters 1 and 2 (Oct1/Oct2 [Slc22a1/Slc22a2]) in Mice Abolishes Renal Secretion of Organic Cations. *Molecular and Cellular Biology*. 2003;23(21):7902-7908. doi:10.1128/mcb.23.21.7902-7908.2003
165. Jonker JW, Wagenaar E, Mol CAAM, et al. Reduced Hepatic Uptake and Intestinal Excretion of Organic Cations in Mice with a Targeted Disruption of the Organic Cation Transporter 1 (Oct1 [Slc22a1]) Gene. *Molecular and Cellular Biology*. 2001;21(16):5471-5477. doi:10.1128/mcb.21.16.5471-5477.2001
166. Chae YK, Arya A, Malecek MK, et al. Repurposing metformin for cancer treatment: Current clinical studies. *Oncotarget*. 2016;7(26):40767-40780. doi:10.18632/oncotarget.8194
167. Heckman-Stoddard BM, Gandini S, Puntoni M, Dunn BK, Decensi A, Szabo E. Repurposing old drugs to chemoprevention: The case of metformin. *Seminars in Oncology*. 2016;43(1):123-133. doi:10.1053/j.seminoncol.2015.09.009
168. Higgins JW, Bedwell DW, Zamek-Gliszczyński MJ. Ablation of both organic cation transporter (oct)1 and oct2 alters metformin pharmacokinetics but has no effect on tissue drug exposure and pharmacodynamics. *Drug Metabolism and Disposition*. 2012;40(6):1170-1177. doi:10.1124/dmd.112.044875
169. Tzvetkov M V., Matthaai J, Pojar S, et al. Increased Systemic Exposure and Stronger Cardiovascular and Metabolic Adverse Reactions to Fenoterol in Individuals with Heritable OCT1 Deficiency. *Clinical Pharmacology and Therapeutics*. 2018;103(5):868-878. doi:10.1002/cpt.812
170. Fukuda T, Chidambaran V, Mizuno T, et al. OCT1 genetic variants influence the pharmacokinetics of morphine in children. *Pharmacogenomics*. 2013;14(10):1141-1151. doi:10.2217/pgs.13.94
171. Matthaai J, Kuron D, Faltraco F, et al. OCT1 mediates hepatic uptake of sumatriptan and loss-of-function OCT1 polymorphisms affect sumatriptan pharmacokinetics. *Clinical Pharmacology and Therapeutics*. 2016;99(6):633-641. doi:10.1002/cpt.317
172. Chen L, Shu Y, Liang X, et al. OCT1 is a high-capacity thiamine transporter that regulates hepatic steatosis and is a target of metformin. *Proceedings of the National Academy of Sciences of the United States of America*. 2014;111(27):9983-9988. doi:10.1073/pnas.1314939111
173. Tzvetkov M V., Saadatmand AR, Lötsch J, Tegeder I, Stingl JC, Brockmöller J. Genetically polymorphic OCT1: Another piece in the puzzle of the variable pharmacokinetics and pharmacodynamics of the opioidergic drug tramadol.

- Clinical Pharmacology and Therapeutics*. 2011;90(1):143-150.
doi:10.1038/clpt.2011.56
174. Tzvetkov M V., Saadatmand AR, Bokelmann K, Meineke I, Kaiser R, Brockmüller J. Effects of OCT1 polymorphisms on the cellular uptake, plasma concentrations and efficacy of the 5-HT₃ antagonists tropisetron and ondansetron. *Pharmacogenomics Journal*. 2012;12(1):22-29. doi:10.1038/tpj.2010.75
 175. Gomez A, Ingelman-Sundberg M. Pharmacoeugenetics: Its role in interindividual differences in drug response. *Clinical Pharmacology and Therapeutics*. 2009;85(4):426-430. doi:10.1038/clpt.2009.2
 176. Giacomini KM, Yee SW, Ratain MJ, Weinshilboum RM, Kamatani N, Nakamura Y. Pharmacogenomics and patient care: One size does not fit all. *Science Translational Medicine*. 2012;4(153). doi:10.1126/scitranslmed.3003471
 177. Schaeffeler E, Hellerbrand C, Nies AT, et al. DNA methylation is associated with downregulation of the organic cation transporter OCT1 (SLC22A1) in human hepatocellular carcinoma. *Genome Medicine*. 2011;3(12). doi:10.1186/gm298
 178. Mehrens T, Lelleck S, Çetinkaya I, et al. The affinity of the organic cation transporter rOCT1 is increased by protein kinase C-dependent phosphorylation. *Journal of the American Society of Nephrology*. 2000;11(7):1216-1224.
 179. Czuba LC, Hillgren KM, Swaan PW. Post-translational modifications of transporters. *Pharmacology and Therapeutics*. 2018;192:88-99. doi:10.1016/j.pharmthera.2018.06.013
 180. Sprowl JA, Ong SS, Gibson AA, et al. A phosphotyrosine switch regulates organic cation transporters. *Nature Communications*. 2016;7. doi:10.1038/ncomms10880
 181. Tanaka M, Herr W. Differential transcriptional activation by Oct-1 and Oct-2: Interdependent activation domains induce Oct-2 phosphorylation. *Cell*. 1990;60(3):375-386. doi:10.1016/0092-8674(90)90589-7
 182. Sprowl JA, Ciarimboli G, Lancaster CS, et al. Oxaliplatin-induced neurotoxicity is dependent on the organic cation transporter OCT2. *Proceedings of the National Academy of Sciences of the United States of America*. 2013;110(27):11199-11204. doi:10.1073/pnas.1305321110
 183. Pabla N, Gibson AA, Buege M, et al. Mitigation of acute kidney injury by cell-cycle inhibitors that suppress both CDK4/6 and OCT2 functions. *Proceedings of the National Academy of Sciences of the United States of America*. 2015;112(16):5231-5236. doi:10.1073/pnas.1424313112

184. Huang F, Ni M, Chalishazar MD, et al. Inosine Monophosphate Dehydrogenase Dependence in a Subset of Small Cell Lung Cancers. *Cell Metabolism*. 2018;28(3):369-382.e5. doi:10.1016/j.cmet.2018.06.005
185. Leblanc AF, Huang K, Uddin ME, Anderson J, Chen M, Hu S. Murine Pharmacokinetic Studies. *Bio-Protocol*. 2018;8(20). doi:10.21769/bioprotoc.3056
186. Mato EPM, Guewo-Fokeng M, Essop MF, Owira PMO. Genetic polymorphisms of organic cation transporter 1 (OCT1) and responses to metformin therapy in individuals with type 2 diabetes. *Medicine (United States)*. 2018;97(27). doi:10.1097/MD.00000000000011349
187. Minematsu T, Giacomini KM. Interactions of tyrosine kinase inhibitors with organic cation transporters and multidrug and toxic compound extrusion proteins. *Molecular Cancer Therapeutics*. 2011;10(3):531-539. doi:10.1158/1535-7163.MCT-10-0731
188. Furmanski BD, Hu S, Fujita KI, et al. Contribution of ABCC4-mediated gastric transport to the absorption and efficacy of dasatinib. *Clinical Cancer Research*. 2013;19(16):4359-4370. doi:10.1158/1078-0432.CCR-13-0980
189. Meyer MJ, Tuerkova A, Römer S, et al. Differences in metformin and thiamine uptake between human and mouse organic cation transporter OCT1: structural determinants and potential consequences for intrahepatic concentrations . *Drug Metabolism and Disposition*. 2020;48(12):DMD-AR-2020-000170. doi:10.1124/dmd.120.000170
190. Floerl S, Kuehne A, Hagos Y. Functional and pharmacological comparison of human, mouse, and rat organic cation transporter 1 toward drug and pesticide interaction. *International Journal of Molecular Sciences*. 2020;21(18):1-15. doi:10.3390/ijms21186871
191. Holle SK, Ciarimboli G, Edemir B, Neugebauer U, Pavenstädt H, Schlatter E. Properties and regulation of organic cation transport in freshly isolated mouse proximal tubules analyzed with a fluorescence reader-based method. *Pflügers Archiv European Journal of Physiology*. 2011;462(2):359-369. doi:10.1007/s00424-011-0969-7
192. Luo L, Ramanathan R, Horlbogen L, et al. A Multiplexed HILIC-MS/HRMS Assay for the Assessment of Transporter Inhibition Biomarkers in Phase i Clinical Trials: Isobutyryl-Carnitine as an Organic Cation Transporter (OCT1) Biomarker. *Analytical Chemistry*. 2020;92(14):9745-9754. doi:10.1021/acs.analchem.0c01144
193. Klaeger S, Heinzlmeir S, Wilhelm M, et al. The target landscape of clinical kinase drugs. *Science*. 2017;358(6367). doi:10.1126/science.aan4368

194. KINOMEScan data - HMS LINCS Project. Accessed December 19, 2020. <https://lincs.hms.harvard.edu/kinomescan/>
195. Li J, Rix U, Fang B, et al. A chemical and phosphoproteomic characterization of dasatinib action in lung cancer. *Nature Chemical Biology*. 2010;6(4):291-299. doi:10.1038/nchembio.332
196. Du J, Bernasconi P, Clauser KR, et al. Bead-based profiling of tyrosine kinase phosphorylation identifies SRC as a potential target for glioblastoma therapy. *Nature Biotechnology*. 2009;27(1):77-83. doi:10.1038/nbt.1513
197. Jensen O, Matthaai J, Blome F, Schwab M, Tzvetkov M V., Brockmüller J. Variability and Heritability of Thiamine Pharmacokinetics With Focus on OCT1 Effects on Membrane Transport and Pharmacokinetics in Humans. *Clinical Pharmacology and Therapeutics*. 2020;107(3):628-638. doi:10.1002/cpt.1666
198. Lautem A, Heise M, Gräsel A, et al. Downregulation of organic cation transporter 1 (SLC22A1) is associated with tumor progression and reduced patient survival in human cholangiocellular carcinoma. *International Journal of Oncology*. 2013;42(4):1297-1304. doi:10.3892/ijo.2013.1840
199. O'Brien VP, Bokelmann K, Ramírez J, et al. Hepatocyte nuclear factor 1 regulates the expression of the organic cation transporter 1 via binding to an evolutionary conserved region in intron 1 of the OCT1 Gene. *Journal of Pharmacology and Experimental Therapeutics*. 2013;347(1):181-192. doi:10.1124/jpet.113.206359
200. Saborowski M, Kullak-Ublick GA, Eloranta JJ. The human organic cation transporter-1 gene is transactivated by hepatocyte nuclear factor-4 α . *Journal of Pharmacology and Experimental Therapeutics*. 2006;317(2):778-785. doi:10.1124/jpet.105.099929
201. Le Vee M, Lecureur V, Moreau A, Stieger B, Fardel O. Differential regulation of drug transporter expression by hepatocyte growth factor in primary human hepatocytes. *Drug Metabolism and Disposition*. 2009;37(11):2228-2235. doi:10.1124/dmd.109.028035
202. Ciarimboli G, Ludwig T, Lang D, et al. Cisplatin nephrotoxicity is critically mediated via the human organic cation transporter 2. *American Journal of Pathology*. 2005;167(6):1477-1484. doi:10.1016/S0002-9440(10)61234-5
203. Tzvetkov M V., Dos Santos Pereira JN, Meineke I, Saadatmand AR, Stingl JC, Brockmüller J. Morphine is a substrate of the organic cation transporter OCT1 and polymorphisms in OCT1 gene affect morphine pharmacokinetics after codeine administration. *Biochemical Pharmacology*. 2013;86(5):666-678. doi:10.1016/j.bcp.2013.06.019

204. Sandoval PJ, Zorn KM, Clark AM, Ekins S, Wright SH. Assessment of substrate-dependent ligand interactions at the organic cation transporter OCT2 using six model substrates. *Molecular Pharmacology*. 2018;94(3):1057-1068. doi:10.1124/mol.117.111443
205. Kim HI, Raffler J, Lu W, et al. Fine Mapping and Functional Analysis Reveal a Role of SLC22A1 in Acylcarnitine Transport. *American Journal of Human Genetics*. 2017;101(4):489-502. doi:10.1016/j.ajhg.2017.08.008
206. Lancaster CS, Hu C, Franke RM, et al. Cisplatin-induced downregulation of OCTN2 affects carnitine wasting. *Clinical Cancer Research*. 2010;16(19):4789-4799. doi:10.1158/1078-0432.CCR-10-1239
207. Uddin ME, Talebi Z, Chen S, et al. In Vitro and In Vivo Inhibition of MATE1 by Tyrosine Kinase Inhibitors. *Pharmaceutics*. 2021;13(12):2004. doi:10.3390/pharmaceutics13122004
208. Kaback HR, Sahin-Tóth M, Weinglass AB. The kamikaze approach to membrane transport. *Nature reviews Molecular cell biology*. 2001;2(8):610-620. doi:10.1038/35085077
209. Borst P, Elferink RO. Mammalian ABC Transporters in Health and Disease. *Annual Review of Biochemistry*. Published online 2002. doi:10.1146/annurev.biochem.71.102301.093055
210. Borst P, Evers R, Kool M, Wijnholds J. The multidrug resistance protein family. *Biochimica et biophysica acta*. 1999;1461(2):347-357. doi:10.1016/s0005-2736(99)00167-4
211. Sprowl JA, Sparreboom A. Uptake carriers and oncology drug safety. *Drug metabolism and disposition: the biological fate of chemicals*. 2014;42(4):611-622. doi:10.1124/dmd.113.055806
212. Giacomini KM, Yee SW, Ratain MJ, Weinshilboum RM, Kamatani N, Nakamura Y. Pharmacogenomics and patient care: one size does not fit all. *Science translational medicine*. 2012;4(153):153ps18. doi:10.1126/scitranslmed.3003471
213. Koepsell H. Update on drug-drug interaction at organic cation transporters: mechanisms, clinical impact, and proposal for advanced in vitro testing. *Expert opinion on drug metabolism & toxicology*. 2021;17(6):635-653. doi:10.1080/17425255.2021.1915284
214. Uddin ME, Garrison DA, Kim K, et al. Influence of YES1 Kinase and Tyrosine Phosphorylation on the Activity of OCT1. *Frontiers in pharmacology*. 2021;12:644342. doi:10.3389/fphar.2021.644342

215. Huang KM, Zavoroka Thomas M, Magdy T, et al. Targeting OCT3 attenuates doxorubicin-induced cardiac injury. *Proceedings of the National Academy of Sciences of the United States of America*. 2021;118(5). doi:10.1073/pnas.2020168118
216. Pabla N, Gibson AA, Buege M, et al. Mitigation of acute kidney injury by cell-cycle inhibitors that suppress both CDK4/6 and OCT2 functions. *Proceedings of the National Academy of Sciences of the United States of America*. 2015;112(16):5231-5236. doi:10.1073/pnas.1424313112
217. Sprowl JA, Ciarimboli G, Lancaster CS, et al. Oxaliplatin-induced neurotoxicity is dependent on the organic cation transporter OCT2. *Proceedings of the National Academy of Sciences of the United States of America*. 2013;110(27):11199-11204. doi:10.1073/pnas.1305321110
218. Minematsu T, Giacomini KM. Interactions of tyrosine kinase inhibitors with organic cation transporters and multidrug and toxic compound extrusion proteins. *Molecular cancer therapeutics*. 2011;10(3):531-539. doi:10.1158/1535-7163.MCT-10-0731
219. Tátrai P, Schweigler P, Poller B, et al. A Systematic In Vitro Investigation of the Inhibitor Preincubation Effect on Multiple Classes of Clinically Relevant Transporters. *Drug metabolism and disposition: the biological fate of chemicals*. 2019;47(7):768-778. doi:10.1124/dmd.118.085993
220. George B, Wen X, Jaimes EA, Joy MS, Aleksunes LM. In Vitro Inhibition of Renal OCT2 and MATE1 Secretion by Antiemetic Drugs. *International journal of molecular sciences*. 2021;22(12). doi:10.3390/ijms22126439
221. Omote S, Matsuoka N, Arakawa H, Nakanishi T, Tamai I. Effect of tyrosine kinase inhibitors on renal handling of creatinine by MATE1. *Sci Rep*. 2018;8(1):9237. doi:10.1038/s41598-018-27672-y
222. Kajiwara M, Terada T, Ogasawara K, et al. Identification of multidrug and toxin extrusion (MATE1 and MATE2-K) variants with complete loss of transport activity. *Journal of Human Genetics*. 2009;54(1):40-46. doi:10.1038/jhg.2008.1
223. Terada T, Masuda S, Asaka JI, Tsuda M, Katsura T, Inui KI. Molecular cloning, functional characterization and tissue distribution of rat H⁺/organic cation antiporter MATE1. *Pharmaceutical Research*. 2006;23(8):1696-1701. doi:10.1007/s11095-006-9016-3
224. Dangprapai Y, Wright SH. Interaction of H⁺ with the extracellular and intracellular aspects of hMATE1. *American journal of physiology Renal physiology*. 2011;301(3):F520-8. doi:10.1152/ajprenal.00075.2011

225. Filipski KK, Loos WJ, Verweij J, Sparreboom A. Interaction of cisplatin with the human organic cation transporter 2. *Clinical Cancer Research*. 2008;14(12):3875-3880. doi:10.1158/1078-0432.CCR-07-4793
226. Dixon SL, Smondirev AM, Knoll EH, Rao SN, Shaw DE, Friesner RA. PHASE: A new engine for pharmacophore perception, 3D QSAR model development, and 3D database screening: 1. Methodology and preliminary results. *Journal of Computer-Aided Molecular Design*. 2006;20(10-11):647-671. doi:10.1007/s10822-006-9087-6
227. Friesner RA, Murphy RB, Repasky MP, et al. Extra precision glide: Docking and scoring incorporating a model of hydrophobic enclosure for protein-ligand complexes. *Journal of Medicinal Chemistry*. 2006;49(21):6177-6196. doi:10.1021/jm051256o
228. Farhat NH. Photonit neural networks and learning mathines the role of electron-trapping materials. *IEEE Expert-Intelligent Systems and their Applications*. 1992;7(5):63-72. doi:10.1109/64.163674
229. Rumelhart DE, Hinton GE, Williams RJ. Learning representations by back-propagating errors. *Nature*. 1986;323(6088):533-536. doi:10.1038/323533a0
230. Leblanc AF, Huang KM, Uddin ME, Anderson JT, Chen M, Hu S. Murine Pharmacokinetic Studies. *Bio-protocol*. 2018;8(20). doi:10.21769/bioprotoc.3056
231. Filipski KK, Mathijssen RH, Mikkelsen TS, Schinkel AH, Sparreboom A. Contribution of organic cation transporter 2 (OCT2) to cisplatin-induced nephrotoxicity. *Clinical Pharmacology and Therapeutics*. 2009;86(4):396-402. doi:10.1038/clpt.2009.139
232. Furmanski BD, Hu S, Fujita KI, et al. Contribution of ABCC4-mediated gastric transport to the absorption and efficacy of dasatinib. *Clinical cancer research : an official journal of the American Association for Cancer Research*. 2013;19(16):4359-4370. doi:10.1158/1078-0432.CCR-13-0980
233. Sprowl JA, van Doorn L, Hu S, et al. Conjunctive therapy of cisplatin with the OCT2 inhibitor cimetidine: influence on antitumor efficacy and systemic clearance. *Clinical pharmacology and therapeutics*. 2013;94(5):585-592. doi:10.1038/clpt.2013.145
234. Belzer M, Morales M, Jagadish B, Mash EA, Wright SH. Substrate-dependent ligand inhibition of the human organic cation transporter OCT2. *The Journal of pharmacology and experimental therapeutics*. 2013;346(2):300-310. doi:10.1124/jpet.113.203257

235. Smith RD, Lu J, Carlson HA. Are there physicochemical differences between allosteric and competitive ligands? *PLoS Computational Biology*. 2017;13(11):1-18. doi:10.1371/journal.pcbi.1005813
236. Jumper J, Evans R, Pritzel A, et al. Highly accurate protein structure prediction with AlphaFold. *Nature*. 2021;596(7873):583-589. doi:10.1038/s41586-021-03819-2
237. Koepsell H. Organic Cation Transporters in Health and Disease. *Pharmacological reviews*. 2020;72(1):253-319. doi:10.1124/pr.118.015578
238. Freitas-Lima LC, Budu A, Arruda AC, et al. PPAR- α Deletion Attenuates Cisplatin Nephrotoxicity by Modulating Renal Organic Transporters MATE-1 and OCT-2. *International journal of molecular sciences*. 2020;21(19). doi:10.3390/ijms21197416
239. Arruda AC, Perilhão MS, Santos WA, et al. PPAR α -Dependent Modulation by Metformin of the Expression of OCT-2 and MATE-1 in the Kidney of Mice. *Molecules* . 2020;25(2). doi:10.3390/molecules25020392
240. Wongwan T, Chatsudthipong V, Soodvilai S. Farnesoid X Receptor Activation Stimulates Organic Cations Transport in Human Renal Proximal Tubular Cells. *International Journal of Molecular Sciences* . 2020;21(17). doi:10.3390/ijms21176078
241. Kajiwara M, Terada T, Asaka J ichi, et al. Critical roles of Sp1 in gene expression of human and rat H⁺/organic cation antiporter MATE1. *American Journal of Physiology-Renal Physiology*. 2007;293(5):F1564-F1570. doi:10.1152/ajprenal.00322.2007
242. Ha Choi J, Wah Yee S, Kim MJ, et al. Identification and characterization of novel polymorphisms in the basal promoter of the human transporter, MATE1. *Pharmacogenetics and genomics*. 2009;19(10):770-780. doi:10.1097/FPC.0b013e328330eeca
243. Kim TH, Kim KH, Park HJ, Kim S, Choi JH. Identification and functional characterization of novel MATE1 genetic variations in Koreans. *Biochemical and Biophysical Research Communications*. 2013;434(2):334-340. doi:https://doi.org/10.1016/j.bbrc.2013.03.072
244. Shapira S, Granot G, Mor-Tzuntz R, et al. Second-generation tyrosine kinase inhibitors reduce telomerase activity in K562 cells. *Cancer Letters*. 2012;323(2):223-231. doi:https://doi.org/10.1016/j.canlet.2012.04.022

245. Miyake T, Mizuno T, Takehara I, et al. Elucidation of N (1)-methyladenosine as a Potential Surrogate Biomarker for Drug Interaction Studies Involving Renal Organic Cation Transporters. *Drug metabolism and disposition: the biological fate of chemicals*. 2019;47(11):1270-1280. doi:10.1124/dmd.119.087262
246. Li Q, Peng X, Yang H, Wang H, Shu Y. Deficiency of multidrug and toxin extrusion 1 enhances renal accumulation of paraquat and deteriorates kidney injury in mice. *Molecular pharmaceutics*. 2011;8(6):2476-2483. doi:10.1021/mp200395f
247. Jonker JW, Wagenaar E, Van Eijl S, Schinkel AH. Deficiency in the organic cation transporters 1 and 2 (Oct1/Oct2 [Slc22a1/Slc22a2]) in mice abolishes renal secretion of organic cations. *Molecular and cellular biology*. 2003;23(21):7902-7908. doi:10.1128/MCB.23.21.7902-7908.2003
248. Huang KM, Leblanc AF, Uddin ME, et al. Neuronal uptake transporters contribute to oxaliplatin neurotoxicity in mice. *The Journal of clinical investigation*. 2020;130(9):4601-4606. doi:10.1172/JCI136796
249. Miyake T, Kimoto E, Luo L, et al. Identification of Appropriate Endogenous Biomarker for Risk Assessment of Multidrug and Toxin Extrusion Protein-Mediated Drug-Drug Interactions in Healthy Volunteers. *Clinical pharmacology and therapeutics*. 2021;109(2):507-516. doi:10.1002/cpt.2022
250. Levêque D, Becker G, Bilger K, Natarajan-Amé S. Clinical Pharmacokinetics and Pharmacodynamics of Dasatinib. *Clinical pharmacokinetics*. 2020;59(7):849-856. doi:10.1007/s40262-020-00872-4
251. Lipka DB, Wagner MC, Dziadosz M, et al. Intracellular retention of ABL kinase inhibitors determines commitment to apoptosis in CML cells. *PloS one*. 2012;7(7):e40853-e40853. doi:10.1371/journal.pone.0040853
252. He K, Lago MW, Iyer RA, Shyu WC, Humphreys WG, Christopher LJ. Lacteal secretion, fetal and maternal tissue distribution of dasatinib in rats. *Drug metabolism and disposition: the biological fate of chemicals*. 2008;36(12):2564-2570. doi:10.1124/dmd.108.022764
253. Graham MA, Lockwood GF, Greenslade D, Brienza S, Bayssas M, Gamelin E. Clinical pharmacokinetics of oxaliplatin: a critical review. *Clinical cancer research : an official journal of the American Association for Cancer Research*. 2000;6(4):1205-1218.
254. Yokoo S, Yonezawa A, Masuda S, Fukatsu A, Katsura T, Inui KI. Differential contribution of organic cation transporters, OCT2 and MATE1, in platinum agent-

- induced nephrotoxicity. *Biochemical pharmacology*. 2007;74(3):477-487.
doi:10.1016/j.bcp.2007.03.004
255. Nakamura T, Yonezawa A, Hashimoto S, Katsura T, Inui KI. Disruption of multidrug and toxin extrusion MATE1 potentiates cisplatin-induced nephrotoxicity. *Biochemical pharmacology*. 2010;80(11):1762-1767.
doi:10.1016/j.bcp.2010.08.019
256. Li Q, Guo D, Dong Z, et al. Ondansetron can enhance cisplatin-induced nephrotoxicity via inhibition of multiple toxin and extrusion proteins (MATEs). *Toxicology and applied pharmacology*. 2013;273(1):100-109.
doi:10.1016/j.taap.2013.08.024
257. Mizuno T, Sato W, Ishikawa K, et al. Significance of downregulation of renal organic cation transporter (SLC47A1) in cisplatin-induced proximal tubular injury. *Oncotargets and therapy*. 2015;8:1701-1706. doi:10.2147/OTT.S86743
258. Sauzay C, White-Koning M, Hennebelle I, et al. Inhibition of OCT2, MATE1 and MATE2-K as a possible mechanism of drug interaction between pazopanib and cisplatin. *Pharmacological research*. 2016;110:89-95.
doi:10.1016/j.phrs.2016.05.012
259. Shen H, Yang Z, Zhao W, Zhang Y, Rodrigues AD. Assessment of vandetanib as an inhibitor of various human renal transporters: inhibition of multidrug and toxin extrusion as a possible mechanism leading to decreased cisplatin and creatinine clearance. *Drug metabolism and disposition: the biological fate of chemicals*. 2013;41(12):2095-2103. doi:10.1124/dmd.113.053215
260. Iwata K, Aizawa K, Kamitsu S, et al. Effects of genetic variants in SLC22A2 organic cation transporter 2 and SLC47A1 multidrug and toxin extrusion 1 transporter on cisplatin-induced adverse events. *Clinical and experimental nephrology*. 2012;16(6):843-851. doi:10.1007/s10157-012-0638-y
261. Qian CY, Zheng Y, Wang Y, et al. Associations of genetic polymorphisms of the transporters organic cation transporter 2 (OCT2), multidrug and toxin extrusion 1 (MATE1), and ATP-binding cassette subfamily C member 2 (ABCC2) with platinum-based chemotherapy response and toxicity in non-small cell lung cancer patients. *Chinese journal of cancer*. 2016;35(1):85. doi:10.1186/s40880-016-0145-8
262. Chang C, Hu Y, Hogan SL, et al. Pharmacogenomic Variants May Influence the Urinary Excretion of Novel Kidney Injury Biomarkers in Patients Receiving Cisplatin. *International journal of molecular sciences*. 2017;18(7).
doi:10.3390/ijms18071333

263. Belzer M, Morales M, Jagadish B, Mash EA, Wright SH. Substrate-dependent ligand inhibition of the human organic cation transporter OCT2. *Journal of Pharmacology and Experimental Therapeutics*. 2013;346(2):300-310. doi:10.1124/jpet.113.203257
264. El-Arabey AA. Dual function of OCT2 and MATE1 in cisplatin induced nephrotoxicity. *Pharmacological research*. 2017;119:493. doi:10.1016/j.phrs.2016.11.023
265. Vlaming MLH, van Esch A, Pala Z, et al. Abcc2 (Mrp2), Abcc3 (Mrp3), and Abcg2 (Bcrp1) are the main determinants for rapid elimination of methotrexate and its toxic metabolite 7-hydroxymethotrexate in vivo. *Molecular cancer therapeutics*. 2009;8(12):3350-3359. doi:10.1158/1535-7163.MCT-09-0668
266. Lancaster CS, Sprowl JA, Walker AL, Hu S, Gibson AA, Sparreboom A. Modulation of OATP1B-type transporter function alters cellular uptake and disposition of platinum chemotherapeutics. *Molecular cancer therapeutics*. 2013;12(8):1537-1544. doi:10.1158/1535-7163.MCT-12-0926
267. Huang KM, Uddin ME, DiGiacomo D, Lustberg MB, Hu S, Sparreboom A. Role of SLC transporters in toxicity induced by anticancer drugs. *Expert opinion on drug metabolism & toxicology*. 2020;16(6):493-506. doi:10.1080/17425255.2020.1755253
268. Uddin ME, Sun X, Huang KM, et al. Development and validation of a UPLC-MS/MS analytical method for dofetilide in mouse plasma and urine, and its application to pharmacokinetic study. *J Pharm Biomed Anal*. 2019;172:183-188. doi:10.1016/j.jpba.2019.04.041
269. Savelieva I, Camm J. Anti-arrhythmic drug therapy for atrial fibrillation: current anti-arrhythmic drugs, investigational agents, and innovative approaches. *Europace*. 2008;10(6):647-665. doi:10.1093/europace/eun130
270. Bianconi L, Castro A, Dinelli M, et al. Comparison of intravenously administered dofetilide versus amiodarone in the acute termination of atrial fibrillation and flutter. A multicentre, randomized, double-blind, placebo-controlled study. *Eur Heart J*. 2000;21(15):1265-1273. doi:10.1053/euhj.1999.2039
271. Wolbrette DL, Hussain S, Maraj I, Naccarelli GV. A Quarter of a Century Later: What is Dofetilide's Clinical Role Today? *J Cardiovasc Pharmacol Ther*. 2019;24(1):3-10. doi:10.1177/1074248418784288
272. Jaiswal A, Goldbarg S. Dofetilide induced torsade de pointes: mechanism, risk factors and management strategies. *Indian Heart J*. 2014;66(6):640-648. doi:10.1016/j.ihj.2013.12.021

273. Shenasa F, Shenasa M. Dofetilide: Electrophysiologic Effect, Efficacy, and Safety in Patients with Cardiac Arrhythmias. *Card Electrophysiol Clin.* 2016;8(2):423-436. doi:10.1016/j.ccep.2016.02.006
274. Yin J, Wang J. Renal drug transporters and their significance in drug-drug interactions. *Acta pharmaceutica Sinica B.* 2016;6(5):363-373. doi:10.1016/j.apsb.2016.07.013
275. Ivanyuk A, Livio F, Biollaz J, Buclin T. Renal Drug Transporters and Drug Interactions. *Clin Pharmacokinet.* 2017;56(8):825-892. doi:10.1007/s40262-017-0506-8
276. Walker DK, Smith DA, Stopher DA. Liquid-liquid extraction and high-performance liquid chromatography for the determination of a novel antidysrhythmic agent (UK-68,798) in human urine. *J Chromatogr.* 1991;568(2):475-480. doi:10.1016/0378-4347(91)80186-g
277. Smith DA, Rasmussen HS, Stopher DA, Walker DK. Pharmacokinetics and metabolism of dofetilide in mouse, rat, dog and man. *Xenobiotica.* 1992;22(6):709-719. doi:10.3109/00498259209053133
278. Tunblad K, Lindbom L, McFadyen L, Jonsson EN, Marshall S, Karlsson MO. The use of clinical irrelevance criteria in covariate model building with application to dofetilide pharmacokinetic data. *J Pharmacokinet Pharmacodyn.* 2008;35(5):503-526. doi:10.1007/s10928-008-9099-z
279. Kaddar N, Pilote S, Wong S, et al. Simultaneous determination of dofetilide and amlodipine in plasma by HPLC. *Journal of Chromatography and Separation Techniques.* 2013;4(6):192.
280. van Amsterdam P, Companjen A, Brudny-Kloeppel M, Golob M, Luedtke S, Timmerman P. The European Bioanalysis Forum community's evaluation, interpretation and implementation of the European Medicines Agency guideline on Bioanalytical Method Validation. *Bioanalysis.* 2013;5(6):645-659.
281. Administration F and D. Guidance for industry: bioanalytical method validation. <http://www.fda.gov/cder/Guidance/4252fnl.pdf>. Published online 2001.
282. Li L, Zhao M, Navid F, et al. Quantitation of sorafenib and its active metabolite sorafenib N-oxide in human plasma by liquid chromatography-tandem mass spectrometry. *J Chromatogr B Analyt Technol Biomed Life Sci.* 2010;878(29):3033-3038. doi:10.1016/j.jchromb.2010.08.049

283. Fu Q, Chen M, Hu S, et al. Development and validation of an analytical method for regorafenib and its metabolites in mouse plasma. *J Chromatogr B Analyt Technol Biomed Life Sci.* 2018;1090:43-51. doi:10.1016/j.jchromb.2018.05.005
284. Caban M, Migowska N, Stepnowski P, Kwiatkowski M, Kumirska J. Matrix effects and recovery calculations in analyses of pharmaceuticals based on the determination of β -blockers and β -agonists in environmental samples. *J Chromatogr A.* 2012;1258:117-127. doi:10.1016/j.chroma.2012.08.029
285. Leblanc AF, Huang KM, Uddin ME, Anderson JT, Chen M, Hu S. Murine Pharmacokinetic Studies. *Bio Protoc.* 2018;8(20):e3056. doi:10.21769/BioProtoc.3056
286. Smith DA, Rasmussen HS, Stopher DA, Walker DK. Pharmacokinetics and metabolism of dofetilide in mouse, rat, dog and man. *Xenobiotica.* 1992;22(6):709-719. doi:10.3109/00498259209053133
287. Yáñez JA, Remsberg CM, Sayre CL, Forrest ML, Davies NM. Flip-flop pharmacokinetics--delivering a reversal of disposition: challenges and opportunities during drug development. *Therapeutic delivery.* 2011;2(5):643-672. doi:10.4155/tde.11.19
288. Sharma A, Benbrook DM, Woo S. Pharmacokinetics and interspecies scaling of a novel, orally-bioavailable anti-cancer drug, SHetA2. *PLoS One.* 2018;13(4):e0194046. doi:10.1371/journal.pone.0194046
289. Naccarelli GV, Varker H, Lin J, Schulman KL. Increasing prevalence of atrial fibrillation and flutter in the United States. *Am J Cardiol.* 2009;104(11):1534-1539. doi:10.1016/j.amjcard.2009.07.022
290. Morillo CA, Banerjee A, Perel P, Wood D, Jouven X. Atrial fibrillation: the current epidemic. *J Geriatr Cardiol.* 2017;14(3):195-203. doi:10.11909/j.issn.1671-5411.2017.03.011
291. Chugh SS, Havmoeller R, Narayanan K, et al. Worldwide epidemiology of atrial fibrillation: a Global Burden of Disease 2010 Study. *Circulation.* 2014;129(8):837-847. doi:10.1161/CIRCULATIONAHA.113.005119
292. Krijthe BP, Kunst A, Benjamin EJ, et al. Projections on the number of individuals with atrial fibrillation in the European Union, from 2000 to 2060. *Eur Heart J.* 2013;34(35):2746-2751. doi:10.1093/eurheartj/eh280
293. Alonso A, Krijthe BP, Aspelund T, et al. Simple risk model predicts incidence of atrial fibrillation in a racially and geographically diverse population: the

- CHARGE-AF consortium. *Journal of the American Heart Association*. 2013;2(2):e000102. doi:10.1161/JAHA.112.000102
294. Rahman F, Kwan GF, Benjamin EJ. Global epidemiology of atrial fibrillation. *Nat Rev Cardiol*. 2014;11(11):639-654. doi:10.1038/nrcardio.2014.118
 295. Coyne KS, Paramore C, Grandy S, Mercader M, Reynolds M, Zimetbaum P. Assessing the direct costs of treating nonvalvular atrial fibrillation in the United States. *Value Health*. 2006;9(5):348-356. doi:10.1111/j.1524-4733.2006.00124.x
 296. Reynolds MR, Essebag V, Zimetbaum P, Cohen DJ. Healthcare resource utilization and costs associated with recurrent episodes of atrial fibrillation: the FRACTAL registry. *J Cardiovasc Electrophysiol*. 2007;18(6):628-633. doi:10.1111/j.1540-8167.2007.00819.x
 297. Wattigney WA, Mensah GA, Croft JB. Increased atrial fibrillation mortality: United States, 1980-1998. *Am J Epidemiol*. 2002;155(9):819-826.
 298. Wu EQ, Birnbaum HG, Mareva M, et al. Economic burden and co-morbidities of atrial fibrillation in a privately insured population. *Curr Med Res Opin*. 2005;21(10):1693-1699. doi:10.1185/030079905X65475
 299. Kim MH, Johnston SS, Chu BC, Dalal MR, Schulman KL. Estimation of total incremental health care costs in patients with atrial fibrillation in the United States. *Circ Cardiovasc Qual Outcomes*. 2011;4(3):313-320. doi:10.1161/circoutcomes.110.958165
 300. Pokorney SD, Yen DC, Campbell KB, et al. Dofetilide dose reductions and discontinuations in women compared with men. *Heart rhythm*. 2018;15(4):478-484. doi:10.1016/j.hrthm.2018.01.027
 301. Masuda S, Terada T, Yonezawa A, et al. Identification and functional characterization of a new human kidney-specific H⁺/organic cation antiporter, kidney-specific multidrug and toxin extrusion 2. *Journal of the American Society of Nephrology : JASN*. 2006;17(8):2127-2135. doi:10.1681/asn.2006030205
 302. Nies AT, Damme K, Kruck S, Schaeffeler E, Schwab M. Structure and function of multidrug and toxin extrusion proteins (MATEs) and their relevance to drug therapy and personalized medicine. *Archives of toxicology*. 2016;90(7):1555-1584. doi:10.1007/s00204-016-1728-5
 303. Chen Y, Zhang S, Sorani M, Giacomini KM. Transport of paraquat by human organic cation transporters and multidrug and toxic compound extrusion family. *J Pharmacol Exp Ther*. 2007;322(2):695-700. doi:10.1124/jpet.107.123554

304. Tsuda M, Terada T, Ueba M, et al. Involvement of human multidrug and toxin extrusion 1 in the drug interaction between cimetidine and metformin in renal epithelial cells. *J Pharmacol Exp Ther*. 2009;329(1):185-191. doi:10.1124/jpet.108.147918
305. Oh J, Chung H, Park SI, et al. Inhibition of the multidrug and toxin extrusion (MATE) transporter by pyrimethamine increases the plasma concentration of metformin but does not increase antihyperglycaemic activity in humans. *Diabetes Obes Metab*. 2016;18(1):104-108. doi:10.1111/dom.12577
306. Torp-Pedersen C, Brendorp B, Kober L. Dofetilide: a class III anti-arrhythmic drug for the treatment of atrial fibrillation. *Expert Opin Investig Drugs*. 2000;9(11):2695-2704. doi:10.1517/13543784.9.11.2695
307. Rowland M, Peck C, Tucker G. Physiologically-based pharmacokinetics in drug development and regulatory science. *Annual review of pharmacology and toxicology*. 2011;51:45-73. doi:10.1146/annurev-pharmtox-010510-100540
308. Jones HM, Chen Y, Gibson C, et al. Physiologically based pharmacokinetic modeling in drug discovery and development: A pharmaceutical industry perspective. *Clinical Pharmacology & Therapeutics*. 2015;97(3):247-262. doi:10.1002/cpt.37
309. Yamazaki S, Loi CM, Kimoto E, Costales C, Varma MV. Application of Physiologically Based Pharmacokinetic Modeling in Understanding Bosutinib Drug-Drug Interactions: Importance of Intestinal P-Glycoprotein. *Drug Metabolism and Disposition*. Published online 2018:dmd.118.080424. doi:10.1124/dmd.118.080424
310. Huang SM, Rowland M. The role of physiologically based pharmacokinetic modeling in regulatory review. *Clinical pharmacology and therapeutics*. 2012;91(3):542-549. doi:10.1038/clpt.2011.320
311. Shebley M, Sandhu P, Emami Riedmaier A, et al. Physiologically Based Pharmacokinetic Model Qualification and Reporting Procedures for Regulatory Submissions: A Consortium Perspective. *Clinical pharmacology and therapeutics*. 2018;104(1):88-110. doi:10.1002/cpt.1013
312. König J, Zolk O, Singer K, Hoffmann C, Fromm MF. Double-transfected MDCK cells expressing human OCT1/MATE1 or OCT2/MATE1: determinants of uptake and transcellular translocation of organic cations. *Br J Pharmacol*. 2011;163(3):546-555. doi:10.1111/j.1476-5381.2010.01052.x
313. Müller F, Weitz D, Mertsch K, König J, Fromm MF. Importance of OCT2 and MATE1 for the Cimetidine-Metformin Interaction: Insights from Investigations of

Polarized Transport in Single- And Double-Transfected MDCK Cells with a Focus on Perpetrator Disposition. *Mol Pharm.* 2018;15(8):3425-3433. doi:10.1021/acs.molpharmaceut.8b00416

314. Liu B, Ho HT, Velez-Cortes F, et al. Genetic ablation of ryanodine receptor 2 phosphorylation at Ser-2808 aggravates Ca(2+)-dependent cardiomyopathy by exacerbating diastolic Ca2+ release. *J Physiol.* 2014;592(9):1957-1973. doi:10.1113/jphysiol.2013.264689
315. Györke S, Lukyanenko V, Györke I. Dual effects of tetracaine on spontaneous calcium release in rat ventricular myocytes. *J Physiol.* 1997;500 (Pt 2):297-309. doi:10.1113/jphysiol.1997.sp022021
316. Mezache L, Struckman HL, Greer-Short A, et al. Vascular endothelial growth factor promotes atrial arrhythmias by inducing acute intercalated disk remodeling. *Sci Rep.* 2020;10(1):20463. doi:10.1038/s41598-020-77562-5
317. Koleske M, Bonilla I, Thomas J, et al. Tetrodotoxin-sensitive Navs contribute to early and delayed afterdepolarizations in long QT arrhythmia models. *J Gen Physiol.* 2018;150(7):991-1002. doi:10.1085/jgp.201711909
318. Wang L, Swirp S, Duff H. Age-dependent response of the electrocardiogram to K(+) channel blockers in mice. *Am J Physiol Cell Physiol.* 2000;278(1):C73-80. doi:10.1152/ajpcell.2000.278.1.C73
319. Chaves AA, Dech SJ, Nakayama T, Hamlin RL, Bauer JA, Carnes CA. Age and anesthetic effects on murine electrocardiography. *Life Sci.* 2003;72(21):2401-2412. doi:10.1016/s0024-3205(03)00137-1
320. Li Q, Peng X, Yang H, Wang H, Shu Y. Deficiency of multidrug and toxin extrusion 1 enhances renal accumulation of paraquat and deteriorates kidney injury in mice. *Mol Pharm.* 2011;8(6):2476-2483. doi:10.1021/mp200395f
321. Uddin ME, Garrison DA, Kim K, et al. Influence of YES1 Kinase and Tyrosine Phosphorylation on the Activity of OCT1. *Front Pharmacol.* 2021;12:644342. doi:10.3389/fphar.2021.644342
322. Uddin ME, Sun X, Huang KM, et al. Development and validation of a UPLC-MS/MS analytical method for dofetilide in mouse plasma and urine, and its application to pharmacokinetic study. *J Pharm Biomed Anal.* 2019;172:183-188. doi:10.1016/j.jpba.2019.04.041
323. Neuhoff S, Gaohua L, Burt H, et al. Accounting for Transporters in Renal Clearance: Towards a Mechanistic Kidney Model (Mech KiM). In: Sugiyama Y, Steffansen B, eds. *Transporters in Drug Development: Discovery, Optimization,*

- Clinical Study and Regulation*. Springer New York; 2013:155-177.
doi:10.1007/978-1-4614-8229-1_7
324. US Food and Drug Administration. *Drug Approval Package: Tikosyn (Dofetilide) NDA# 20-931*.; 1999. Accessed February 13, 2022.
https://www.accessdata.fda.gov/drugsatfda_docs/nda/99/20-931_Tikosyn.cfm
 325. Lee N, Duan H, Hebert MF, Liang CJ, Rice KM, Wang J. Taste of a pill: organic cation transporter-3 (OCT3) mediates metformin accumulation and secretion in salivary glands. *J Biol Chem*. 2014;289(39):27055-27064.
doi:10.1074/jbc.M114.570564
 326. Bell RM, Mocanu MM, Yellon DM. Retrograde heart perfusion: the Langendorff technique of isolated heart perfusion. *Journal of molecular and cellular cardiology*. 2011;50(6):940-950. doi:10.1016/j.yjmcc.2011.02.018
 327. Huang KM, Leblanc AF, Uddin ME, et al. Neuronal uptake transporters contribute to oxaliplatin neurotoxicity in mice. *J Clin Invest*. 2020;130(9):4601-4606.
doi:10.1172/JCI136796
 328. J. Paul Mounsey, John P. DiMarco. Dofetilide. *Circulation*. 2000;102(21):2665-2670. doi:doi:10.1161/01.CIR.102.21.2665
 329. Saliba WI. Dofetilide (Tikosyn): a new drug to control atrial fibrillation. *Cleve Clin J Med*. 2001;68(4):353-363.
 330. Cho MJ, Thompson DP, Cramer CT, Vidmar TJ, Scieszka JF. The Madin Darby canine kidney (MDCK) epithelial cell monolayer as a model cellular transport barrier. *Pharmaceutical research*. 1989;6(1):71-77.
 331. Quan Y, Jin Y, Faria TN, et al. Expression Profile of Drug and Nutrient Absorption Related Genes in Madin-Darby Canine Kidney (MDCK) Cells Grown under Differentiation Conditions. *Pharmaceutics*. 2012;4(2):314-333.
doi:10.3390/pharmaceutics4020314
 332. Braun A, Hammerle S, Suda K, et al. Cell cultures as tools in biopharmacy. *European journal of pharmaceutical sciences : official journal of the European Federation for Pharmaceutical Sciences*. 2000;11 Suppl 2:S51-60.
 333. Walker DK, Alabaster CT, Congrave GS, et al. Significance of metabolism in the disposition and action of the antidysrhythmic drug, dofetilide. In vitro studies and correlation with in vivo data. *Drug metabolism and disposition: the biological fate of chemicals*. 1996;24(4):447-455.

334. Abel S, Nichols DJ, Brearley CJ, Eve MD. Effect of cimetidine and ranitidine on pharmacokinetics and pharmacodynamics of a single dose of dofetilide. *Br J Clin Pharmacol*. 2000;49(1):64-71. doi:10.1046/j.1365-2125.2000.00114.x
335. Johnson BF, Cheng SL, Venitz J. Transient kinetic and dynamic interactions between verapamil and dofetilide, a class III antiarrhythmic. *Journal of clinical pharmacology*. 2001;41(11):1248-1256.
336. Diaz AL, Clifton GD. Dofetilide: A New Class III Antiarrhythmic for the Management of Atrial Fibrillation. *Progress in Cardiovascular Nursing*. 2001;16(3):126-129. doi:10.1111/j.0889-7204.2001.00595.x
337. Launay-Vacher V, Izzedine H, Karie S, Hulot JS, Baumelou A, Deray G. Renal Tubular Drug Transporters. *Nephron Physiology*. 2006;103(3):p97-p106. doi:10.1159/000092212
338. Lepist EI, Ray AS. Renal Transporter-Mediated Drug-Drug Interactions: Are They Clinically Relevant? *The Journal of Clinical Pharmacology*. 2016;56(S7):S73-S81. doi:10.1002/jcph.735
339. Teuma C, Perier-Muzet M, Pelletier S, et al. New insights into renal toxicity of the B-RAF inhibitor, vemurafenib, in patients with metastatic melanoma. *Cancer chemotherapy and pharmacology*. 2016;78(2):419-426. doi:10.1007/s00280-016-3086-7
340. Jhaveri KD, Sakhiya V, Fishbane S. Nephrotoxicity of the BRAF Inhibitors Vemurafenib and Dabrafenib. *JAMA oncology*. 2015;1(8):1133-1134. doi:10.1001/jamaoncol.2015.1713
341. Yamreudeewong W, DeBisschop M, Martin LG, Lower DL. Potentially significant drug interactions of class III antiarrhythmic drugs. *Drug Saf*. 2003;26(6):421-438. doi:10.2165/00002018-200326060-00004
342. Walker DK, Alabaster CT, Congrave GS, et al. Significance of metabolism in the disposition and action of the antidysrhythmic drug, dofetilide. In vitro studies and correlation with in vivo data. *Drug Metab Dispos*. 1996;24(4):447-455.
343. CDER. Clinical Drug Interaction Studies - Study Design, Data Analysis, and Clinical Implications. Guidance for Industry (draft).
344. CDER. In Vitro Metabolism and Transporter Mediated Drug-Drug Interaction Studies. Guidance for Industry (draft).